INTEGRATED RESERVOIR CHARACTERIZATION OF UPPER LEONARDIAN DETRITAL CARBONATE ROCKS, GLASSCOCK COUNTY, TEXAS, USA

A Thesis

by

ROY AUGUSTINE CONTE

Submitted to the Office of Graduate and Professional Studies of
Texas A&M University
in partial fulfillment of the requirements for the degree of

MASTER OF SCIENCE

Chair of Committee,	Michael C. Pope
Committee Members,	Zoya Heidari
	Juan Carlos Laya
Head of Department,	Rick E. Giardino

December 2014

Major Subject: Geology

ABSTRACT

Wells on the eastern side of the Midland Basin near its Eastern Shelf in Glasscock County, Texas, penetrate an Upper Leonardian succession of detrital carbonate, deposited in slope and basinal environments. Hydrocarbon production from this interval in Veterans and St. Lawrence Fields is highly variable - some wells produced oil at economic rates following fracture stimulation, whereas the coeval section in other wells failed to produce oil after fracture stimulation.

The depositional texture and diagenetic attributes of the Upper Leonardian detrital carbonate succession were described from slabbed cores, plain light and cathodoluminescence (CL) petrography, scanning electron microscope (SEM) images, and formation micro-imager (FMI) logs. Depth-by-depth assessment of petrophysical properties were interpreted from conventional wireline logs and laboratory core plug measurements using the multimineral analysis method.

Nine main lithofacies were identified on the basis of depositional texture, constituent composition (skeletal and non-skeletal grains, detrital component, and mineralogy) and diagenetic features. The upper and middle slope lithofacies are: mud-lean fusulinid-crinoid packstone and clast-supported polymict conglomerate deposited in channelized settings. The middle and lower slope deposits are: fusulinid-crinoid packstone, fusulinid wackestone, skeletal wackestone and partially silicified skeletal wackestone to mudstone. Occasional intraclasts in these deposits suggest they were deposited by debris flows. The lower slope facies is matrix-supported conglomerate

deposited by debris flow at the toe-of-slope. Carbonate mudstone was deposited on the lower slope and on unchannelized parts of the slope. Shale was deposited in the basin.

The Upper Leonardian detrital carbonate succession in Veterans and St. Lawrence Fields was deposited in carbonate aprons developed along relatively gentle to steep slopes ($1\text{-}5^0$) that were fed by small submarine canyons that by-passed fine-grained upper slope sediments. The rocks were affected most by burial diagenesis. The effects of burial diagenesis on the formation are mechanical and chemical compaction, resulting in reduced pore sizes and loss of primary interparticle porosity, reduced pore throat diameter, stylolite development, grain penetration, grain deformation, and grain fracturing. The pore system throughout the carbonate units is characterized by intraparticle pores mainly in skeletal grains and interparticle pores which are interconnected solution-enhanced pores between grains created by partial dissolution of skeletal grains.

This reservoir characterization indicates that, in Veterans and St. Lawrence Fields, the failure of some wells to produce oil at economic rates could be attributed to the heterogeneities associated with the stratigraphic framework and spatial distribution of depositional facies of the Upper Leonardian detrital carbonate succession. The potential reservoir rocks developed in the channelized portion of the slope whereas non-reservoir rocks accumulated in the lower slope and on interchannel highs on the upper and middle slope.

DEDICATION

This thesis is dedicated to Jesus Christ, the same yesterday, today and forevermore.

ACKNOWLEDGEMENTS

I would like to express my profound gratitude to my committee chair, Dr. Mike Pope, and my committee members Dr. Zoya Heidari and Dr. Juan Carlos Laya, for their guidance, and support throughout the course of this research.

I wish to thank McClure Oil Company, Midland, TX, for providing all the data for this research, and Berg Hughes Center for Sedimentary and Petroleum Studies, Texas A&M University, for providing funding for this research.

I also would like to thank my friends, colleagues and faculty and staff members of the Department of Geology and Geophysics for making my time at Texas A&M University a great experience.

Finally, I would like to thank my family for their support and encouragement throughout the course of my study.

NOMENCLATURTE

CL	Cathodoluminescence
Csh	Volumetric Concentration of Shale
FMI	Formation Micro Imager
F	Fahrenheit (measured in degrees)
GR	Gamma Ray (measured in API)
kV	Kilovolt
mA	Milliamp
ϕ_e	Interconnected Porosity
$\emptyset_N$	Neutron Porosity
PEF	Photo Electric Factor
$\emptyset_s$	Non-Shale Porosity
Rd	Deep Resistivity
SEM	Scanning Electron Microscope
So	Oil Saturation
Sw	Water Saturation
Sxo	Flushed Zone Fluid Saturation
U	Volumetric Photoelectric Factor
Δt	Interval Transit Time
ρ_b	Bulk Density

TABLE OF CONTENTS

LIST OF FIGURES

LIST OF TABLES

Page

INTRODUCTION

Carbonate reservoirs typically are heterogeneous, and determining the controls that characterize the reservoir for successful hydrocarbon exploration, reservoir development and hydrocarbon production can be difficult. For example, post-depositional processes such as diagenesis and fracturing can significantly alter a reservoir's depositional texture and may ultimately control its spatial distribution of porosity and permeability (Ahr, 2008). Consequently, exploration for hydrocarbon accumulations in carbonate reservoirs requires a thorough understanding of the relationships among depositional environments, diagenesis, regional stratigraphy, and the spatial distribution of petrophysical properties such as porosity, permeability, and fluid saturation.

This study area is located in Glasscock County, Texas, on the eastern side of the Midland Basin near its Eastern Shelf (Figure 1). The stratigraphic interval is an Upper Leonardian succession of detrital carbonate deposited in slope and basinal environments (Figure 2). Hydrocarbon production from this interval in Veterans and St. Lawrence Fields is highly variable. For instance, Well 1 produced oil at economic rates following fracture stimulation, however, the coeval section in Well 2 failed to produce oil after fracture stimulation (Figure 1b).

In carbonate reservoirs, the three-dimensional distribution of petrophysical properties usually is a product of multiple geological processes, and sometimes it reflects several episodes of diagenetic alteration during its burial and exhumation history (Ahr, 2008). Therefore, a reservoir characterization study to predict the spatial distribution of reservoir zones must carefully identify the sequence of events that led to the reservoir's

rock properties and pore characteristics. This paper presents the results of a reservoir characterization study of Upper Leonardian detrital carbonate rocks on the Eastern Shelf of the Midland Basin. The reservoir characterization relates the stratigraphic framework of the depositional facies and diagenetic overprints to the vertical and lateral variations of reservoir zones that have the highest combined values of porosity and permeability with low initial water saturation. The results provide a basic framework to better understand the heterogeneities in the Upper Leonardian detrital carbonate reservoir which can influence future hydrocarbon exploration and exploitation, as well as reservoir development.

Geologic setting

The Permian Basin of West Texas and southern New Mexico is located in the foreland basin of the Marathon – Ouachita orogenic belt (Yang and Dorobek, 1995b). Structurally, it is sub-divided into several sub-basins that are separated by fault-bounded uplifts of the Central Basin Platform, Diablo Platform, and Ozona Arch (Figure 1a). The Midland Basin, a major structural subdivision on the eastern flank of the Permian Basin, is separated by the north-south trending Central Basin Platform from the Delaware Basin on its western flank.

The Midland Basin covers an area of about 15,200 square miles, and is largely filled with Phanerozoic shallow-marine shelf to shelf-margin carbonate and deep-basin deposits that are, at the deepest point, approximately 5000 m thick (Handford, 1981; Hills, 1985). During the Early to Middle Paleozoic, the current Permian Basin region was occupied by a relatively shallow, semi-circular basin called the Tobosa Basin, which

probably formed during an initial extensional event in Late Precambrian – Early Cambrian (Yang and Dorobek, 1995b). From Early Cambrian to Middle Mississippian, gradual subsidence occurred throughout the Tobosa Basin, which led to the formation of a broad marine basin in which vast carbonate and siliciclastic sediments were deposited (Yang and Dorobek, 1995b). During the Late Mississippian, the Appalachian-Ouachita Orogeny initiated the structural evolution of the Permian Basin as Laurasia collided with Gondwanaland, and the Marathon-Ouachita orogenic belt started to form (Hills, 1984; Ross and Ross, 1985; Yang and Dorobek, 1995b). Consequently, the antecedent Tobosa Basin was tectonically differentiated into the crustal uplifts and sub-basins that now characterize the Permian basin region. By Late Paleozoic, the Permian Basin was structurally stable, and vast siliciclastic units were deposited in the deep asymmetrical basins, whereas carbonate units were deposited on the shallow water shelves and their slopes.

In the Midland basin, rimmed platforms which prograded basinward developed during the Middle and Late Leonardian (Mazzullo, 1995). Early Permian eustatic curves indicate that reciprocal highstand carbonates and lowstand siliciclastic sedimentation was prevalent in the Midland and Delaware Basins in the Leonardian time (Mazzullo, 1995). During sea level highstands, carbonate and evaporite rocks were deposited in shelf lagoons as thick and laterally continuous platform margin reefs, and as allochthonous detritus in slope settings (Mazzullo, 1995; Mazzullo and Reid, 1989; Saller et al., 1989; Silvers and Todd, 1969). The Upper Leonardian detrital carbonate succession was likely deposited during an intervening sea level highstand. The Permian basin was not subjected to

significant deformation since the late Paleozoic, so the present structural features are essentially the same as those that existed at the end of the Permian (Yang and Dorobek, 1995a).

METHODS

The depositional texture and diagenetic attributes of the Upper Leonardian detrital carbonate succession were described from slabbed cores and thin sections using plain light and cathodoluminescence (CL) petrography, scanning electron microscopy (SEM), and formation micro-imager (FMI) logs. Petrophysical and compositional properties such as porosity, water saturation and volumetric concentrations of the formation's minerals were interpreted from conventional wireline logs and laboratory core plug measurements using the multimineral analysis method.

Approximately 994 ft. (303 m) of slabbed cores (Figures 3 to 7) from nine wells were examined and described at the bed-by-bed scale. The cores were examined for depositional texture, constituent composition (skeletal and non-skeletal grains, detrital components, and mineralogy), pore types, pore-filling cements, sedimentary structures and boundary between units. The depositional textures were classified according to Dunham's (1962) classification.

Seventy Seven **(**77) thin-sections from five (5) wells were analyzed (Figures 8 and 9) for depositional texture and fabric, as well as for digenetic events that complement the core description study. The thin-sections were impregnated with blue dye to indicate porosity. A small portion of each thin-section was stained with Alizarin Red S to determine the relative abundance of calcite and dolomite. The thin-sections were examined under a petrographic microscope that is equipped with a high-resolution digital camera attached to a desktop computer. The petrographic images were captured using Axiovision® 4.8 software. The pore characteristics are classified using Ahr and Hammel's

(1999) genetic classification scheme in which pores are classified as depositional, diagenetic, or fracture. The pore spaces were then described as intraparticle and interparticle pores. The intraparticle pores occur primarily as intrafossil pores in skeletal grains whereas the interparticle pores occur as interconnected solution-enhanced pores between grains. Some of the solution-enhanced interparticle pores are "vugs" that are significantly larger than the surrounding framework grains (Ahr, 2008). Thin-sections also were examined with a petrographic microscope attached to a TECHNOSYN Model 8200 MKII cathodoluminescence stage to determine the compositional variations in calcite and dolomite cements. The operating conditions were gun current of 200-300 mA and voltage of 10–15 kV. The grains were imaged using a Coolsnap-Procf camera attached to a desktop computer.

The QuantiElan work flow in Schlumberger's Techlog® software was used to conduct a depth-by-depth assessment of interconnected porosity, initial water saturation, initial oil saturation, flushed zone fluid saturation, and volumetric concentrations of clay and non-clay mineral constituents. The QuantiElan solver uses a semi-linear joint inversion method to quantify the rock's mineral and fluid composition based on input data from well logs. The volumetric concentrations of mineral and fluid constituents are obtained by minimizing the difference between the linearly estimated and actual well log measurements (Heidari et al., 2012) , expressed as

$$min\|A \cdot x - b\|_2^2 , \ 0 \leq x_i \leq 1 \qquad (1)$$

Subject to

$$\sum_{i=1}^{n} x_i = 1 \qquad (2)$$

Where x is the n-size vector of volumetric mineral and fluid concentrations, given by

$$x = [C_1 \quad C_2 \ldots \quad C_p \; C_{sh} \quad \emptyset_s]^T \tag{3}$$

$$A = \begin{bmatrix} \rho_{b,1} & \rho_{b,2} \ldots & \rho_{b,p} & \rho_{b,sh} & \rho_{fluid} \\ \emptyset_{N,1} & \emptyset_{N,2} \ldots & \emptyset_{N,p} & \emptyset_{N,sh} & \emptyset_{N,fluid} \\ \Delta t_1 & \Delta t_2 \ldots & \Delta t_p & \Delta t_{sh} & \Delta t_{sh} \\ U_1 & U_2 \ldots & U_p & U_{sh} & U_{fluid} \end{bmatrix} \tag{4}$$

$$b = [\rho_b \quad \emptyset_N \quad \Delta t \quad U]^T \tag{5}$$

Where C is volumetric concentration of the assumed mineral constituents, C_{sh} is the volumetric concentration of shale, $\emptyset_s$ is non-shale porosity, ρ_b is the bulk density, U is the volumetric photoelectric factor, Δt is the interval transit time, and $\emptyset_N$ is the neutron porosity. Conventional well logs from 17 wells were used for the input data. The well logs include: gamma ray (GR), electrical resistivity, bulk density, neutron porosity, photoelectric factor (PEF) and compressional-wave slowness. The output results are: interconnected porosity (ϕ_e), initial water saturation (S_w), initial oil saturation (S_o) and flushed zone water saturation (S_{xo}). Core plug data (porosity and water saturation) from eight (8) wells were used to verify the accuracy of the output results. A reservoir characterization report for well 1 and well 2 indicates that the measured connate water restivity is 0.0308 ohm-m at 98^0 F (Geosystem LLP, 2011). The dominant clay type in the Upper Leonardian detrital carbonate succession is illite-smectite composition, whereas the non-clay matrix component consists of calcite, dolomite, silt and secondary quartz (chalcedony). The formation fluids are saline connate water and oil. The initial water saturation was estimated using Archie's (1942) equation. It is assumed that Archie's (1942) equation is reliable in this formation, and values of 1, 2 and 1.9 were used for

Archie's factor a, n and m respectively. Log-log plots of porosity vs permeability were used to derive equations for the porosity-permeability relationships. The derived equations were then used to estimate the depth-by-depth permeability in all the wells. Figure 10 shows an example of a multimineral analysis result from Well 7.

The formation tops and bases of the Upper Leonard detrital carbonate succession were picked from well logs and, where available, the slabbed core data was used to verify the position of the formation tops. Where there was a depth mismatch, slabbed core data was shifted to match the well log depth. The tops and bases of the clast-supported polymict conglomerate and the mud-lean fusulinid-crinoid packstone were picked as are sub-zones within the Upper Leonardian detrital carbonate succession. The formation tops and bases were used as input to Petrel® software to develop a depositional model for the Upper Leonardian detrital carbonate succession. Subsequently, the interconnected porosity, initial water saturation, initial oil saturation, flushed zone water saturation and permeability values that were estimated using the QuantiElan workflow in Techlog®,were imported into Petrel®.

Using the arithmetic mean method, the petrophysical properties (interconnected porosity, permeability and initial water saturation) of the Upper Leonardian detrital carbonate succession at each well were averaged, and the average values were interpolated between wells to create average maps. Average maps of porosity, permeability and water saturation provide a general knowledge of the spatial distribution of petrophysical properties. However, carbonate reservoirs that were extensively altered by diagenesis may have significant vertical and lateral variations in petrophysical and compositional

properties, and the average values of porosity, permeability, and water saturation may not correspond to the reservoir's flow units. Therefore, to identify the reservoir zones that have the highest combined values of porosity and permeability with low initial water saturation, the net pay thickness in each well was estimated using a logical statement in Petrel® software to select zones with combined cut-off values of; interconnected porosity ≥ 7%; initial oil saturation ≥ 60% (i.e. initial water saturation < 40%); permeability ≥ 0.1 mD; moveable oil saturation ≥ 0%; volumetric concentration of shale < 20%. The moveable oil saturation, S_{mo}, was estimated using equation 6 (Rider and Kennedy, 2011).

$$S_{mo} = S_{xo} - S_w \quad (6)$$

Finally, the net pay thickness was estimated in each well and interpolated between wells to extend the coverage of the one-dimensional data to other portions of the field.

RESULTS

Core description and lithofacies

Nine main lithofacies were identified from the slabbed cores on the basis of depositional texture, constituent composition (skeletal and non-skeletal grains, detrital component, and mineralogy) and diagenetic features (Figures 3-7). The Upper Leonardian detrital carbonate succession thickens basinward (Figure 11b), and it is characterized by a sharp to gradual transition from very high GR log response in the basinal shale to very low GR log response in the carbonate interval. The nine lithofacies are:

1. Mud-lean fusulinid-crinoid packstone: The mud-lean fusulinid crinoid packstone (Figures 3a, c and d) consists primarily of fusulinid grains and crinoid fragments, but fragments of bryozoans and brachiopod shells also are common. This facies is normally graded occurring exclusively at the top of the succession and can be correlated across several wells in Veterans and St. Lawrence fields (Figures 13 and 14a). This unit is interpreted as grain flows and turbidity flows in upper to middle slope environments (Figures 12a, 13 and 14a).
2. Clast-supported polymict conglomerate: The clast-supported polymict conglomerate (Figures 3b, e and f) consists of clasts of skeletal wackestone to grainstone, mudstone and reef boundstone in a matrix of crushed skeletal grains and carbonate mud with occasional silt-sized quartz grains. The skeletal grains are fusulinids, fragments of bryozoans, crinoids, sponges and a few brachiopod shells. This unit grades into the overlying mud-lean fusulinid-crinoid packstone and also can be correlated across several wells in Veterans and St. Lawrence Fields (Figures 13 and 14a). Bioclasts of

bryozoans, sponges and reef boundstones indicate that the materials originate in shallow water carbonate environments. The unit is interpreted as channelized debris flows that were deposited in the upper to middle slope environments (Figures 12b, 13 and 14b).

3. Fusulinid wackestone: The fusulinid wackestone (Figures 4a and c) consists of fusulinids, brachiopod shell fragments, crinoid fragments, rare isolated rugose coral fragments and occasional intraclasts that are randomly oriented in a carbonate mud matrix with occasional silt-sized quartz grains. The facies occurs as relatively laterally discontinuous intervals on the slope (Figure 13). It is interpreted as debris flows deposited in middle to lower slope environments.
4. Skeletal wackestone: The skeletal wackestone (Figures 4b, d and e) consists of abundant brachiopod shell fragments, pelloidal grains, rare fusulinid grains, and occasional intraclasts. It is occasionally bioturbated, and the matrix is a mixture of carbonate mud and crushed skeletal grains with occasional silt-sized quartz grains. The facies occurs as relatively laterally discontinuous intervals on the slope. The unit is interpreted as debris flows deposited in lower slope to basin environments.
5. Fusulinid-crinoid packstone: The fusulinid-crinoid packstone (Figures 5a and c) is composed of fusulinids, crinoid fragments and occasional brachiopod fragments in dark carbonate mud matrix. The orientation of the skeletal grains vary from chaotic and randomly oriented to partially aligned. The facies occurs as a relatively laterally discontinuous intervals on the slope (Figure 13). The unit is interpreted as debris flows containing abundant skeletal grains deposited in the lower slope.

6. Partially silicified skeletal wackestone to mudstone: The partially silicified skeletal wackestone to mudstone (Figures 5b and d) consists of sponge spicules and partially to completely silicified brachiopod shells, crinoid fragments and fusulinid grains. The matrix is a mixture of carbonate mud and crushed skeletal grains. This facies was formed through siliceous diagenesis subsequent to deposition.
7. Carbonate mudstone: The carbonate mudstone (Figures 6b and e) consists of sparsely distributed brachiopod shell fragments, crinoid fragments, pellets, and occasional isolated rugose coral fragments in a lime mud matrix. The facies is occasionally bioturbated, and occurs as relatively laterally discontinuous interval on the slope (Figure 13). The occurrence of bioturbation, carbonate mud and pellets indicate deposition occurred in low energy environments in the lower slope to basin, and on the interchannel highs in the middle and upper slope as carbonate mud settled out of the water column.
8. Matrix-supported conglomerate: The matrix-supported conglomerate (Figures 6a and d) consists of poorly sorted and disorganized granular to cobble size clasts of skeletal packstone to mudstone in a dark, argillaceous carbonate mud matrix. The predominant skeletal grains are brachiopod shell fragments, crinoid fragments and varying amounts of fusulinids. The skeletal packstone to mudstone clasts, shale clasts at its basal contact, argillaceous carbonate mud matrix and slope geometry (Figure 11a) suggest that the materials were resedimented via debris flows from middle and lower slope environments into mud-rich basinal environments. This unit typically has a sharp contact with the underlying shale (Figure 7b).

9. Shale: The Upper Leonardian detrital carbonate succession is underlain and overlain by black, platy to massive shale that is occasionally calcareous (Figure 7a). The dark grey to black color and the presence of pyrite indicate an anoxic basinal depositional setting where organic matter was preserved.

Diagenesis

Thin-section petrography indicates that the detrital carbonate rocks in the Upper Leonardian succession were most affected by burial diagenesis. Cathodoluminescence microscopy did not show any significant luminescence to suggest substantial meteoric diagenesis. The matrix in the carbonate unit is a mixture of carbonate mud and crushed skeletal grains, and most of the larger skeletal grains are either deformed or broken. The results of mechanical and chemical compaction on the succession are: reduction of pore-size and loss of porosity, reduction of pore throat diameter, stylolite development, grain penetration, grain deformation, and grain fracturing. The mechanical and chemical compaction effects are more pronounced in the mud-lean fusulinid-crinoid packstone (Figures 9e and f) indicating lack a of framework cement during its burial.

Calcite is the most abundant cement occurring as poorly- to well-developed blocky fringing cements in the intraparticle pores, syntaxial overgrowth of crinoids, and subhedral to anhedral blocky calcite in both the intraparticle and interparticle pores. Dolomite occurs as euhedral rhombs in the matrix and interparticle pores, and as saddle dolomite (Figure 9d) in the intraparticle and interparticle pores. Silica (chalcedony) replacement (Figure 9c) in grains also is common. The paragenesis in the Upper Leonard detrital carbonate succession is shown in Figure 15.

Classification of pore types

Carbonate porosity can be genetically classified based on end member processes of depositional, diagenetic, or fracture (Ahr, 2008; Ahr and Hammel, 1999). Thin-section petrography and SEM images show that the pore system in the Upper Leonard detrital carbonate succession is the result of depositional and diagenetic processes, occurring as intraparticle and interparticle pores. The intraparticle pores are primary intrafossil pores in skeletal grains (Figures 8c and d), and their spatial distribution is controlled by depositional environment. These pores occasionally are enhanced by dissolution, but they commonly are reduced by blocky fringing calcite cement around the internal walls of the skeletal grains, pore-filling subhedral to anhedral blocky calcite and dolomite rhombs. The interparticle pores are secondary interconnected solution-enhanced pores between grains, created by partial dissolution of grains (Figures 8a and b). The interparticle pores commonly are filled by subhedral to anhedral blocky calcite, poikilotopic blocky calcite and baroque dolomite (saddle dolomite) cements.

Burial diagenesis has altered the original primary intrafossil and interparticle pore spaces resulting in reduction of pore sizes and pore throat diameter. However, subsequent dissolution events resulted in increased porosity (Figures 8a and 9d). The clast-supported polymict conglomerate, which commonly has dissolution vugs, is characterized by both interparticle and intraparticle pores with pore sizes commonly up to 4000 μm. The mud-lean fusulinid-crinoid packstone, with its extensive mechanical and chemical compaction, is characterized primarily by intraparticle pores with lesser amounts of interparticle pores, and the pore sizes are typically less than 1000 μm. The fusulinid wackestone has both

intraparticle and solution-enhanced interparticle pores, with pore sizes occasionally up to 4000 μm. The fusulinid-crinoid packstone has mainly intraparticle pores with lesser amounts of interparticle pores due to syntaxial overgrowth of calcite cement in crinoids. The pore sizes generally are less than 1000 μm in this facies. The skeletal wackestone is characterized by solution-enhanced interparticle pores with pore sizes less than 250 μm. The pore system in the partially silicified skeletal wackestone to mudstone is highly heterogeneous, the silicified portion is characterized by solution-enhanced interparticle pores with less amounts of intraparticle pores, whereas the unsilicified part has negligible porosity. The pore sizes in the partially silicified skeletal wackestone to mudstone typically are less than 1000 μm. The matrix-supported conglomerate has intraparticle and interparticle pores that commonly are filled with various kinds of cement and has no significant porosity. The mudstone has no visible porosity. Table 1 shows a summary of the pore types and sizes in the Upper Leonardian detrital carbonate succession.

Petrophysical characterization and formation evaluation

Heterogeneities caused by different geological processes in carbonate reservoirs may significantly affect a reservoir's vertical and lateral variations in porosity and permeability. However, flow units can be mapped by identifying reservoir zones with the highest combined values of porosity and permeability with low initial water saturation in each well, and subsequently expanding the coverage of the one-dimensional data to other parts of the field.

In the Veterans and St. Lawrence Fields, the average interconnected porosity of the Upper Leonardian carbonate succession varies from 2% to 10% (Figure 16a), whereas

the total porosity varies from 4% to 16% (Figure 16b). The average interconnected porosity increases northward. The average permeability varies from < 0.1 mD to about 7 mD (Figure 17a) and increases northward. The average initial water saturation varies from 36% to 72% (Figure 17b) and it decreases northward. The maps of average interconnected porosity, permeability and initial water saturation provide a general knowledge of the spatial distribution of petrophysical properties, however they do not give information about the flow units in the Upper Leonardian detrital carbonate succession. On the other hand, the net pay thickness, estimated by selecting reservoir zones that have the highest combined values of interconnected porosity and permeability with low initial water saturation (high initial oil saturation), provides more useful information on the flow units within the reservoir. Accordingly, the estimated net pay thickness in each well was interpolated between wells to create a net pay thickness map that outlines the spatial distribution of reservoir zones with the highest combined values of porosity and permeability with low initial water saturation. The net pay thickness map was further constrained by the moveable hydrocarbon saturation (equation 6) using the afore-mentioned cut-off values

A reservoir characterization report for Well 1 and Well 2 indicates that Well 1 produced oil at economic rates following fracture stimulation, but the coeval section in Well 2 did not produce oil after fracturing (Geosystems LLP, 2011). Based on the cut-off values above, Well 2 has about 8 ft. (2.4 m) of net pay whereas Well 1 has about 75 ft. (23 m) of net pay, the thickest pay zone is around Well 4 with about 90 ft. (27.4 m) of net pay (Figure 21a). Wells 11, 8, 10, 16 and 9 do not have pay. Furthermore, based on the

moveable oil saturation, Well 2 has almost no moveable oil whereas Wells 1 and 4 have almost 59 ft. (18 m) and 90 ft. (27.4 m) respectively of moveable oil (Figure 21b).

DISCUSSION

Depositional environments

The isochore thickness map for the clast-supported polymict conglomerate (Figure 14b) suggests that this unit was transported down slope via debris flows and deposited in a lobate fan geometry. The isochore thickness map for the mud-lean fusulinid-crinoid packstone (Figure 14a) suggests that this unit was likely deposited in channelized slope settings. Normal grading in the upper part of the mud-lean fusulinid-crinoid packstone probably resulted from a transition from grain support by dispersive pressure in the lower parts to grain support by turbulence at the top of the unit (Cook and Mullins, 1983). The fusulinid-crinoid packstone, fusulinid wackestone and skeletal wackestone are all characterized by the occurrence of occasional intraclasts in the deposits, and their lateral discontinuity suggests that these units were deposited by a combination of background sedimentation and individual events of isolated debris flows (Figure 13a and b). The occurrence of skeletal packstone to mudstone clasts in dark argillaceous carbonate mud matrix suggests that the matrix-supported conglomerate are debris flows which originated in middle slope and lower slope environments, and have moved down slope into mud-rich basinal environments. The carbonate mudstone represents fine-grained carbonate deposited in low energy environments on the lower slope-to-basin and on interchannel highs in the upper and middle slope (Figures 13a and b).

Stratigraphic architecture

Lower Permian (Wolcampian to Leonardian) detrital limestones form an important regional reservoir in the Permian Basin of West Texas (Montgomery, 1996). In Glasscock County, the detrital carbonates extend from the Eastern Shelf margin into the Midland basin. These re-deposited carbonate rocks may represent a combination of debris flows and submarine fan depositional processes (Cook, 1983). The Upper Leonardian detrital carbonate succession in Veterans and St. Lawrence Fields best fits a base-of-slope apron depositional model in which carbonate aprons develop along relatively steep slopes, and are fed by several small submarine canyons that by-pass fine-grained upper slope sediments (Schalger and Chermak, 1979; Mullins and Cook, 1986; Playton et al., 2010). This model suggests that the submarine canyons act as a line source for the down-slope transportation and distribution of coarse grained sediments (Mullins and Cook, 1986; Playton et al., 2010). Early Permian eustatic curves indicate that the Upper Leonardian detrital carbonate succession was deposited during a prolonged sea level highstand as the rimmed platform prograded basinward (Mazzullo, 1995).

Generally, average down-to-basin carbonate slopes are highly variable ranging from as little as 1 to 60^0 with locally vertical to overhanging scarps (Cook and Mullins, 1983; Mullins and Neumann, 1979). The bases of the clast-supported polymict conglomerate and the matrix-supported conglomerate illustrate two types of slope settings in the Upper Leonardian detrital carbonate succession. Surface map for the base of the matrix-supported conglomerate indicates that the facies was likely deposited on a relatively subtle slope of about 3^0 (Figure 11a). Surface map for the base of the clast-

supported polymict conglomerate indicates that the facies was likely deposited on a relatively gentle to steep slope varying from 1 to 5^0 (Figure 12b). It is interpreted to record sediment by-pass in the upper slope environment, and accumulation of fine-grained carbonate on interchannel highs as indicated by well 11 (Figures 12b and 13a). The sediments, which originated in shallow-water carbonate environments, were deposited via debris flow and sheet flow processes in upper and middle slope environments (Figure 14b). The surface map for the base of the mud-lean fusulinid-crinoid packstone indicates that the facies was likely deposited on a relatively subtle slope varying from 2 to 3^0 (Figure 12a). The slope angle for the mud-lean fusulinid-crinoid packstone is considerably less than the 18 to > 30+ ^{0} slope angle required for most grain flows (Cook and Mullins, 1983). Therefore, the deposit is interpreted as modified grain flows in which a dense interstitial fluid, overlying current, or excess pore-fluid pressure aids significantly in maintaining the dispersion and thus may flow on slope less than 18^0 (Lowe, 1976; Mullins and Buren, 1979). In the mud-lean fusulinid-crinoid packstone, normal grading suggests the top of this unit was turbulent. Turbulence and dense interstitial fluid (fluid density increased by presence of carbonate mud) in the intraparticle pores probably aided dispersive pressure in supporting the grains above the base of the bed causing the deposits to flow on a low angle slope (Cook and Mullins, 1983).

Impact of diagenesis on pore types and reservoir quality

Thin-section petrography and SEM images indicate that the pore system in the Upper Leonardian detrital carbonate succession is a result of depositional and diagenetic processes. The intraparticle pores (Figures 8c and d) occur primarily in fusulinids and

bryozoans and can be related to their depositional environments. The pores are occasionally enhanced by dissolution, however, most skeletal grains commonly are deformed, broken, or crushed due to burial compaction, resulting in an overall pore size reduction (Figures 9e and f). Furthermore, blocky fringing calcite cement, subhedral to anhedral blocky calcite and dolomite rhombs commonly are precipitated in the pores (Figure 9a, e and f). Intraparticle pores occur mainly in the mud-lean fusulinid-crinoid packstone, clast-supported polymict conglomerate, fusulinid-crinoid packstone and fusulinid wackestone. The interparticle pores are created by dissolution due to burial diagenesis (Figures 8a and b), occurring mainly by partial dissolution of grains. However, subhedral to anhedral blocky calcite and saddle dolomite (baroque dolomite) commonly occur in these pore spaces resulting in pore size reduction. Conversely, occasional intense dissolution in the clast-supported polymict conglomerate formed vugs (Figure 9d). Interparticle pores occur mainly in fusulinid wackestone, skeletal wackestone, clast-supported polymict conglomerate, mud-lean fusulinid-crinoid packstone and fusulinid-crinoid packstone. The matrix-supported conglomerate has very low porosity (Figures 6d and 18).

As indicated by their fossil contents, the re-deposited carbonate materials in the clast-supported polymict conglomerate originated in shallow water carbonate environments, whereas the re-deposited carbonate materials in the matrix-supported conglomerate originated in deep water middle and lower slope environments. Re-deposited shelf-derived carbonate clasts contain an abundance of metastable fine- and coarse-grained aragonite and high magnesium calcite, whereas slope-derived re-deposited

sediments consist primarily of more stable calcite (Bornhold and Pilkey, 1971; Mullins and Cook, 1986; Scholle, 1977). Accordingly, this may explain the relatively high degree of dissolution in the clast-supported polymict conglomerate. Thus, the clast-supported polymict conglomerate has the best reservoir potential. Furthermore, based on study of the elastic and petrophysical properties of the Upper Leonardian detrital carbonate succession in Veterans field estimated from conventional well logs, the clast-supported polymict conglomerate is the best reservoir zone for fracture treatment (Saneifer et al., 2014).

Mechanical and chemical compaction effects, which resulted in reduction of pore-size and loss of porosity, reduction of pore throat diameter, stylolite development, grain penetration, grain deformation, and grain fracturing, are more pronounced in the mud-lean fusulinid-crinoid packstone (Figures 9e and f), indicating lack of framework cement during burial. The compaction resulted in pore-size reduction of both the intraparticle and interparticle pores, but subsequent dissolution events resulted in solution-enhanced pores between grains. The fusulinid-crinoid packstone, fusulinid wackestone and skeletal wackestone record varying degree of dissolution vertically and laterally (Figures 8a, and b), and solution-enhanced interparticle pores are the principal pore type in the fusulinid wackestone and skeletal wackestone. The mudstone does not record any significant dissolution effects and is characterized by low porosity and permeability with high initial water saturation (Figures 18 and 19). The pore system in the partially silicified skeletal wackestone to mudstone is complex and highly heterogeneous. The silicified part has relatively high interparticle porosity whereas the unsilicified part has low porosity (Figure 8f).

Spatial distribution of petrophysical properties

Vertical and lateral variations of porosity and permeability in the Upper Leonardian detrital carbonate succession reflect the combination of depositional and diagenetic controls on reservoir development. The porosity varies with the degree of dissolution, and is well-developed in clast-supported polymict conglomerate, fusulinid wackestone, skeletal wackestone, mud-lean fusulinid-crinoid packstone and fusulinid crinoid packstone. The mudstone and matrix-supported conglomerate consistently have low porosity and permeability values (Figure 18). The average interconnected porosity of the Upper Leonardian detrital carbonate succession generally increases northward in the Veterans and St. Lawrence Fields (Figure 16a). Similarly, the average permeability increases northward in these fields (Figure 17a). Conversely, average initial water saturation of the Upper Leonardian detrital carbonate succession decreases northward in the Veterans and St. Lawrence Fields (Figure 16b). Water saturation in the Upper Leonardian detrital carbonate succession decreases with increase in porosity (Figure 19), suggesting that as the pore sizes increase, the pore throat sizes also increase, allowing oil to displace connate water from the pores.

The net pay thickness maps (Figures 21a and b) suggest that reservoir zones with the highest combined values of porosity and permeability with low initial water saturation (Figures 20a and b) mimic the depositional setting of the clast-supported polymict conglomerate (Figure 14b). This probably is because the relatively thick accumulation of carbonate mudstone in well 11 (Figure 13a) was deposited on the interchannel high, thereby acting as a baffle to hydrocarbon flow. Furthermore, although clast-supported

polymict conglomerate and mud-lean fusulinid-crinoid packstone thin onto the interchannel highs, the fusulinid wackestone, skeletal wackestone and fusulinid-crinoid packstone in the northern portion of the field have significantly higher interconnected solution-enhanced interparticle pores (Figures 8a and b) resulting in an increase in porosity and permeability (Figure 18b).

The net pay thickness map based on the aforementioned cut-off values of interconnected porosity, permeability and initial water saturation indicates that the thickest pay zone is located around Wells 3, 7, 4, 1, 18 and 5 (Figure 21 a). The net pay thickness map based on the moveable oil saturation shows a decrease in net pay thickness of almost 60 ft. (18.29 m) in Well 4 (Figure 21b), indicating the need for fracture stimulation.

CONCLUSIONS

Wells on the eastern side of the Midland Basin near its Eastern Shelf in Glasscock County, Texas, penetrate an Upper Leonardian succession of detrital carbonate rocks, deposited in slope and basinal environments. The succession thickens basinward, and the facies do not have systematic vertical stacking patterns, rather, they consist of carbonate mass-transport facies that were deposited areally as debris flows, grain flows and turbidity flows.

The detrital carbonate units in the Upper Leonardian succession were most affected by burial diagenesis. The matrix in all the facies is a mixture of carbonate mud and crushed skeletal grains, and most of the larger skeletal grains also are either deformed or broken. The textural effects of compaction on the succession is reduction of pore-size, loss of primary interparticle porosity, reduction of pore throat diameter, stylolite development, grain penetration, grain deformation, and grain fracturing. Accordingly, the pore system in the Upper Leonard detrital carbonate succession is the result of depositional facies and diagenetic events, and they occur primarily as interparticle and intraparticle pores.

The Upper Leonardian detrital carbonate succession in Veterans and St. Lawrence Fields were deposited in carbonate aprons developed along relatively gentle to steep slopes ($1\text{-}5^0$). This reservoir characterization indicates that in Veterans and St. Lawrence Fields, the potential reservoir rocks were deposited in the channelized portion of the slope whereas non-reservoir rocks accumulated in the lower slope and on interchannel highs in the middle and upper slope.

The clast-supported polymict conglomerate, fusulinid wackestone, mud-lean fusulinid-crinoid packstone, fusulinid-crinoid packstone, and skeletal wackestone are the best potential reservoir rocks in this study area. Conversely, the mudstone, partially silicified skeletal wackestone to mudstone and matrix-supported conglomerate are non-reservoir rocks, whereas shale is possible seal for the detrital carbonate unit. Reservoir zones with highest combined values of porosity and permeability have spatial distribution patterns that correspond closely to deposition of the clast-supported polymict conglomerate, whereas the relatively thick accumulation of carbonate mudstone in well 11 was deposited on an interchannel high, thereby acting as a horizontal baffle to hydrocarbon flow.

REFERENCES

Ahr, W. M., 2008, Geology of carbonate reservoirs:The identification, description, and characterization of hydrocarbon reservoirs in carbonate rocks: Hoboken, New Jersey, John Wiley & Sons, p. 277.

Ahr, W. M., and Hammel, B., 1999, Identification and mapping of flow units in carbonate reservoirs: An example from Happy Spraberry (Permian) Field, Garza County, Texas, USA: Energy Exploration and Exploitation, v. 17, p. 311-334.

Archie, G. E., 1942, The electrical resistivity log as an aid in determining some reservoir characteristics: Transactions of AIME, v. 146, p. 54-62.

Bornhold, B. D., and Pilkey, O. H., 1971, Bioclastic turbidite sedimentation in Columbus Basin, Bahamas: Geological Society of America Bulletin, v. 82, no. 1341-1354.

Cook, H. E., 1983, Sedimentology of some allochthonous deepwater carbonate reservoirs, Lower Permian, West Texas: Carbonate debris sheets, aprons, or submarine fans?: AAPG Bulletin, v. 63, p. 442.

Cook, H. E., and Mullins, H. T., 1983, Basin margin environment, in P. Scholle, D. Bebout and C. Moore eds., Carbonate depositional environments: AAPG Memoir, v. 33, p. 539-618.

Dunham, R. J., 1962, Classification of rocks according to depositional texture, in Classification of carbonate rocks, W.E. Ham (Ed), : AAPG Memoir No. 1 Tulsa Ok., v. 1, p. 108-121.

Geosystem LLP, 2011, Reservoir characterization of Upper Leonard Carbonates Veterans Field, Glasscock County, Texas. Unpublished reservoir characterization report.

Handford, C. R., 1981, Sedimentology and genetic stratigraphy of Dean and Spraberry Formations (Permian), Midland Basin, Texas: American Association of Petroleum Geologists, v. 65, p. 1602 - 1616.

Heidari, Z., Torres-Verdín, C., and Preeg, W. E., 2012, Improved estimation of mineral and fluid volumetric concentrations from well logs in thinly bedded and invaded formations: Geophysics v. 77, no. 3, p. WA79-WA98.

Hills, J. M., 1984 Sedimentation, tectonism, and hydrocarbon generation in Delaware Basin, West Texas and souteastern New Mexico: AAPG Bulletin, v. 68, p. 250 - 267.

Hills, J. M., 1985, Structural evolution of the Permian Basin of West Texas and New Mexico, *in* Dickerson, P.W., and Muehlberger, W.R., eds., Structure and tectonics of Trans-Pecos Texas: West Texas Geological Society: West Texas Geological Society, p. 89 - 99.

Lowe, D. R., 1976, Grain flow and grain flow deposits: Lournal of sedimentary petrology, v. 46, no. 1, p. 188-199.

Mazzullo, S. J., 1995, Permian stratigraphy and facies, Permian Basin (Texas-New Mexico) and adjoining areas in the midcontinent United States, in P.A. Scholle, T.M Peryt, and D.S. Ulmer-Scholle, eds., The Permian of Northern Pangea, v. 2: Sedimentary Basins and Economic Resources; Springer-Verlag, p. 41-60.

Mazzullo, S. J., and Reid, A. M., 1989, Lower Permian platform and basin depositional systems, northern Midland Basin, Texas, in Crevello, P.D., Wilson, J.L., Sarg, J.F.,

Read, J.F., eds., Controls on carbonate platform and basin development: SEPM Special Publication, v. 44, p. 305-320.

Montgomery, S. L., 1996, Permian "Wolfcamp" limestone reservoirs: Powell Ranch Field, Eastern Midland Basin: AAPG Bulletin, v. 80, no. 9, p. 1349-1365.

Mullins, H. T., and Buren, H. M. V., 1979, Modern modified carbonate grain flow deposits: Journal of Sedimentary Petrology, v. 49, no. 3, p. 747-752.

Mullins, H. T., and Cook, H. E., 1986, Carbonate apron models: Alternations to the submarine fan model for paleoenvironmental analysis and hydrocarbon exploration.: Sedimentary geology, v. 48, p. 37-79.

Mullins, H. T., and Neumann, A. C., 1979, Deep carbonate bank margin structure and sedimentation in northern Bahamas SEPM Special Publication, v. 27, p. 165-192.

Playton, T. E., Janson, X., and Kerans, C., 2010, Carbonate slopes, in N. P. James and R. W. Dalrymple, eds., Facies models 4: Geological Association of Canada, p. 449-476.

Rider, M., and Kennedy, M., 2011, The geological interpretation of well logs, 3rd edition, Scotland, Rider-French Consulting Ltd., 432 p.:

Ross, C. A., and Ross, J. R. P., 1985, Paleozoic tectonics and sedimentation in West Texas, southern New Mexico and southern Arizona in Dickepson P. W. and Muehlberger W. R. eds., Structure and tectonics of Trans Pecos Texas: Midland: West Texas Geological Society, no. 85, p. 221-230.

Ruppel, S. C., and Ward, W. B., 2013, Outcrop-based characterization of the Leonardian carbonate platform in west Texas: Implications for sequence-stratigraphic styles

in the Lower Permian: American Association of Petroleum Geologists Bulletin, v. 97, no. 2, p. . 223–250.

Saller, A. H., Barton, J. W., and Barton, R. E., 1989, Slope sedimentation associated with a vertically building reef, Bone Spring Formation, Mescalero Escarpe Field, southeastern New Mexico, in in Crevello, P.D., Wilson, J.L., Sarg, J.F., Read, J.F., eds., Controls on carbonate platform and basin development: SEPM Special Publication, v. 44, p. 275-288.

Saneifer, M., Conte, R., Chen, C., Heidari, Z., and Pope, M., 2014, Integrated rock classification based on elastic and petrophysical properties estimated from conventional well logs.: SPWLA 55th Annual Logging Symposium.

Schalger, W., and Chermak, A., 1979, Sediment facies of platform-basin transition, Tongue of the Ocean, Bahamas: SEPM, v. 27, p. 193-208.

Scholle, P. A., 1977, Deposition, diagenesis and hydrocarbon potential od "deep-water" limestones: AAPG Short Course Notes, p. 25pp.

Silvers, B. A., and Todd, R. G., 1969, Permian cyclic strata, northern Midland and Delaware Basins, West Texas and southeastern New Mexico: American Association of Petroleum Geologists Bulletin, v. 53, no. 11, p. 2223 - 2251.

Yang, K.-M., and Dorobek, S., 1995a, The Permian Basin of West Texas and New Mexico; Tectonic history of a "composite" foreland basin and its effects on stratigraphic development, in Dorobek, S.L., and Ross, G.M. eds., Stratigraphic evolution of foreland basins: Society for Sedimentary Geology Special Publication no. 52, p. 149-174.

Yang, K.-M., and Dorobek, S. T., 1995b, The Permian Basin of West Texas and New Mexico: Flexural modeling and evidence for lithospheric heterogenity across the Marathon foreland, in Dorobek, S.L., and Ross, G.M. eds., Stratigraphic evolution of foreland basins: Society for Sedimentary Geology Special Publication no. 52, p. 37 - 50.

APPENDIX 1

FIGURES

Legends


Shale


Skeletal wackestone


Matrix-supported conglomerate


Mudstone


Fusulinid-crinoid packstone


Clast-supported polymict conglomerate


Mud-lean fusulinid-crinoid packstone


Fusulinid wackestone


Partially silicified skeletal wackestone to mudstone

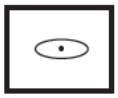
Fusulinid


Broken brachiopod shell


Bryozoan

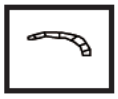
Sponge


Clasts with skeletal grains


Reef clast


Crinoid


Rugose


Shale rip-up clast


Soft sediment deformation

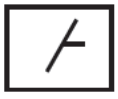
Sponge spicule


Stylolite


Pellets


Bioturbation


Gastropod

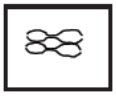
Compaction nodules


Normal grading


Calcite filled fractures


Base of Upper Leonardian detrital carbonate succession


Shallowing upward facies trend


Deepening upward facies trend

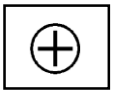
Wells with slabbed cores, thin-sections, well logs and FMI logs

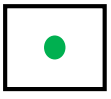
Oil stain in slabbed core

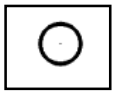
Wells with well logs and FMI logs

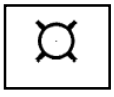
Wells with well logs only

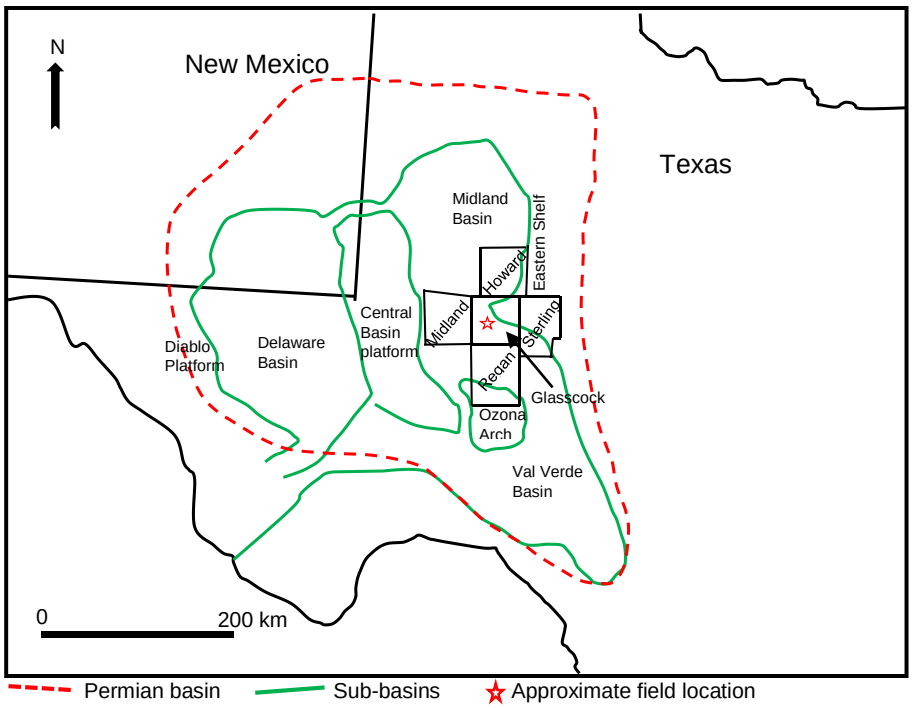

(a)

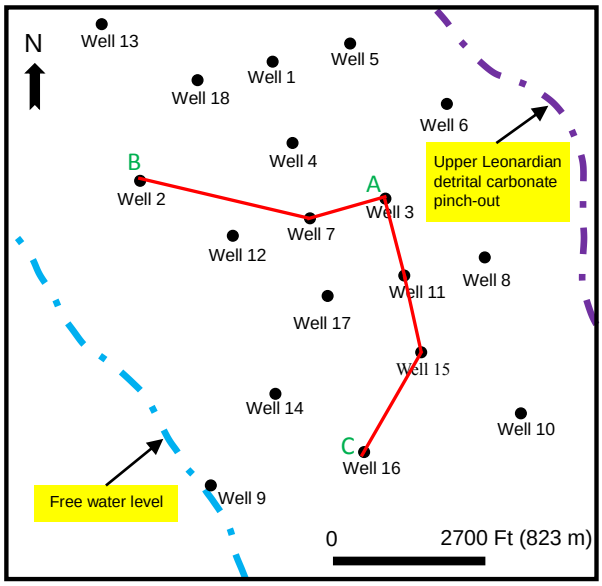

(b)

Figure 1: Location map of the study area. (a) Regional map of the Permian Basin showing Glasscock County and the approximate field location. (b) Field map provided by McClure Oil Company showing the relative position of the wells, the Upper Leonardian detrital carbonate pinch-out and the free-water level. (A-B and A-C are stratigraphic cross-sections correlated for wells with slabbed cores)

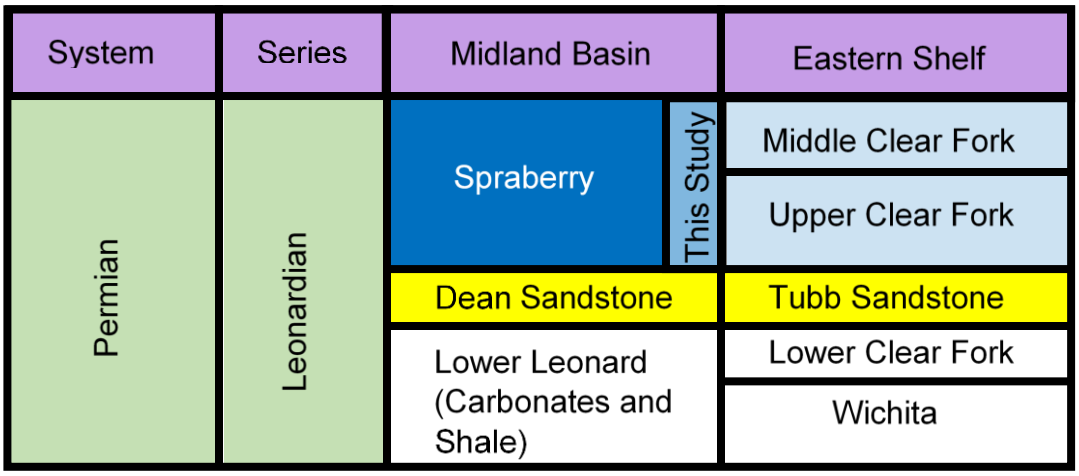

(a)

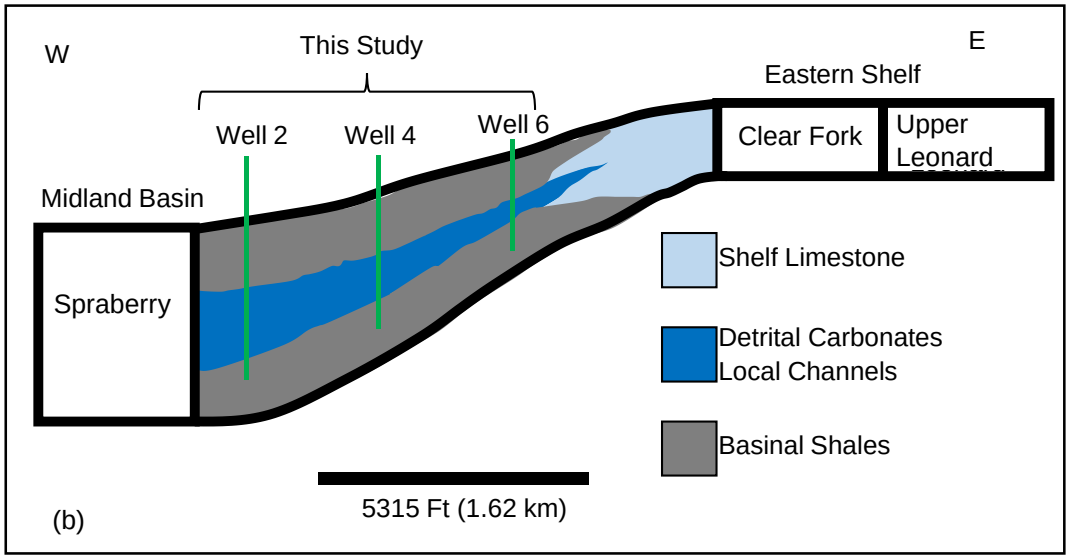

Figure 2: Stratigraphy. (a) Leonardian stratigraphic chart of the Eastern Shelf and Midland Basin stratigraphy. (b) Upper Leonardian detrital carbonate succession stratigraphy in Veterans and St. Lawrence Fields Glasscock County, Texas. The succession is underlain and overlain by shale.

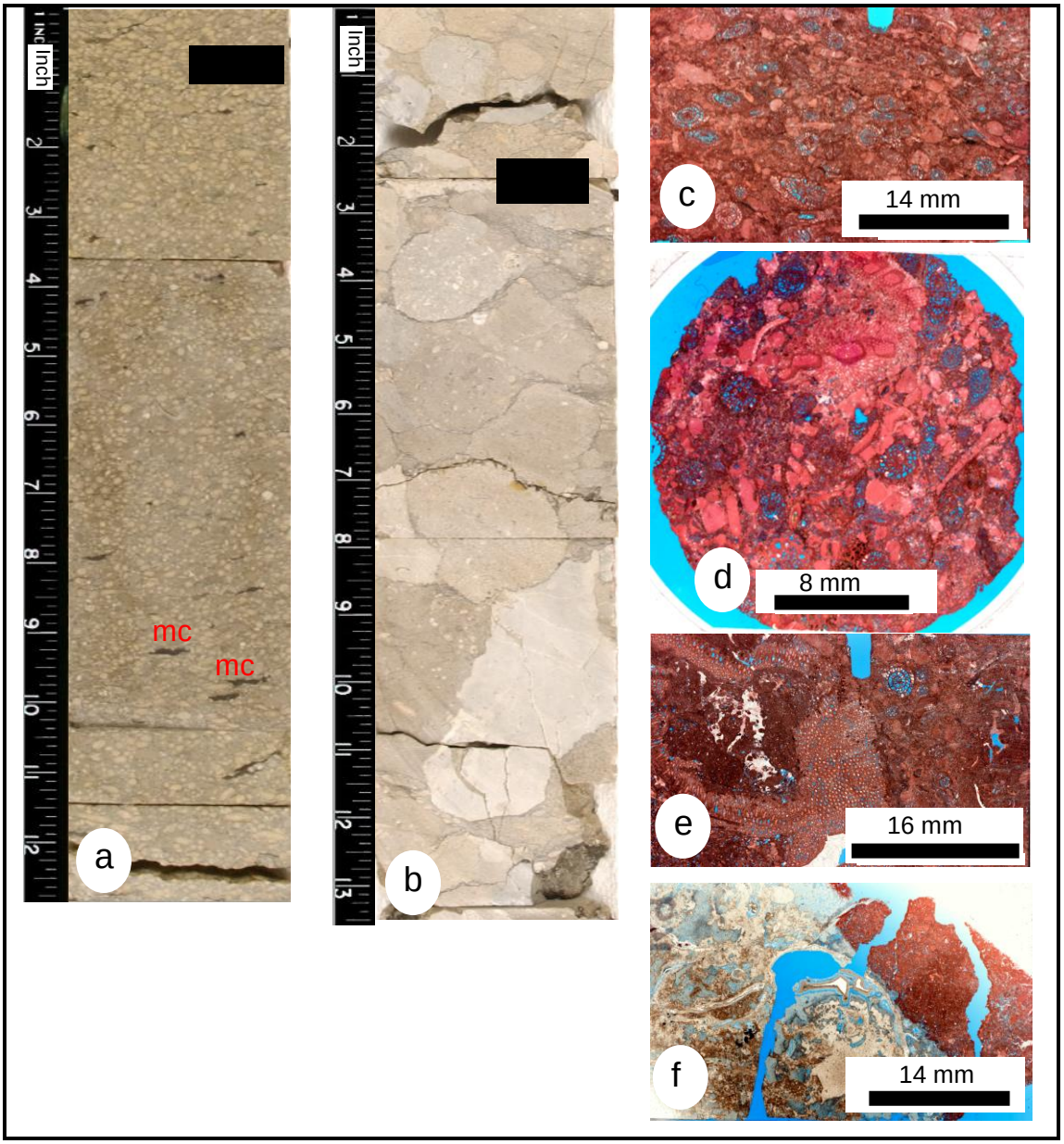

Figure 3: Mud-lean fusulinid-crinoid packstone and clast-supported polymict conglomerate facies. (a) Slabbed core of mud-lean fusulinid-crinoid packstone. Note the mud rip-up clasts (mc) mixed with the skeletal grains indicating high energy flow. (b) Slabbed core of clast-supported polymict conglomerate. (c and d) Thin-section of mud-lean fusulinid-crinoid packstone showing mostly intraparticle pores. (e and f) Thin-section of clast-supported polymict conglomerate showing two different types of clasts. [In the thin-sections, pink is calcite, white is dolomite, off-white/beige is silica (chalcedony) and blue is porosity. Notch in slides indicates depositional way up].

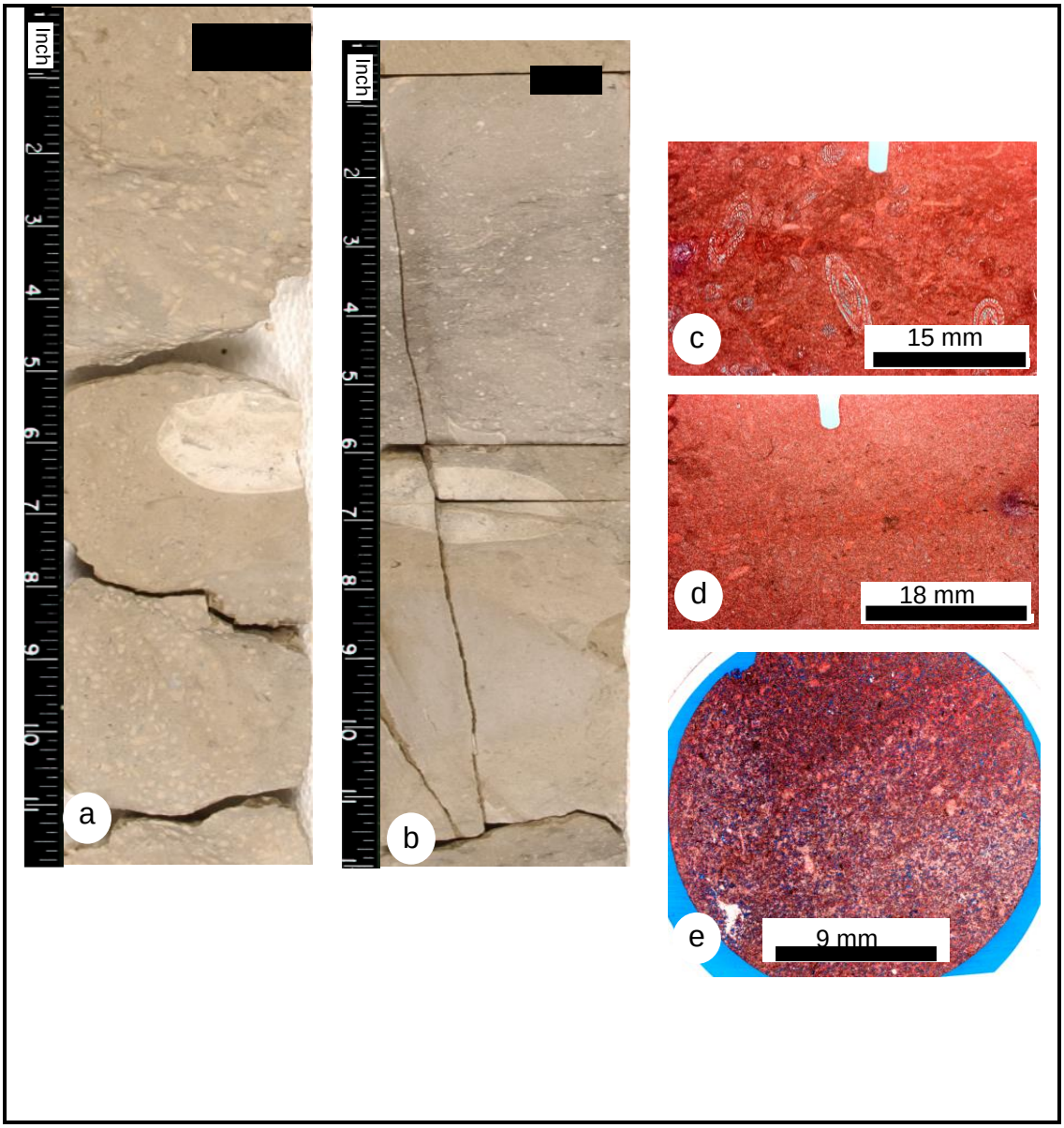

Figure 4: Fusulinid wackestone and skeletal wackestone facies (a) Slabbed core of fusulinid wackestone with chert clast. (b) Slabbed core of skeletal wackestone with chert clast. (c) Thin-section image of fusulinid wackestone. (d) Thin-section image of skeletal wackestone without solution-enhanced pores. (e) Thin-section image of skeletal wackestone. [In the thin-sections, pink is calcite, white is dolomite, off-white/beige is silica (chalcedony) and blue is porosity. Notch in slides indicates depositional way up].

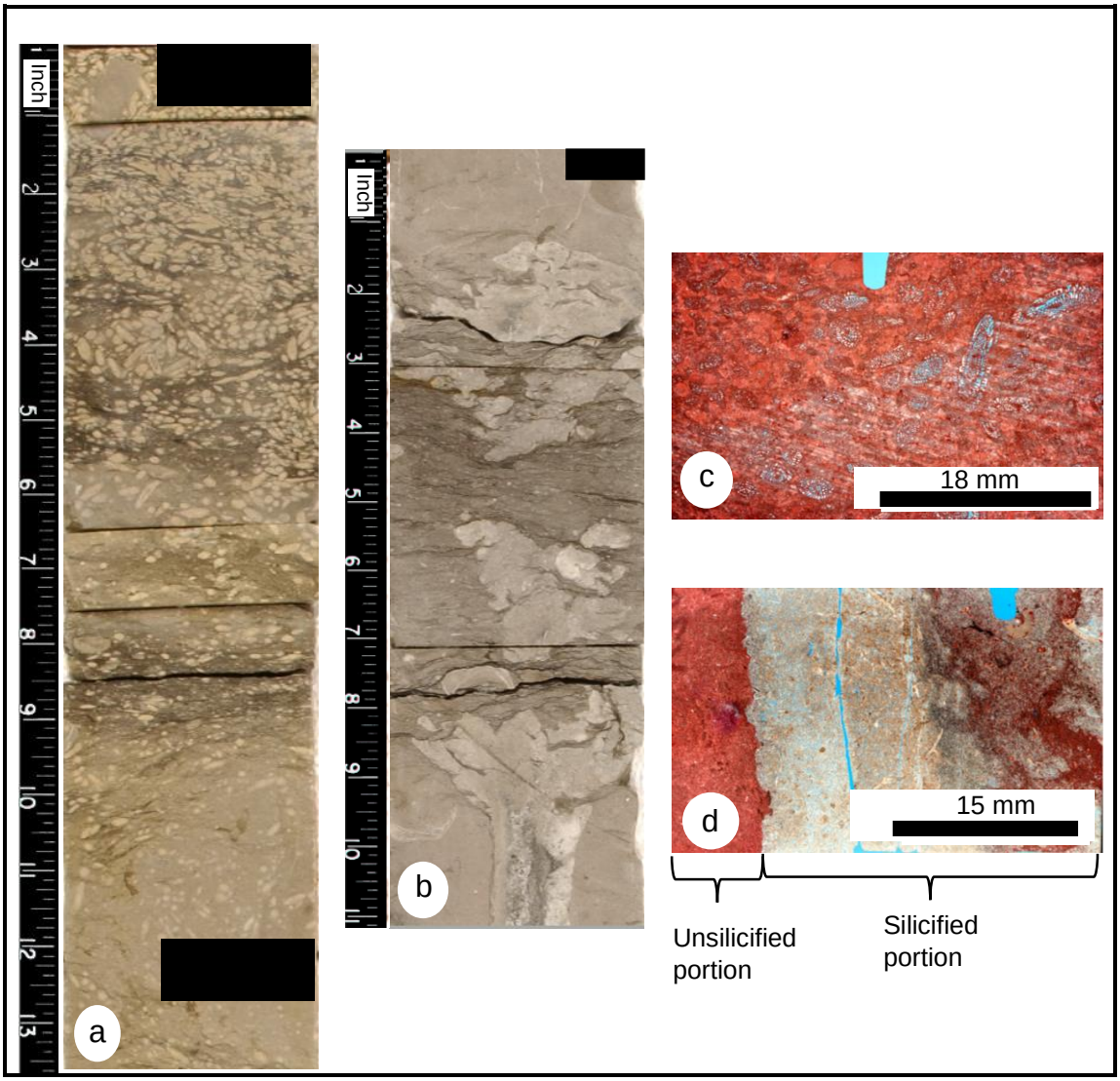

Figure 5: Fusulinid-crinoid packstone and partially silicified skeletal wackestone to mudstone facies. (a) Slabbed core of fusulinid-crinoid packstone. (b) Slabbed core of partially silicified skeletal wackestone to mudstone. (c) Thin-section of fusulinid-crinoid packstone. (d) Thin-section of partially silicified skeletal wackestone to mudstone showing extensive dissolution in silicified portion. [In the thin-sections, pink is calcite, white is dolomite, off-white/beige is silica (chalcedony) and blue is porosity. Notch in slides indicate depositional way up].

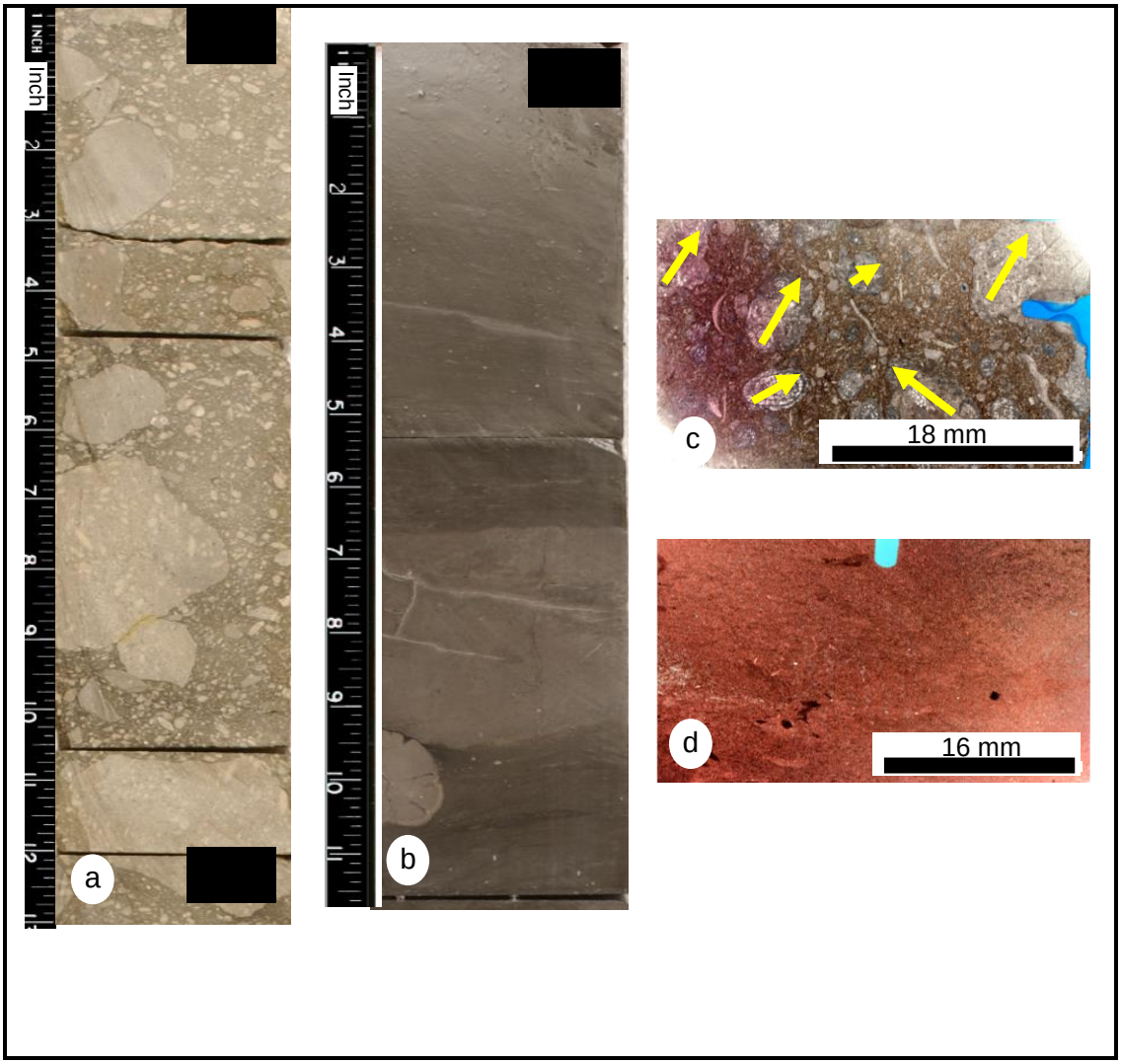

Figure 6: Matrix-supported conglomerate and carbonate mudstone facies. (a) Slabbed core of matrix-supported conglomerate. (b) Slabbed core of carbonate mudstone mudstone. (c) Thin-section of matrix-supported conglomerate (yellow arrows indicate clasts). (d) Thin-section of carbonate mudstone. [In the thin-sections, pink is calcite, white is dolomite, off-white/beige is silica (chalcedony) and blue is porosity. Notch in slides indicate depositional way up].

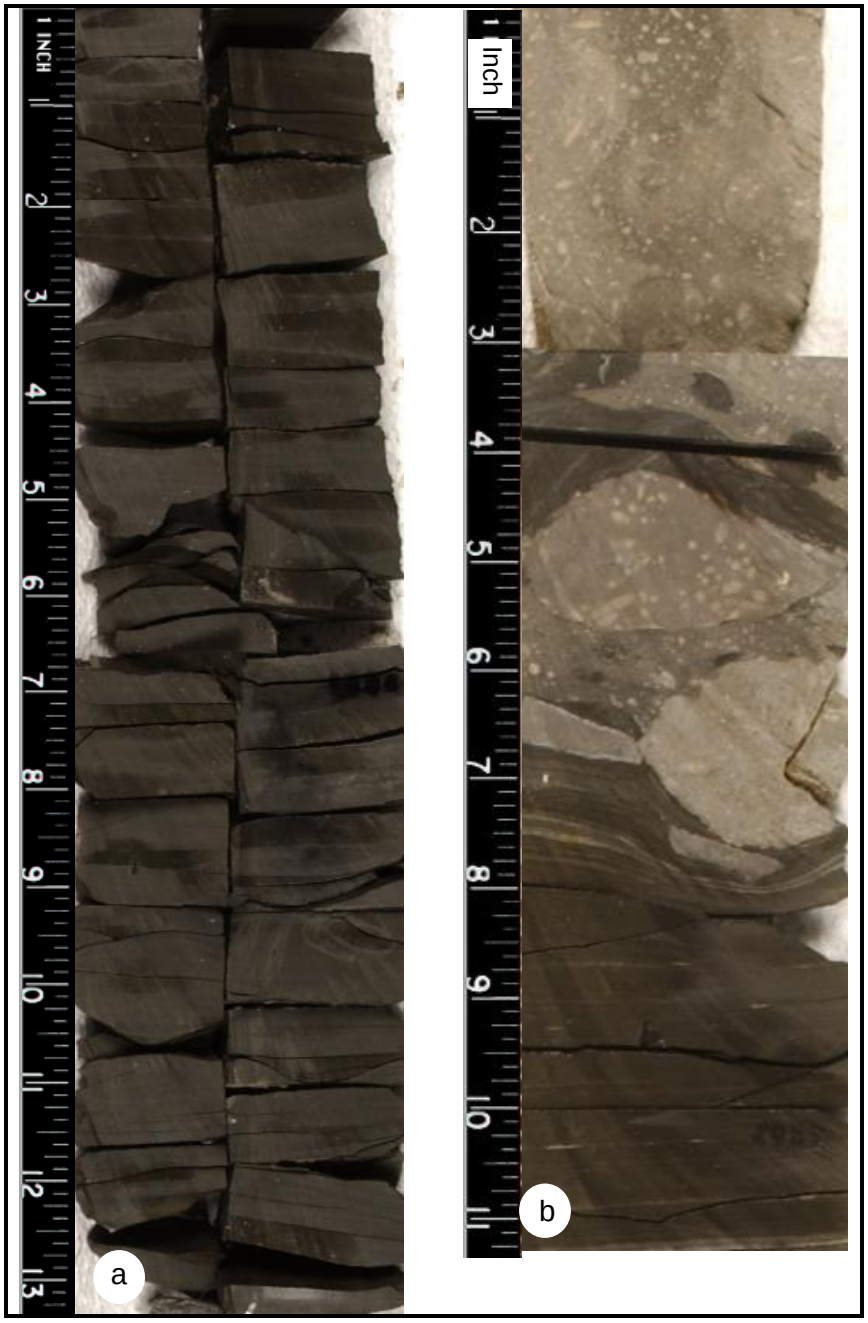

Figure 7: Shale facies. (a) Slabbed core of shale. (b) Slabbed core showing the sharp contact between the matrix-supported conglomerate and the underlying shale. Note the shale is mixed into the base of the matrix-supported conglomerate indicating debris flows into mud rich basinal environments.

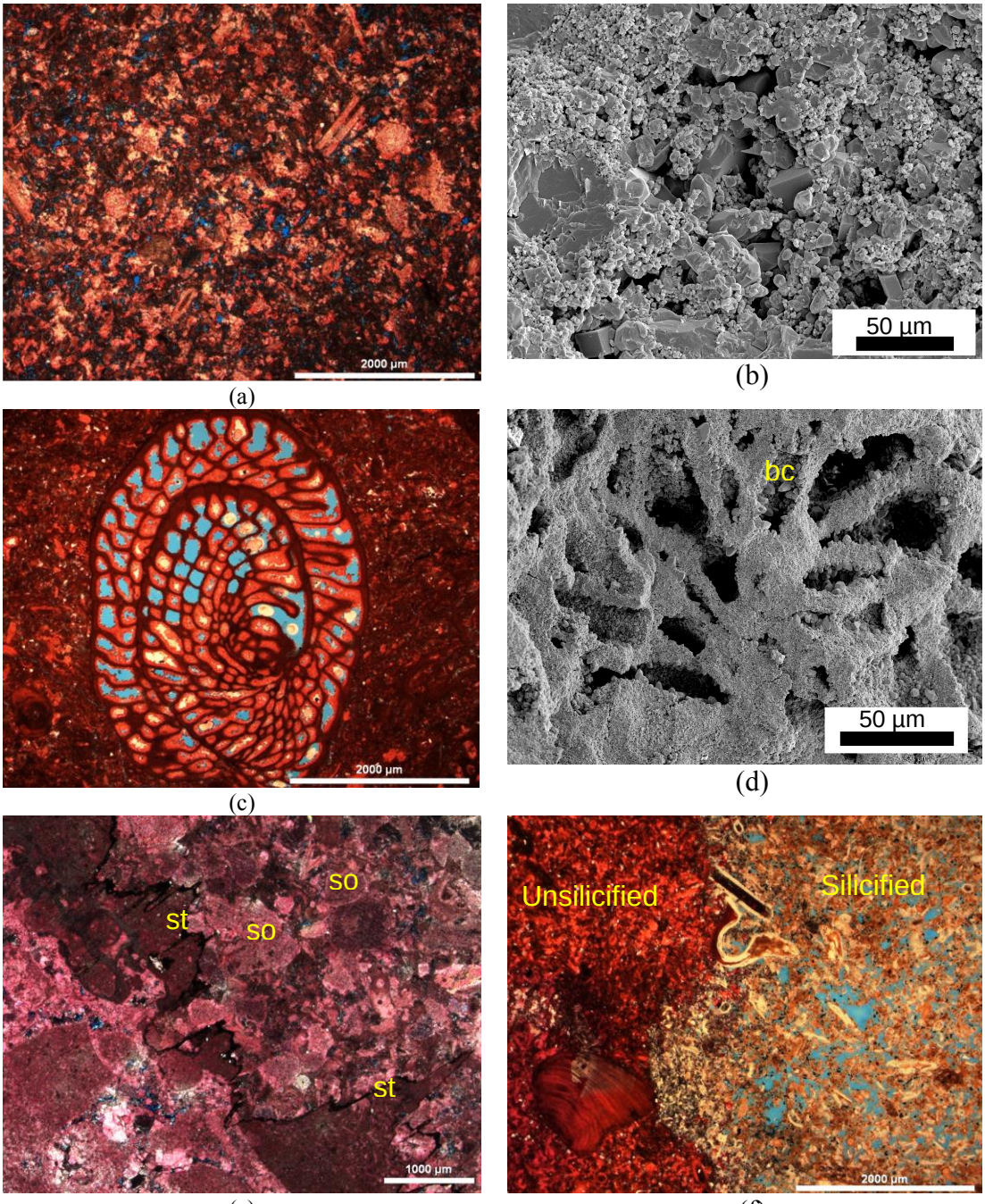

Figure 8: Diagenesis and pore types. (a) Skeletal-wackestone photomicrograph showing solution-enhanced interparticle pores. (b) SEM image of skeletal wackestone showing solution-enhanced interparticle pores. (c) Photomicrograph showing intraparticle pores in fusulinid with small blocky fringing calcite in the pore spaces. (d) SEM image of intraparticle pores in fusulinid with small blocky calcite fringing cement (bc) in the chambers. (e) Photomicrograph showing syntaxial overgrowth (so) of crinoids and stylolite (st) development. The stylolite (st) postdate the syntaxial overgrowth. (f) Photomicrograph of partially silicified skeletal packstone to mudstone showing partial to complete silicification of grains and matrix, and solution enhanced interparticle pores (to right).

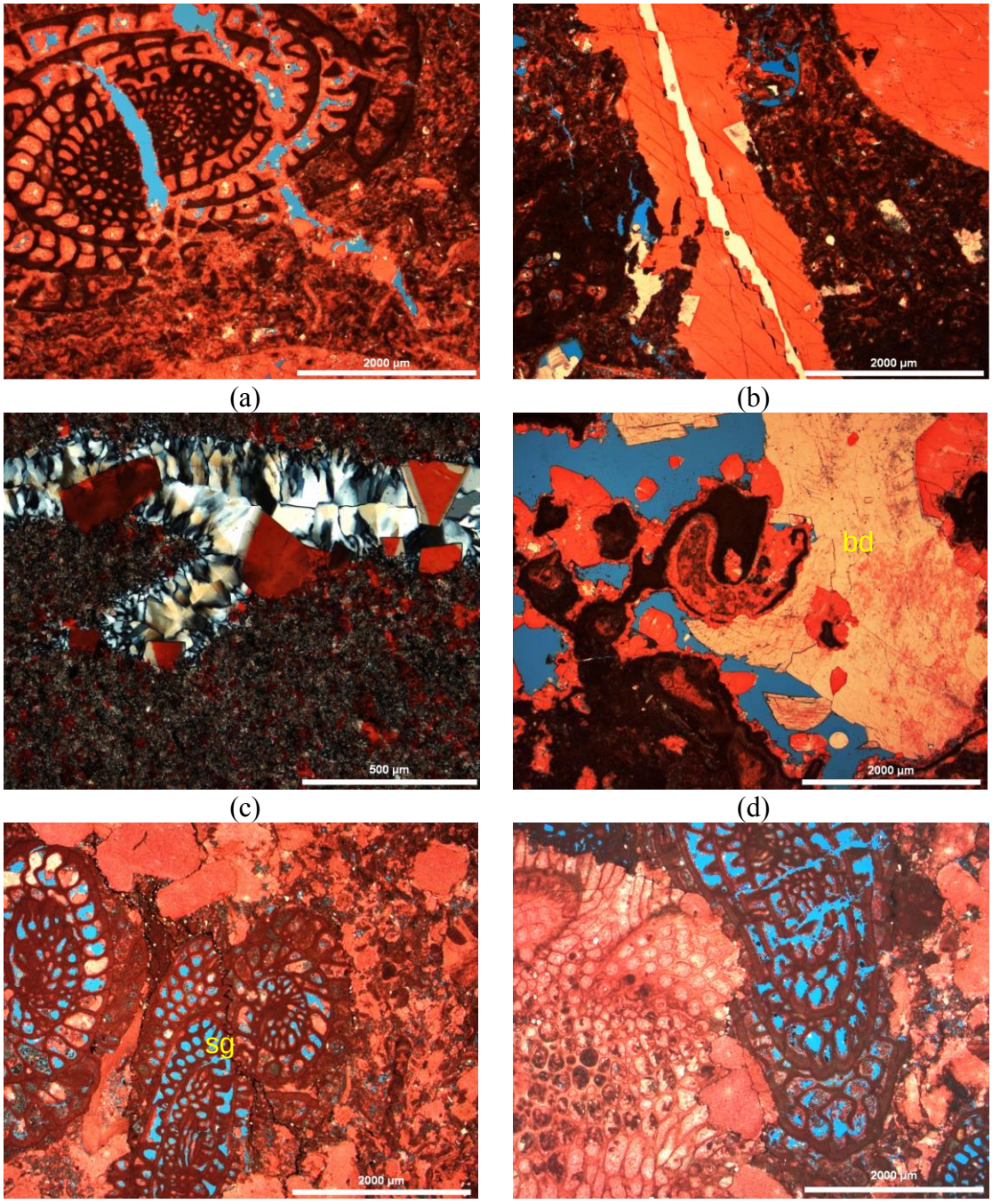

Figure 9: Photomicrographs showing diagenesis of Upper Leonardian detrital succession. (a) Fusulinid wackestone showing dissolution and subsequent development of blocky calcite cement. (b) Fusulinid wackestone showing solution enhanced interparticle pores and late poikilotopic blocky calcite and dolomite cements filling fracture and interparticle pores. (c) Silica replacement in skeletal grain. (d) Clast-supported polymict conglomerate with late blocky calcite and baroque dolomite (bd) filling dissolution vug. (e) Extensive chemical compaction in mud-lean fusulinid-crinoid packstone resulting in sutured grains (sg). (f) Extensive mechanical and chemical compaction in mud-lean fusulinid-crinoid packstone.

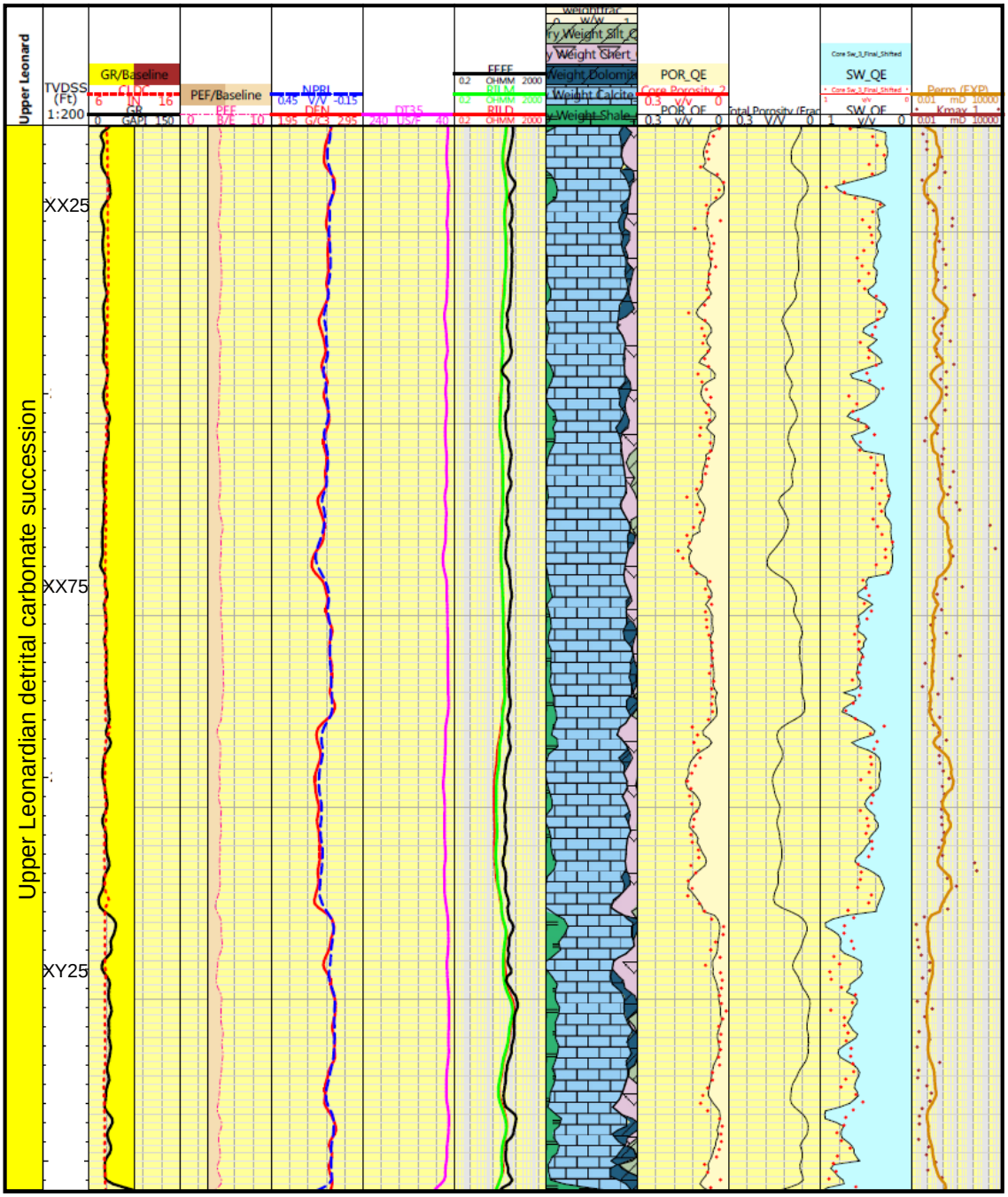

Figure 10: Example of multimineral analysis results from Well 7 showing good match between core measurements and estimated values.

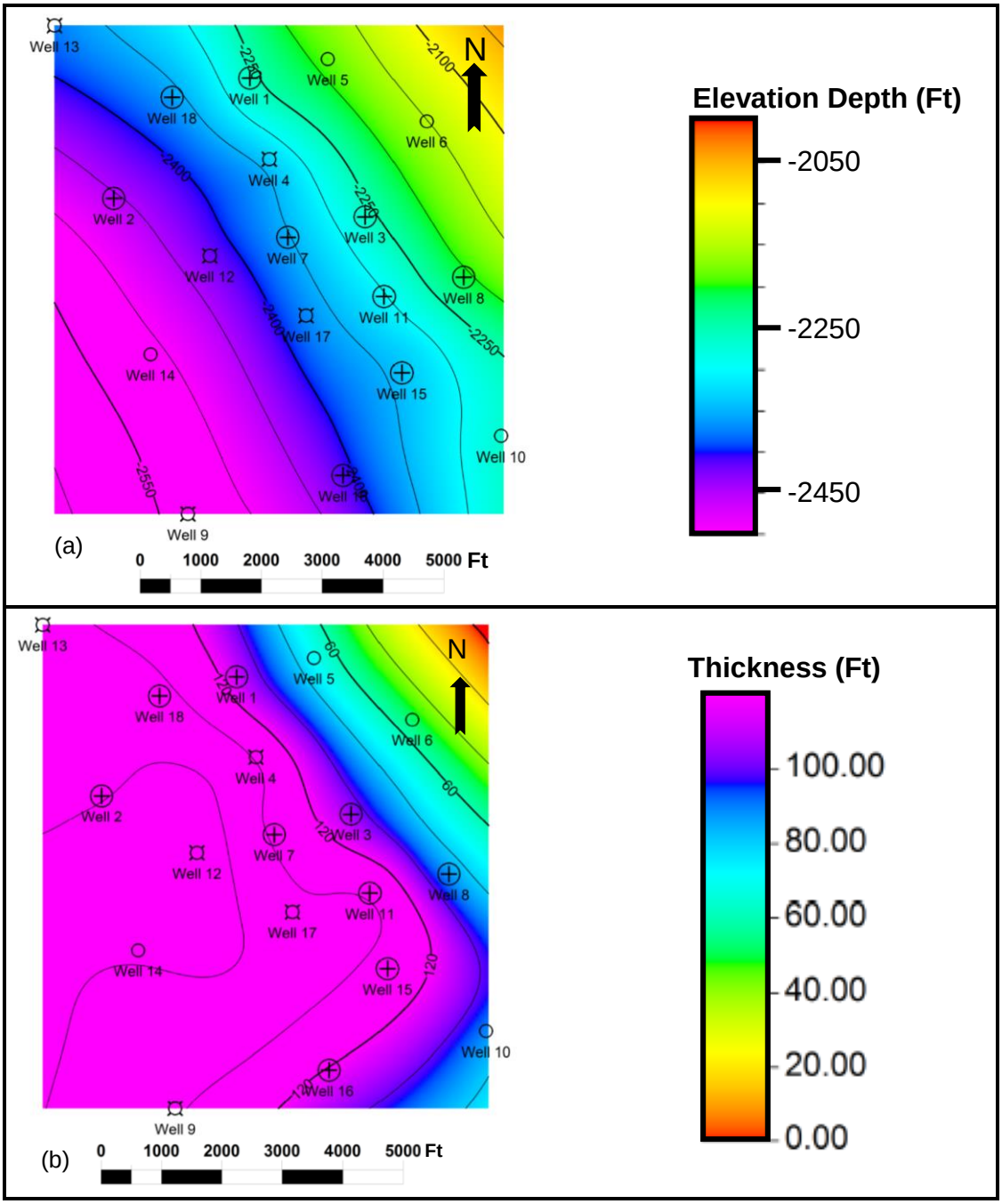

Figure 11: Upper Leonardian detrital carbonate succession maps. (a) Subsurface map for the base of the succession showing a subtle slope of about 3^0. (b) Isochore map showing a basin-ward thickening of the interval.

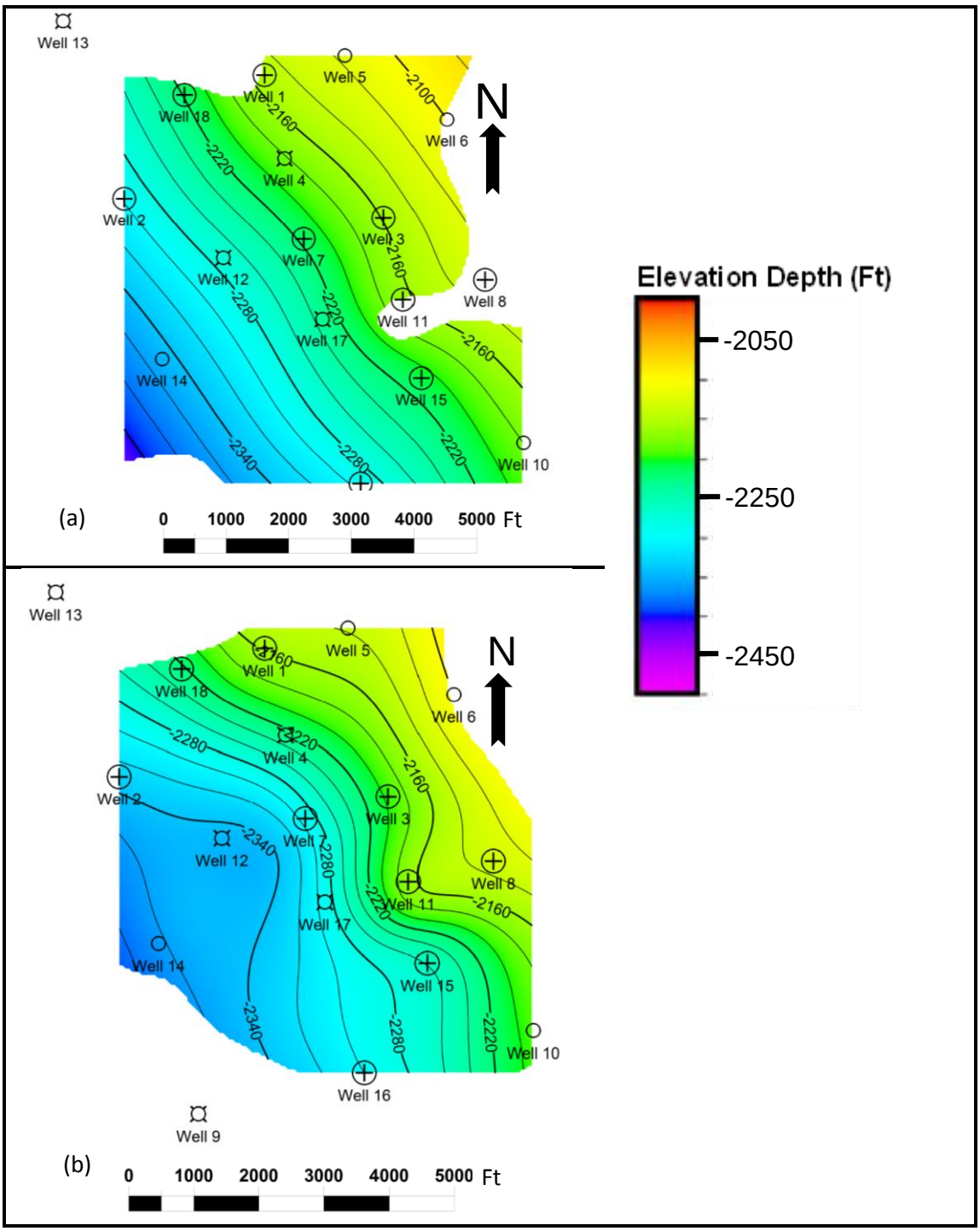

Figure 12: Subsurface maps. (a) Base of mud-lean fusulinid-crinoid packstone with a subtle slope varying from 2 to 3^0. The unit is absent in Well 11. (b) Base of clast-supported polymict conglomerate showing relatively steeper slope varying from 1 to 5^0. Well 11 has thick accumulation of carbonate mudstone and is interpreted to be on the interchannel high.

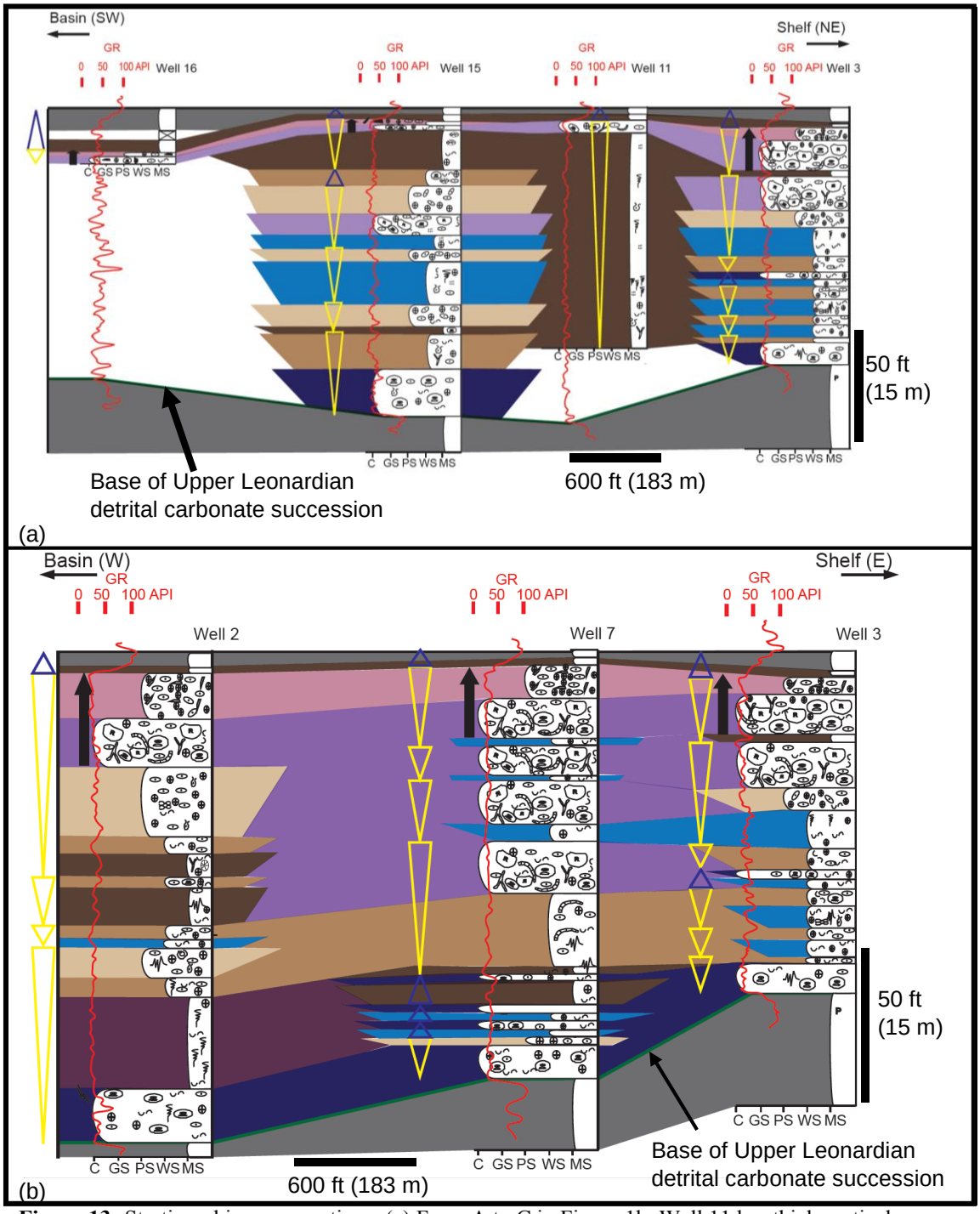

Figure 13: Stratigraphic cross-sections. (a) From A to C in Figure 1b. Well 11 has thick vertical accumulation of carbonate mudstone indicating this was probably an unchannelized portion of the slope. (b) From A to B in Figure 1b.

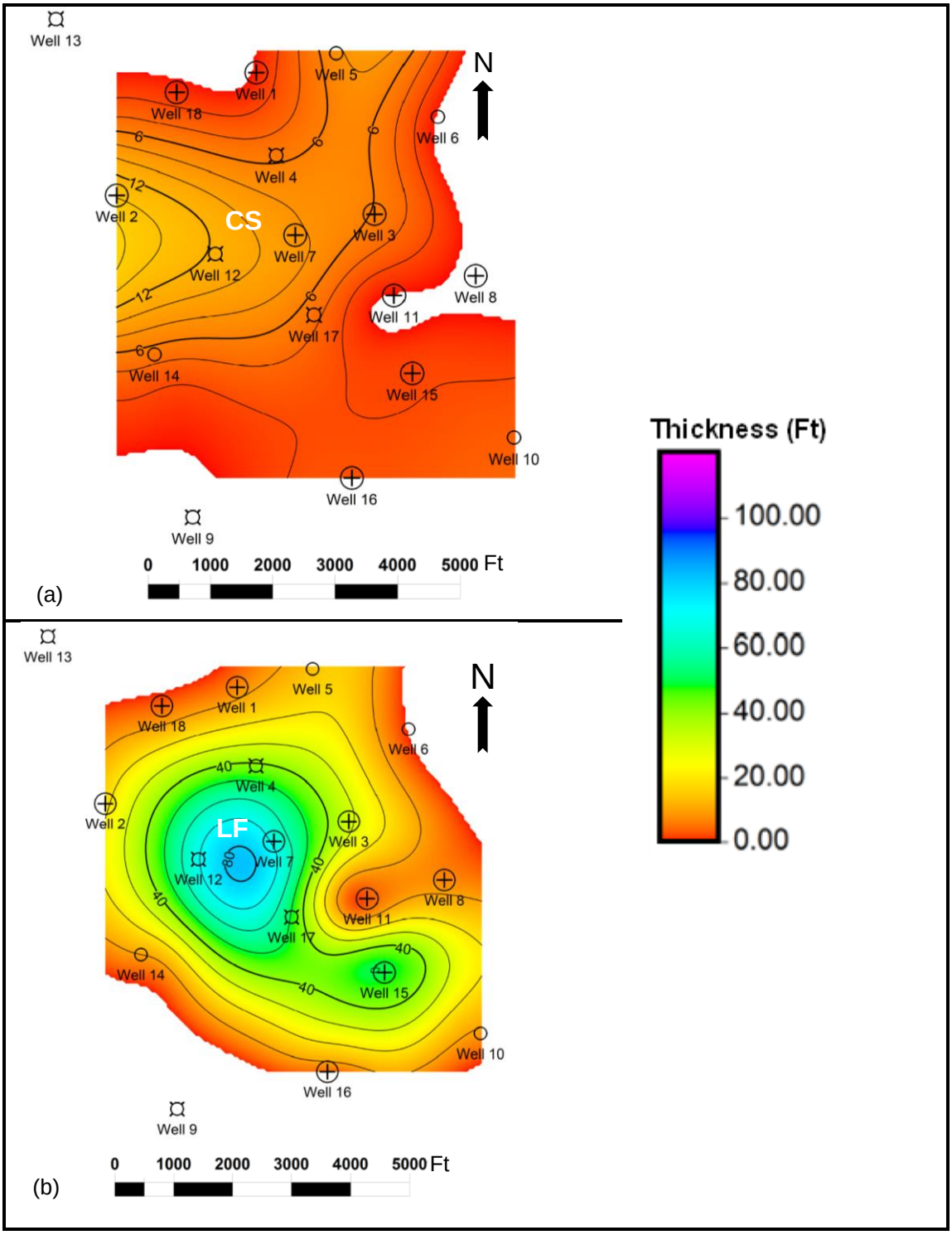

Figure 14: Isochore thickness maps. (a) Mud-lean fusulinid-crinoid packstone showing a possible channelized slope (CS) geometry. The unit is absent in Wells 11 and 8, and thins out in Wells 15, 16, 1 and 18. (b) Clast-supported polymict conglomerate showing lobate fan (LF) depositional geometry. The unit thins out in Wells 11 and 8.

Diagenetic phases observed from thin-section			
Event	**Early**	**Intermediate**	**Late**
Deposition (Intraparticle and interparticle pores)			
Fringing blocky calcite cement in intraparticle pores			
Syntaxial overgrowth of crinoids			
First phase dissolution of grains and matrix			
Pore-filling blocky calcite			
Pore-filling euhedral dolomite rhombs			
Mechanical compaction (crushed skeletal grains)			
Chemical compaction (stylolites and sutured grains)			
Second phase dissolution			
Selective silicification of grains and matrix			
Fracturing			
Pore-filling poikilotopic blocky calcite			
Pore-filling baroque dolomite (saddle dolomite)			

Figure 15: Paragenesis in the Upper Leonardian detrital carbonate succession as observed from thin-section petrography.

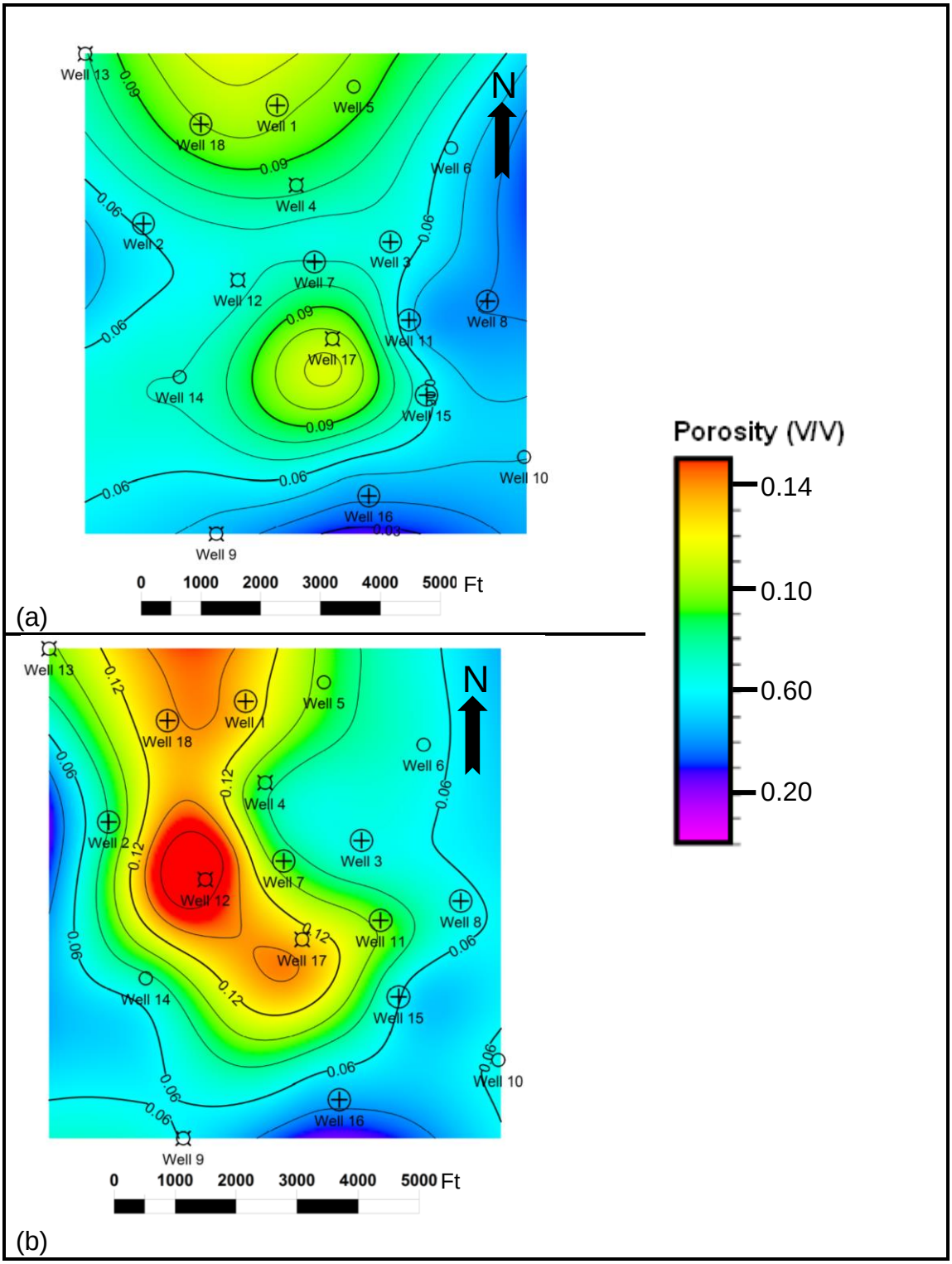

Figure 16: Average porosity maps. (a) Upper Leonardian detrital carbonate interconnected porosity. (b) Upper Leonardian detrital carbonate total porosity

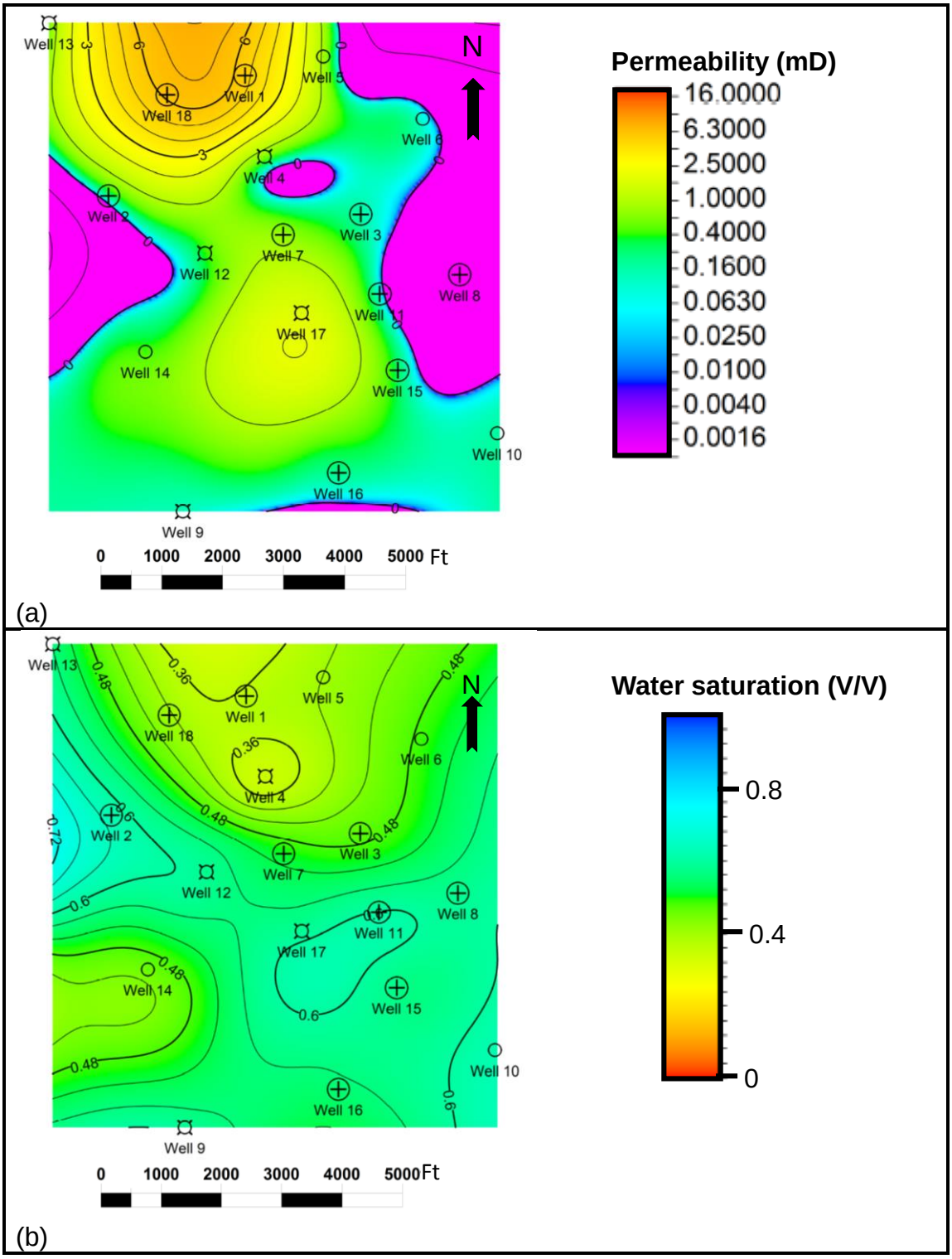

Figure 17: Permeability and water saturation maps. (a) Upper Leonardian detrital carbonate average permeability map. (b) Upper Leonardian detrital carbonate average initial water saturation map.

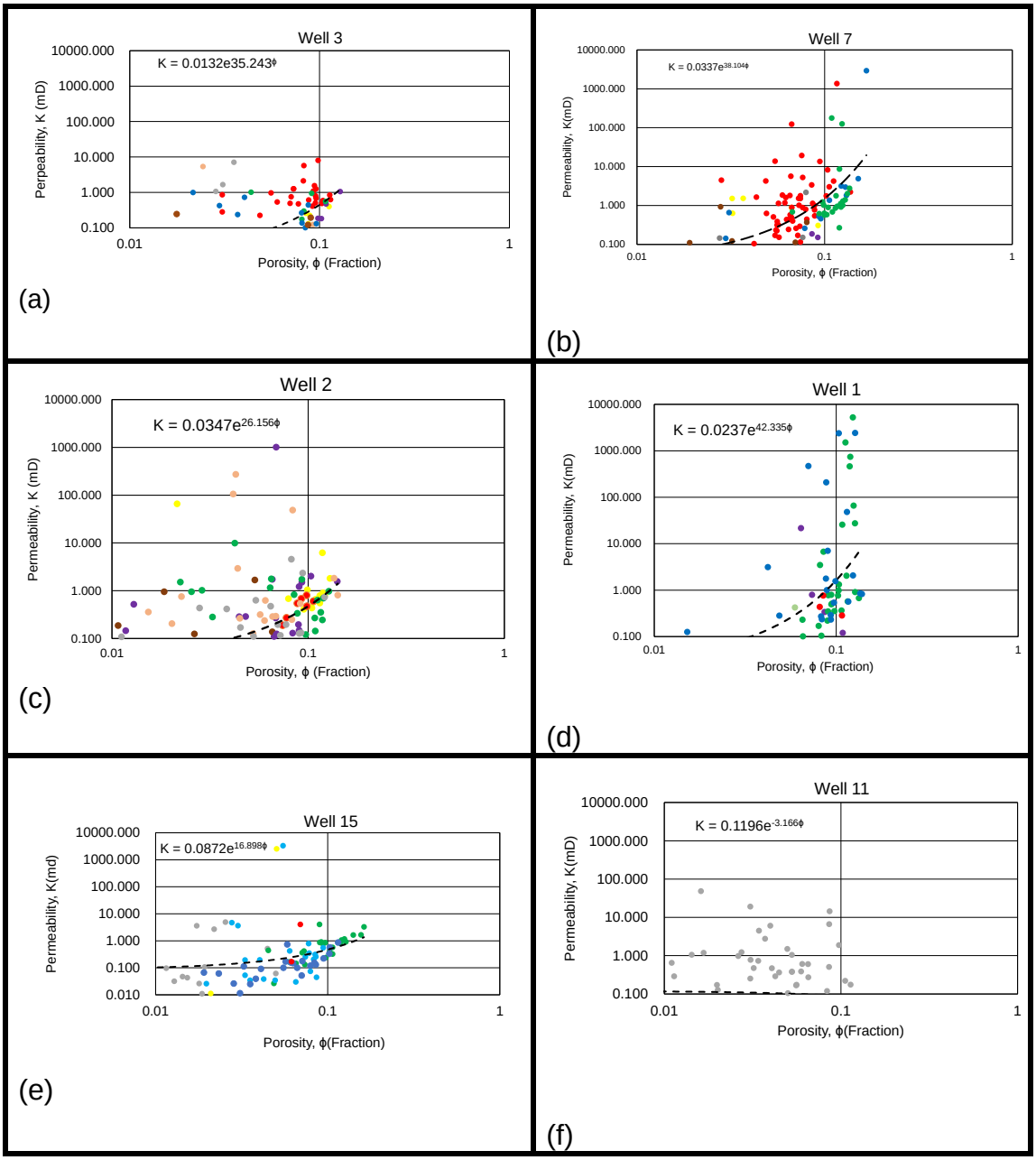

Figure 18: Cross-plots to illustrate the porosity-permeability relationships. (a) Well 3; (b) Well 7; (c) Well 2; (d) Well 1. (e) Well 15; (f) Well 11. The porosity-permeability plots do not show significant trends.

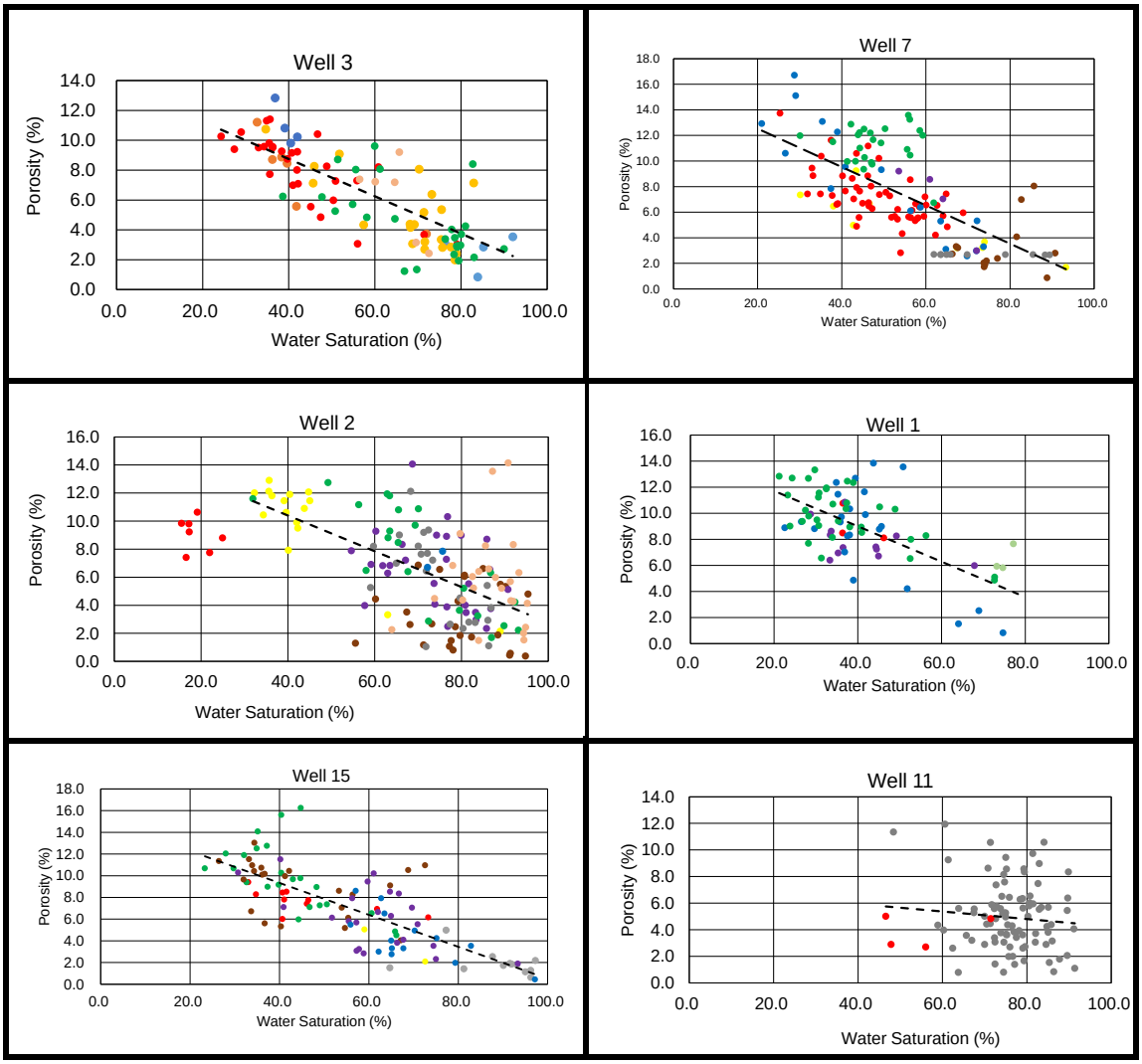

Figure 19: Cross-plot to illustrate porosity – water saturation relationships. (a) Well 3; (b) Well 7; (c) Well 2; (d) Well 1. (e) Well 15. (f) Well 11. Plots 3 to 15 show decrease in water saturation with increase in porosity. Well 11 has thick vertical accumulation of carbonate mudstone with low porosity and high water saturation.

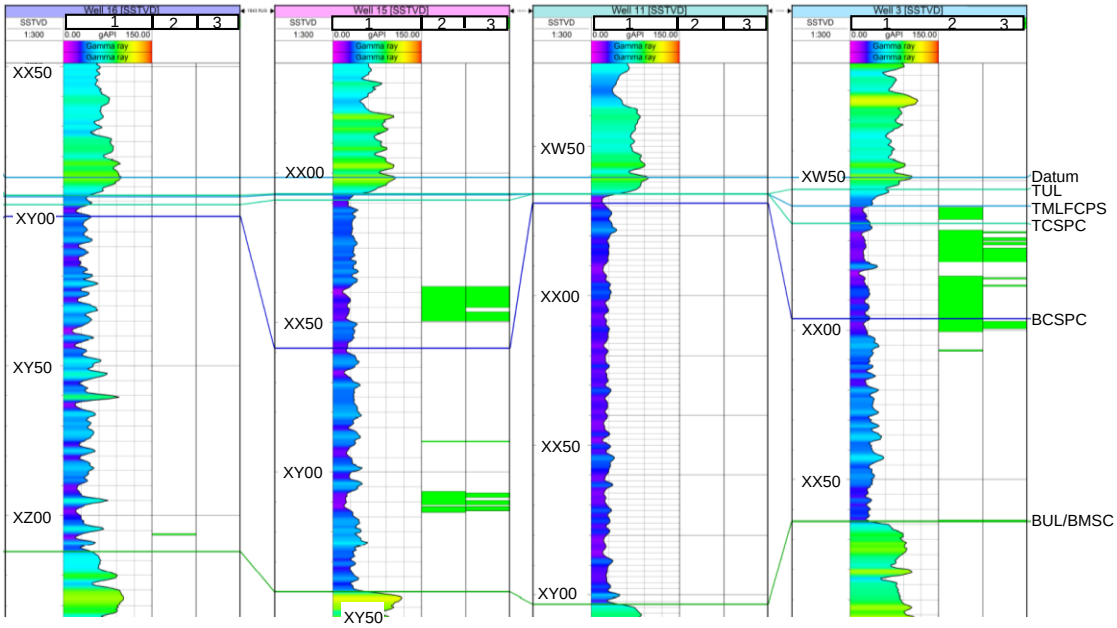

Figure 20a: Cross-section from well 3 to well 16 (Figure 1b A-C) showing net pay isochore thickness in the Upper Leonardian detrital carbonate succession in Veterans and St. Lawrence Fields, Glasscock County. Track 1 = GR log; Track 2 = Net pay thickness based on interconnected porosity ≥ 7%, C_{Sh} < 20%, So ≥ 60%, and permeability ≥ 0.1 mD; Track 3 is based on interconnected porosity ≥ 7%, C_{Sh} < 20%, So ≥ 60%, permeability ≥ 0.1 mD, and moveable oil ($S_{xo} - S_w$); TUL = Top of Upper Leonardian detrital carbonate succession; TMLFCPS = Top of mud-lean fusulinid-crinoid packstone; TCSPC = Top of clast-supported polymict conglomerate; BCSPC = Base of clast-supported polymict conglomerate; BUL = Base of Upper Leonardian detrital carbonate succession. Well 11 which is interpreted to be on an interchannel high does not have pay.

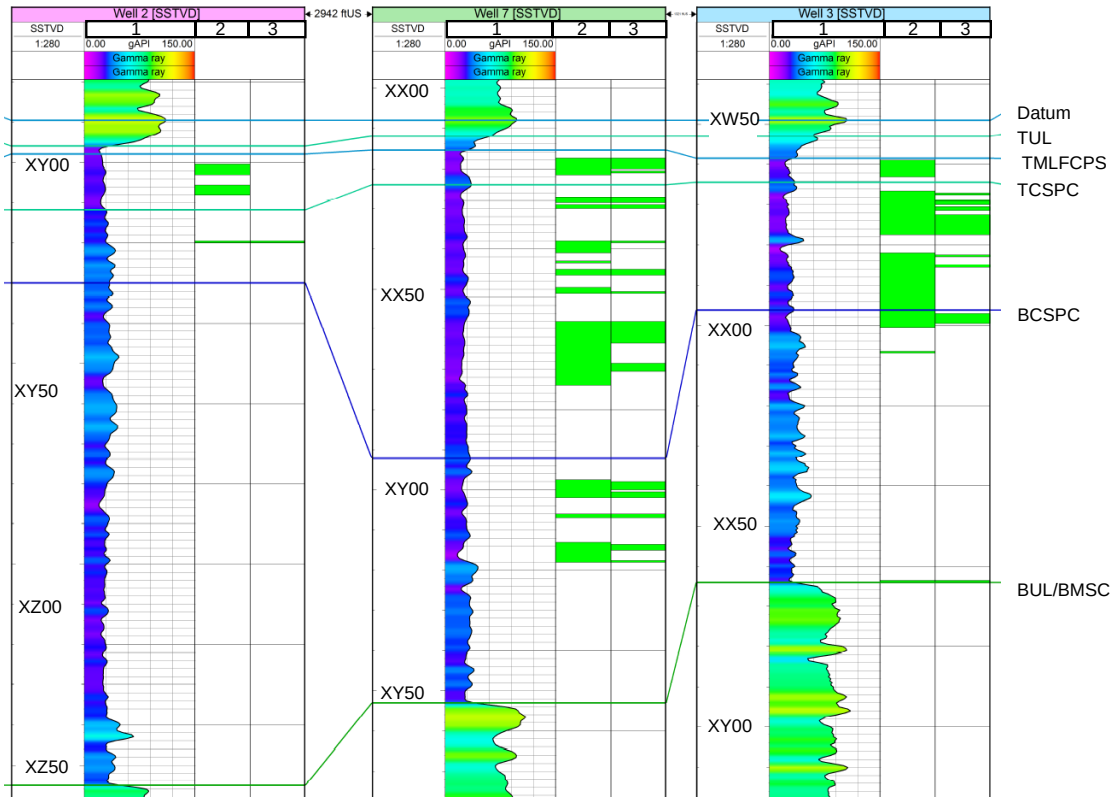

Figure 20 b: Cross-section from well 3 to well 2 (Figure 1b A-B) showing net pay isochore thickness in the Upper Leonardian detrital carbonate succession in Veterans and St. Lawrence Fields, Glasscock County. Track 1 = GR log; Track 2 = Net pay thickness based on interconnected porosity ≥ 7%, C_{Sh} < 20%, So ≥ 60%, and permeability ≥ 0.1 mD; Track 3 is based on interconnected porosity ≥ 7%, C_{Sh} < 20%, So ≥ 60%, permeability ≥ 0.1 mD, and moveable oil ($S_{xo} - S_w$); TUL = Top of Upper Leonardian detrital carbonate succession; TMLFCPS = Top of mud-lean fusulinid-crinoid packstone; TCSPC = Top of clast-supported polymict conglomerate; BCSPC = Base of clast-supported polymict conglomerate; BUL = Base of Upper Leonardian detrital carbonate succession.

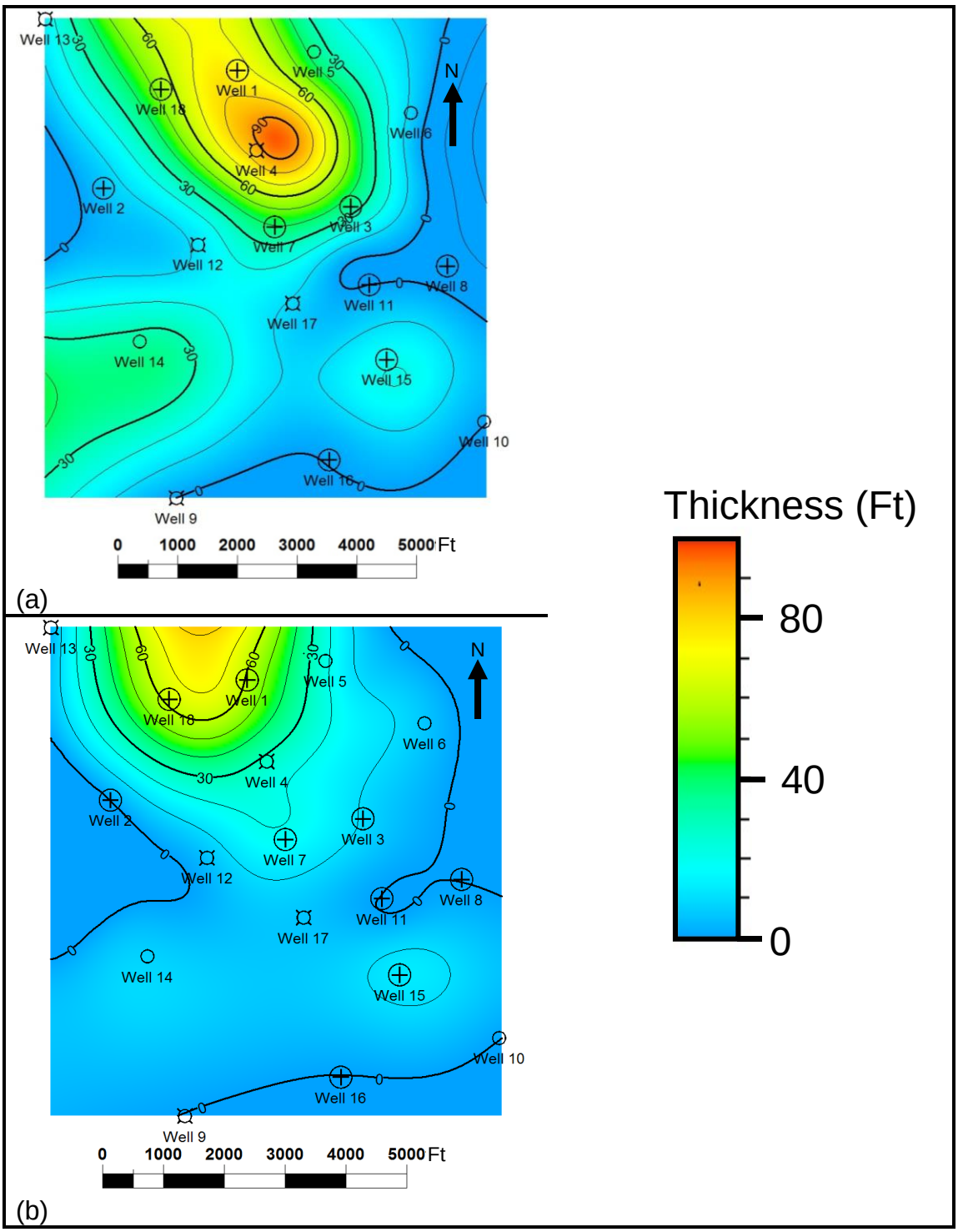

Figure 21: Upper Leonardian detrital carbonate succession net pay isochore thickness maps. (a) based on interconnected porosity ≥ 7%, C_{Sh} < 20%, So ≥ 60%, and permeability ≥ 0.1 m. Based on these cut-offs Wells 11, 8, 16, 9 and 10 do not have pay. (b) based on interconnected porosity ≥ 7%, Csh < 20%, So ≥ 60%, permeability ≥ 0.1 mD, and moveable oil ($S_{xo} - S_w$). Based on the moveable oil saturation, there is a decrease in net pay thickness of almost 60 ft. (18.29 m) in Well 4.

APPENDIX 2

TABLES

Table 1: Summary of porosity types within the facies

Facies	Pore Type
Mud-lean fusulinid-crinoid packstone	Mostly intraparticle pores with less amounts of interparticle pores (pore sizes < 1000 μm)
Clast-supported polymict conglomerate	Solution-enhanced Interparticle and intraparticle pores (pore size up to 4000 μm)
Fusulinid-crinoid packstone	Mostly intraparticle pores with less amounts of interparticle pores (pore sizes < 1000 μm)
Fusulinid wackestone	Intraparticle and solution-enhanced interparticle pores (pore sizes up to 4000 μm)
Skeletal wackestone	Solution-enhanced interparticle pores (Pore sizes < 250 μm)
Partially silicified skeletal wackestone to mudstone	Solution-enhanced interparticle pores with less amounts of intraparticle pores (pore sizes < 1000 μm)
Mudstone	No visible porosity
Matrix-supported conglomerate	No significant porosity
Shale	No visible porosity

APPENDIX 3

CORE DESCRIPTIONS

Well 3

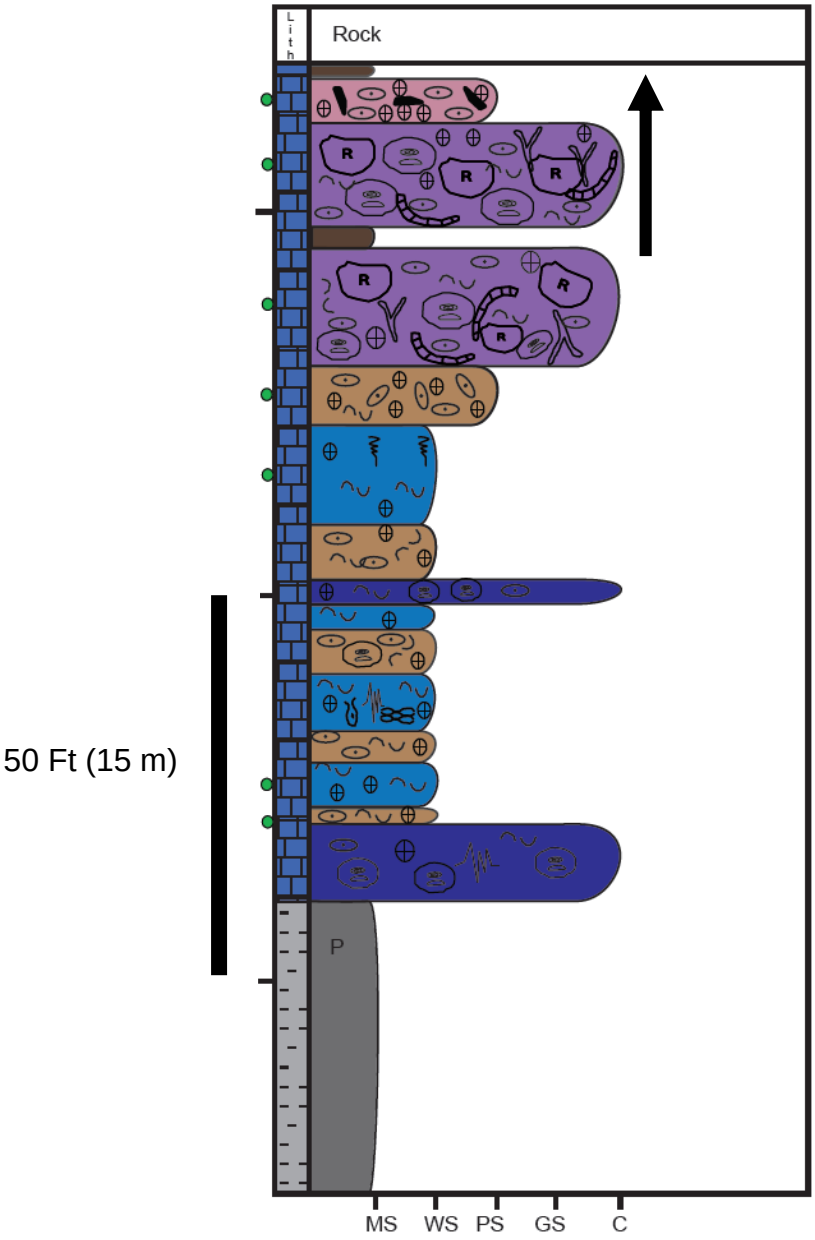

Well 7

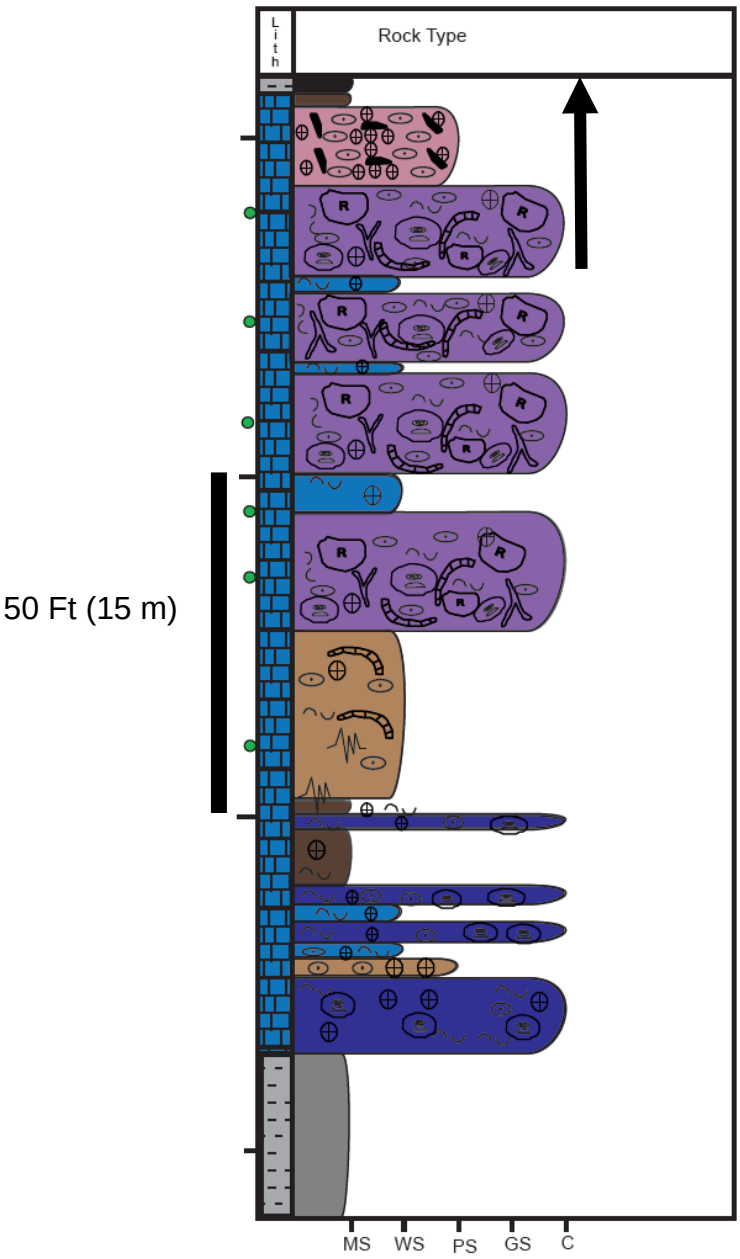

Well 1

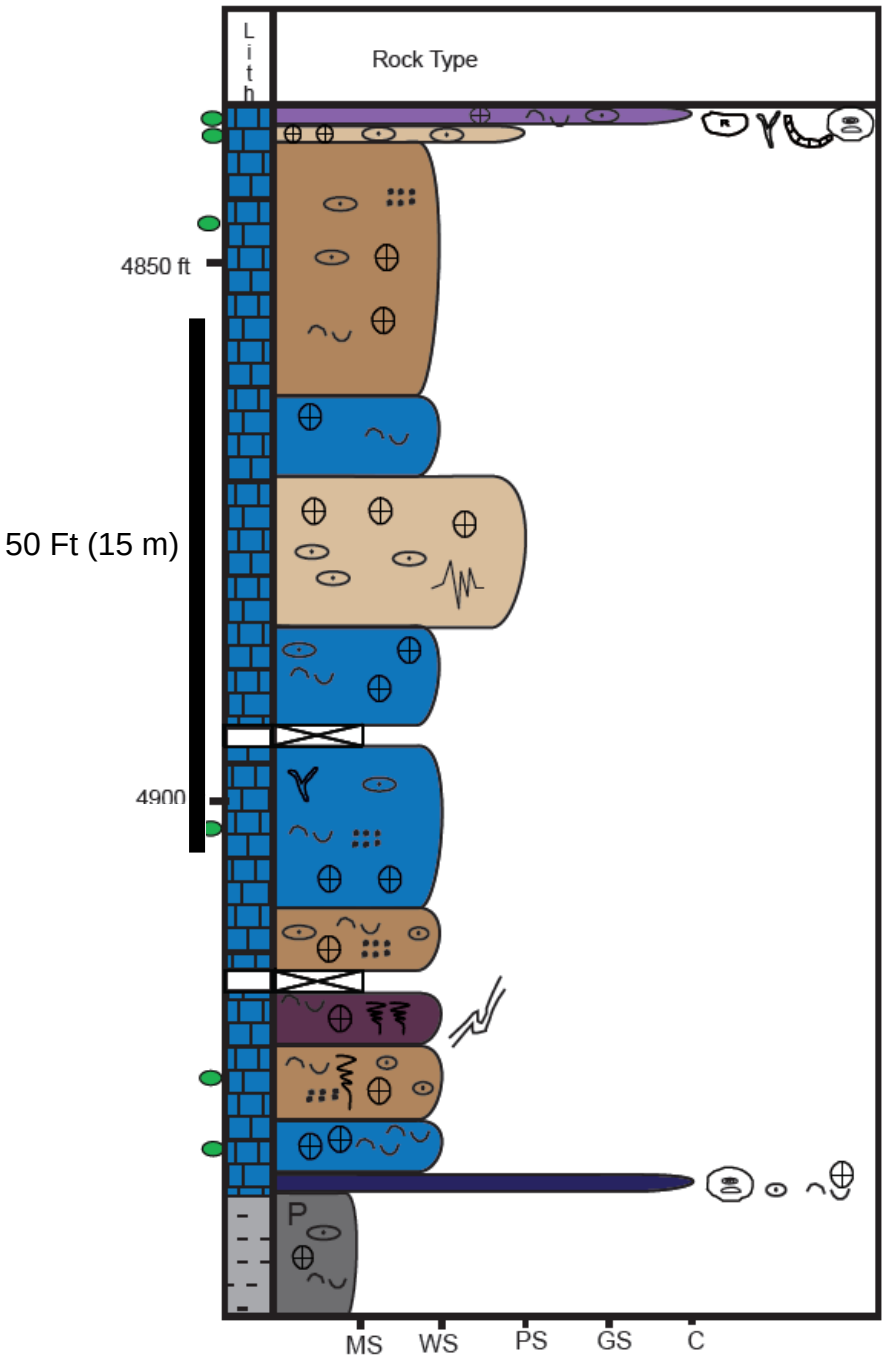

Well 2

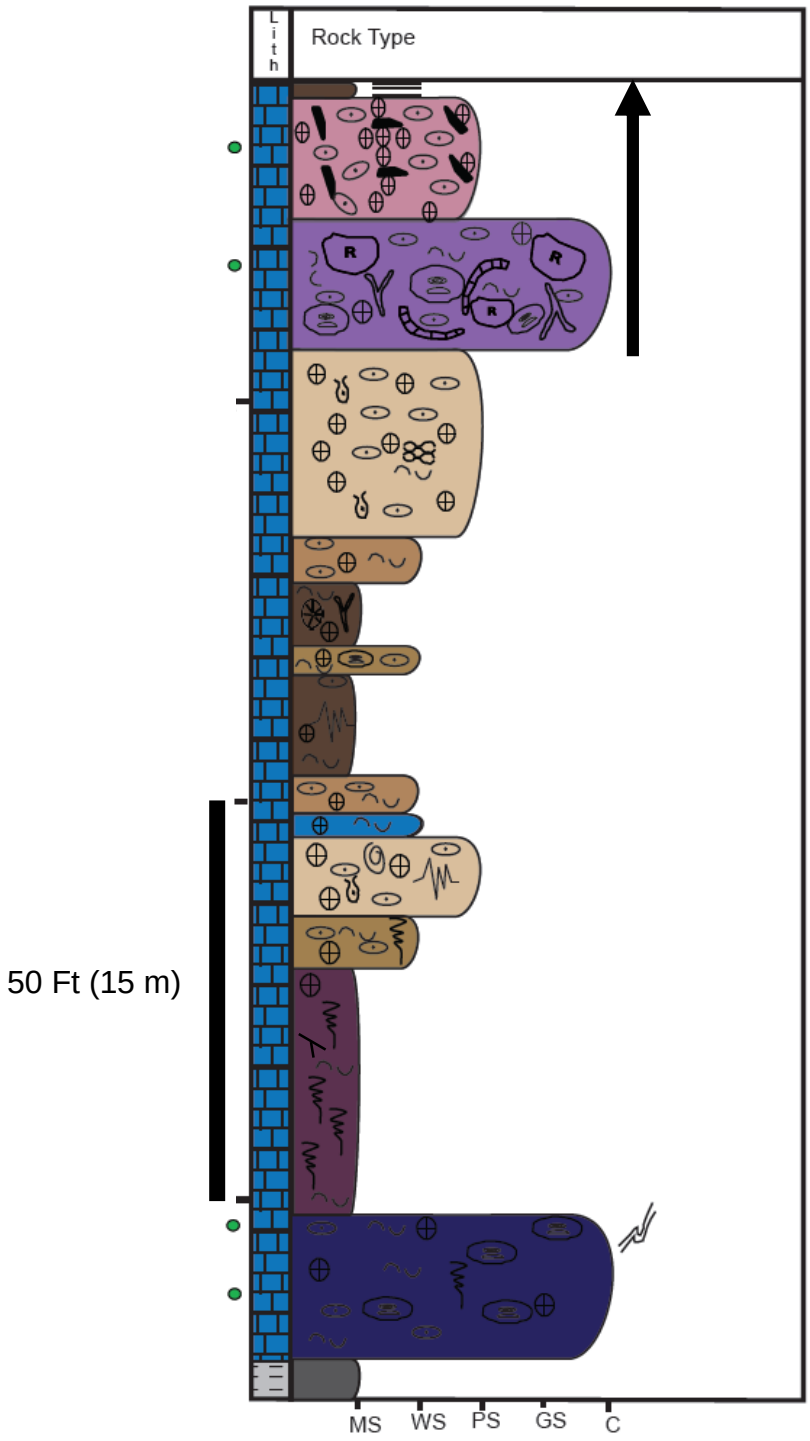
Lith
Rock Type
R
R
R
50 Ft (15 m)
MS
WS
PS
GS
C

Well 15

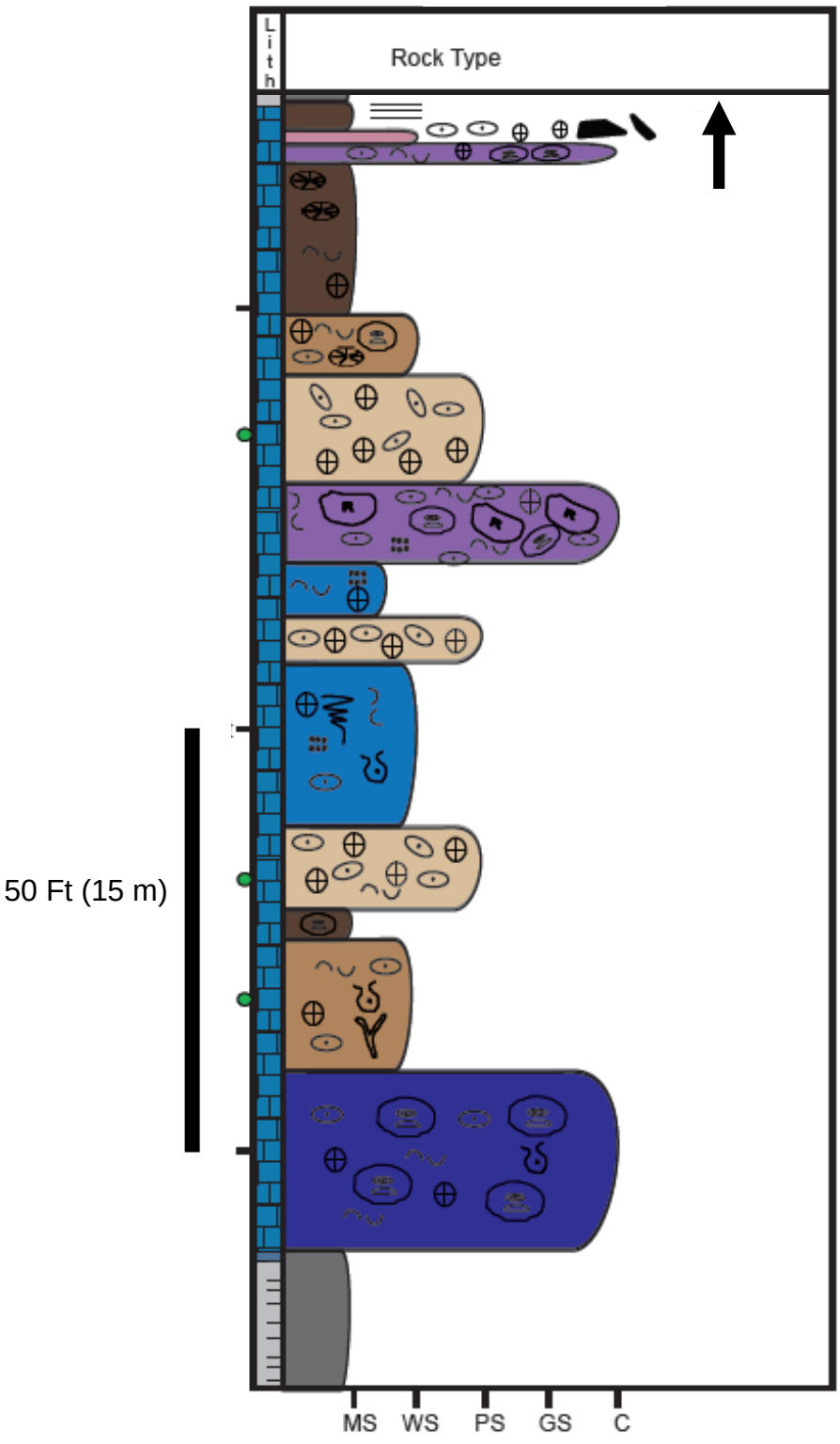

Well 11

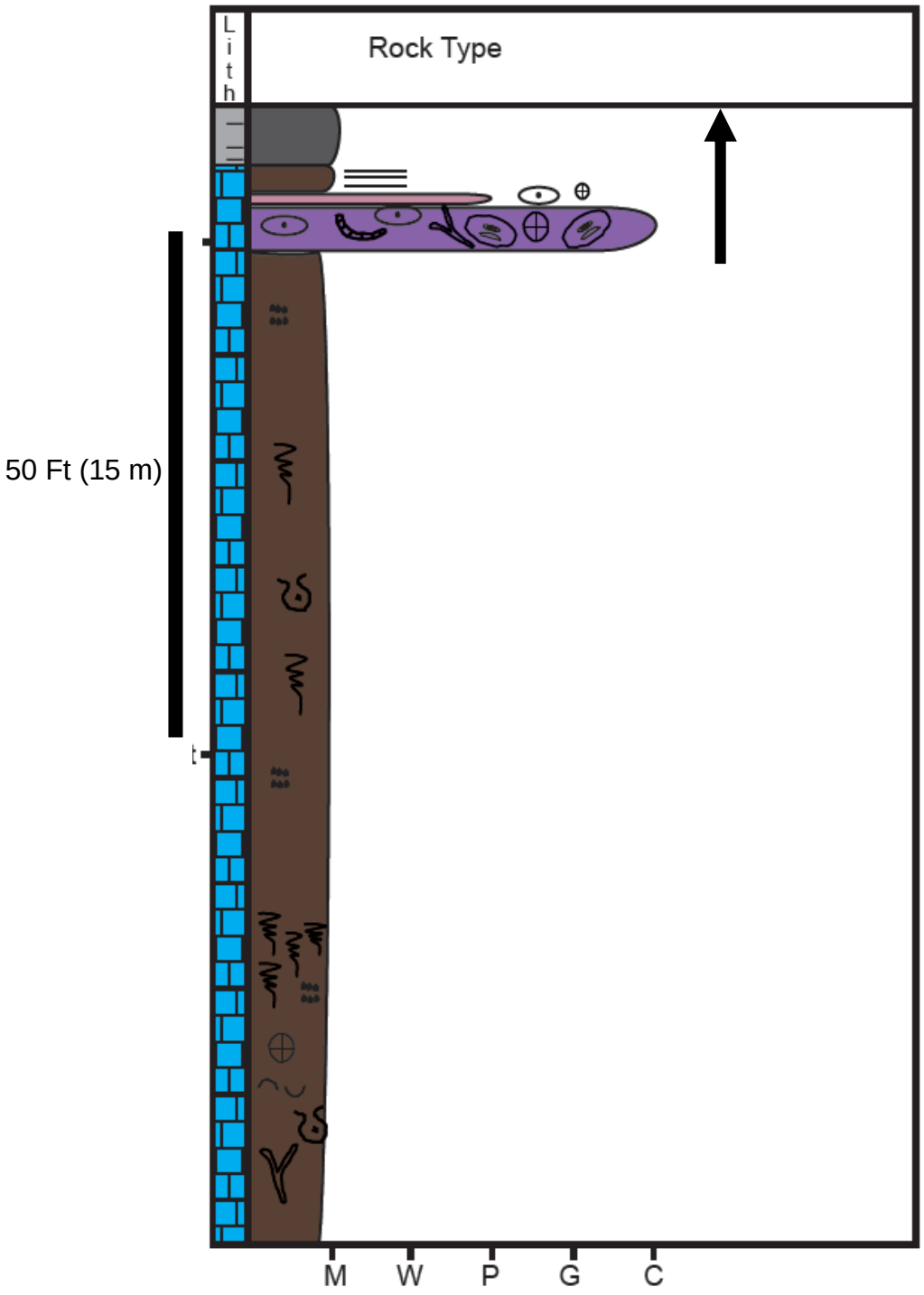

Well 8

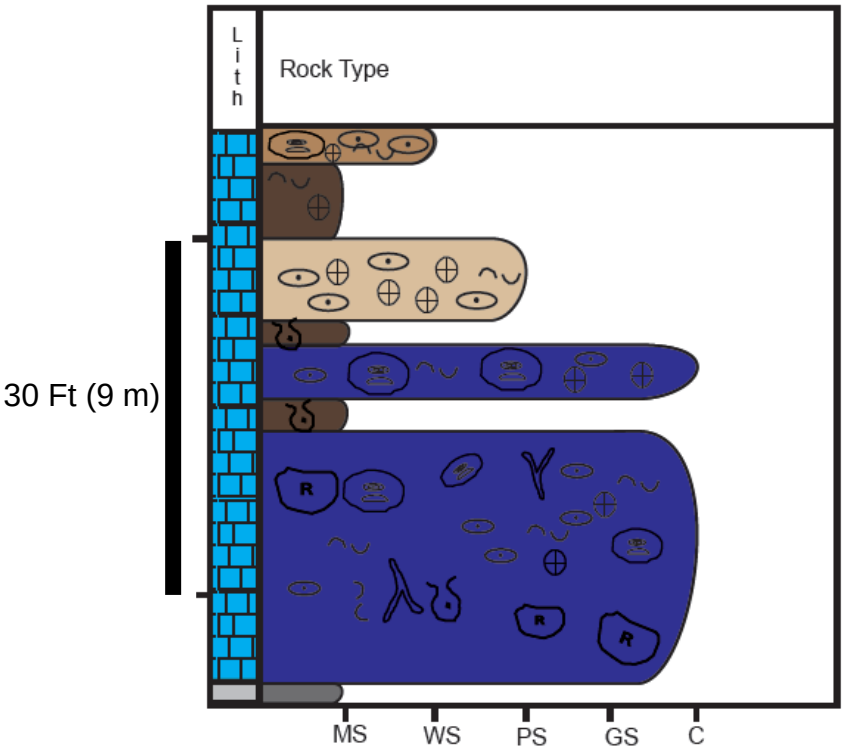

Well 16

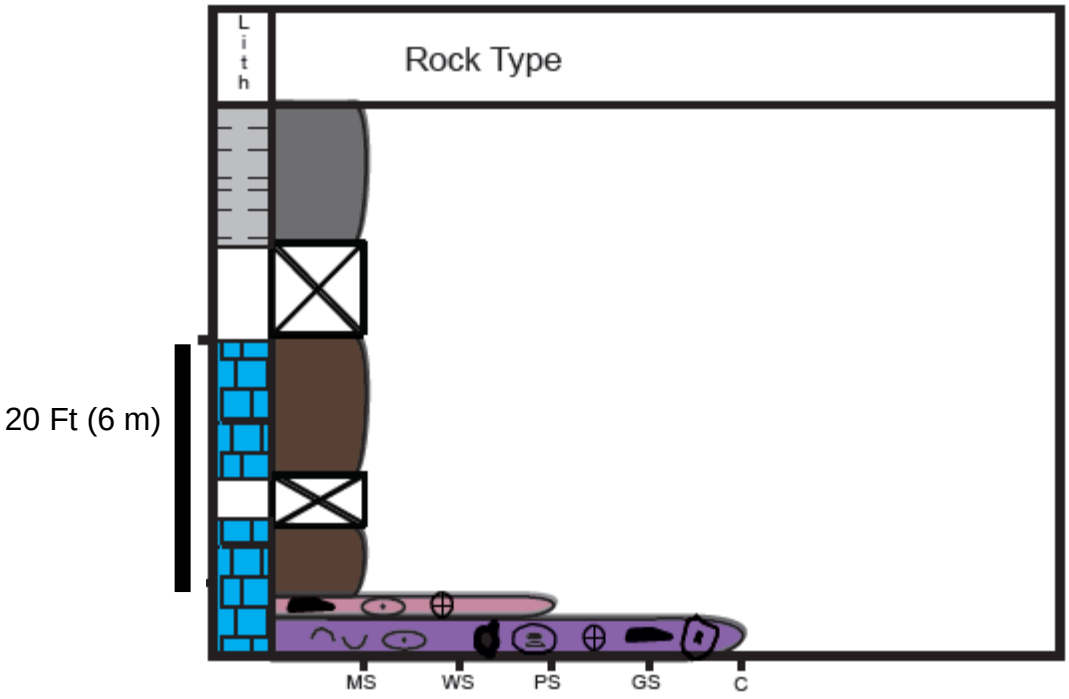

APPENDIX 4

MULTIMINERAL ANALYSIS RESULTS

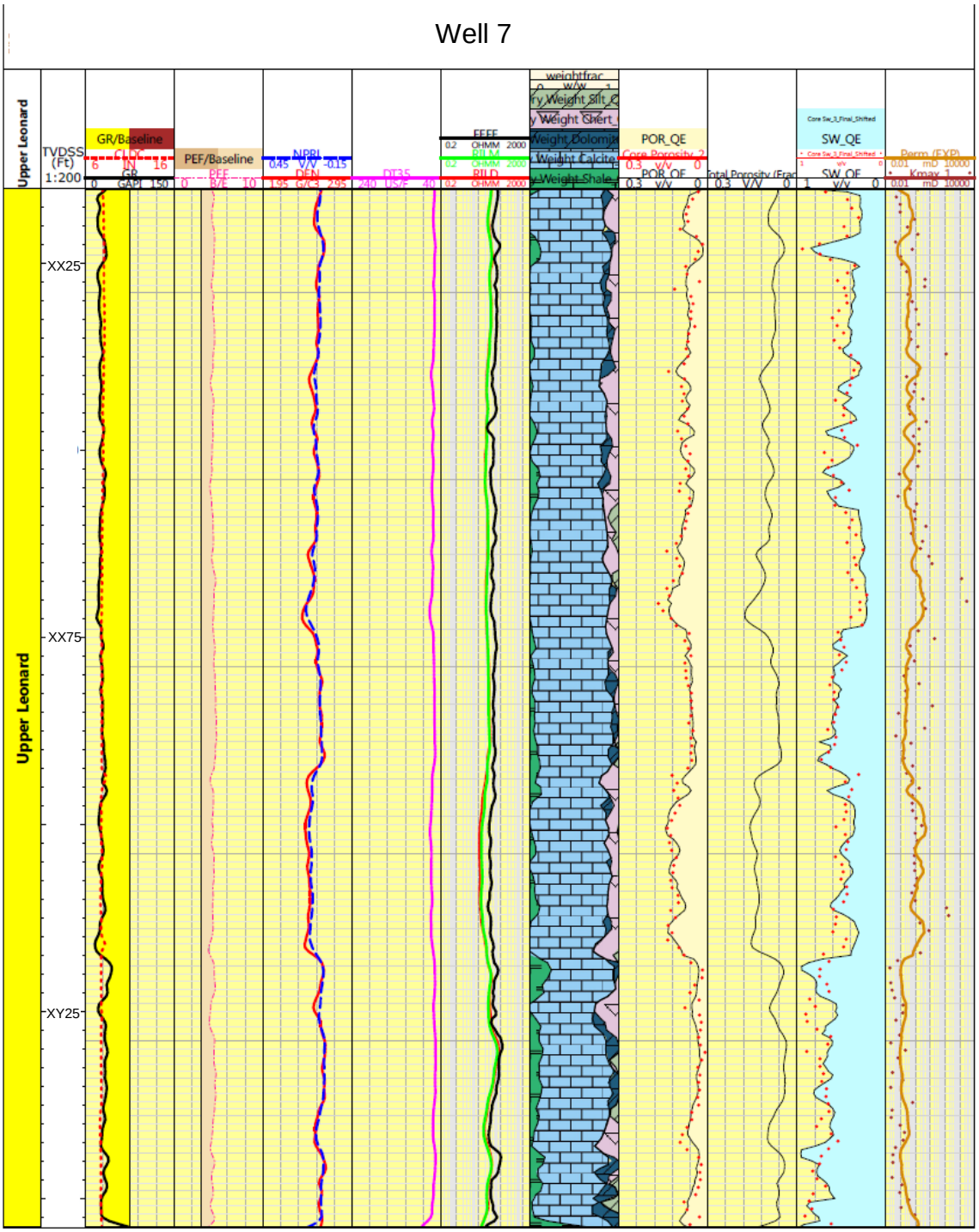

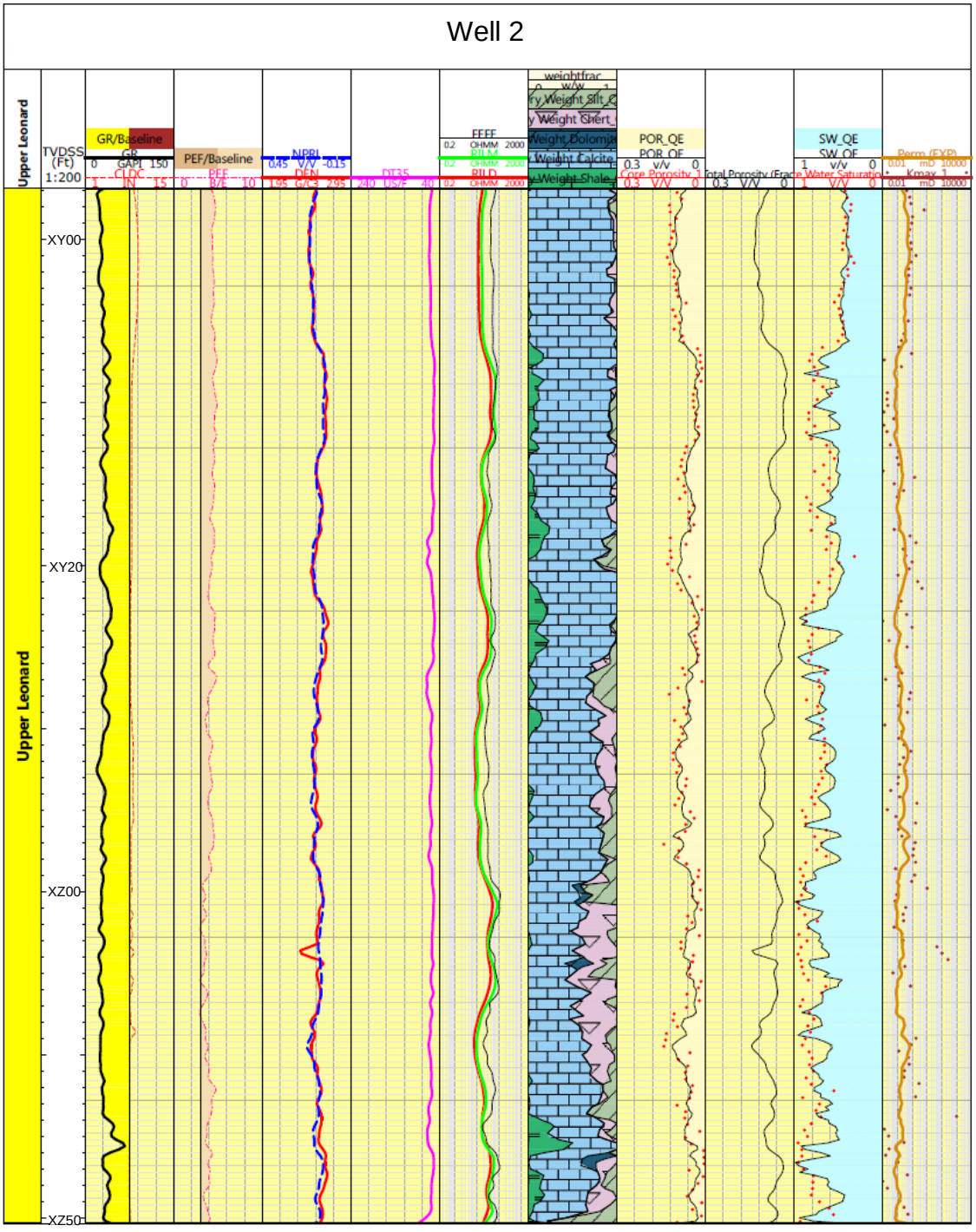
Well 2
Upper Leonard
TVDSS (Ft) 1:200
GR/Baseline
GR
GAPI
CLDC
IN
PEF/Baseline
PEF
B/E
NPRL
DEN
DT35
FEFE
RILM
RILD
OHMM
weightfrac
v/v
Weight Silt_Q
Weight Chert
Weight Dolomite
Weight Calcite
Weight Shale
POR_QE
POR_OE
Core Porosity_1
Total Porosity (Frac
SW_QE
SW_OE
Water Saturation
Perm (EXP)
mD
Kmax
XY00
XY20
XZ00
XZ50

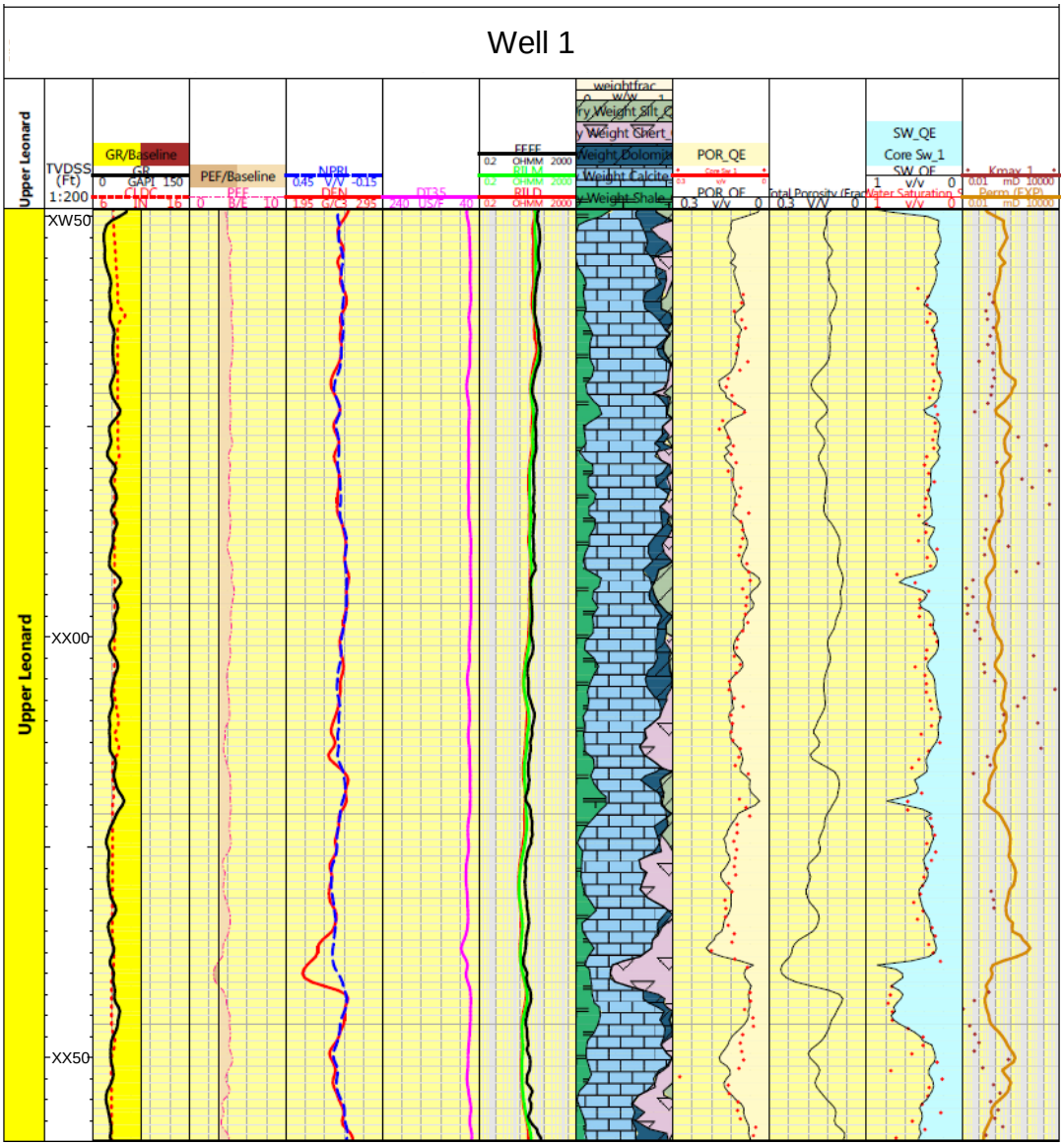
Well 1
Upper Leonard
TVDSS (Ft)
1:200
GR/Baseline
GR
GAPI
CLDC
PEF/Baseline
PEF
RHOB
NPRL
DEN
DT35
RILD
RILM
weightfrac
Weight_Dolomite
Weight_Calcite
Weight_Shale
POR_QE
POR_OE
Total Porosity (Frac
SW_QE
Core Sw_1
SW_OE
Water Saturation
Kmax_1
Perm (EXP)
XW50
XX00
XX50

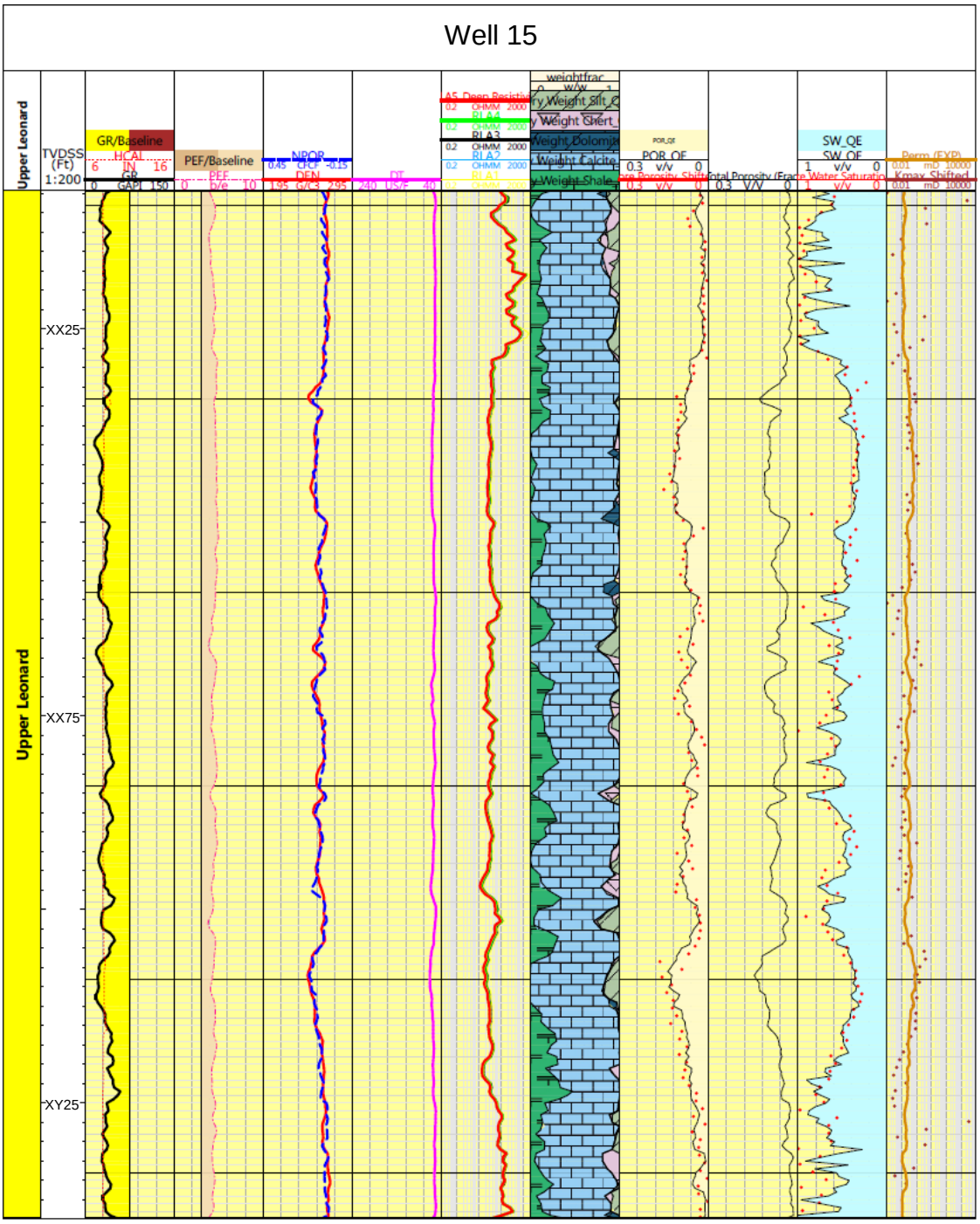
Well 15
Upper Leonard
TVDSS (Ft) 1:200
GR/Baseline
HCAL
CALI
GR
GAPI
PEF/Baseline
PEF
NPOR
DEN
DT
RLA5
RLA4
RLA3
RLA2
RLA1
weightfrac
Dry Weight Silt_C
Dry Weight Chert
Weight Dolomite
Weight Calcite
Weight Shale
POR_QE
POR_QF
Pore Porosity Shift
Total Porosity (Fract
SW_QE
SW_QF
Water Saturation
Perm (EXP)
Kmax_Shifted
XX25
XX75
XY25

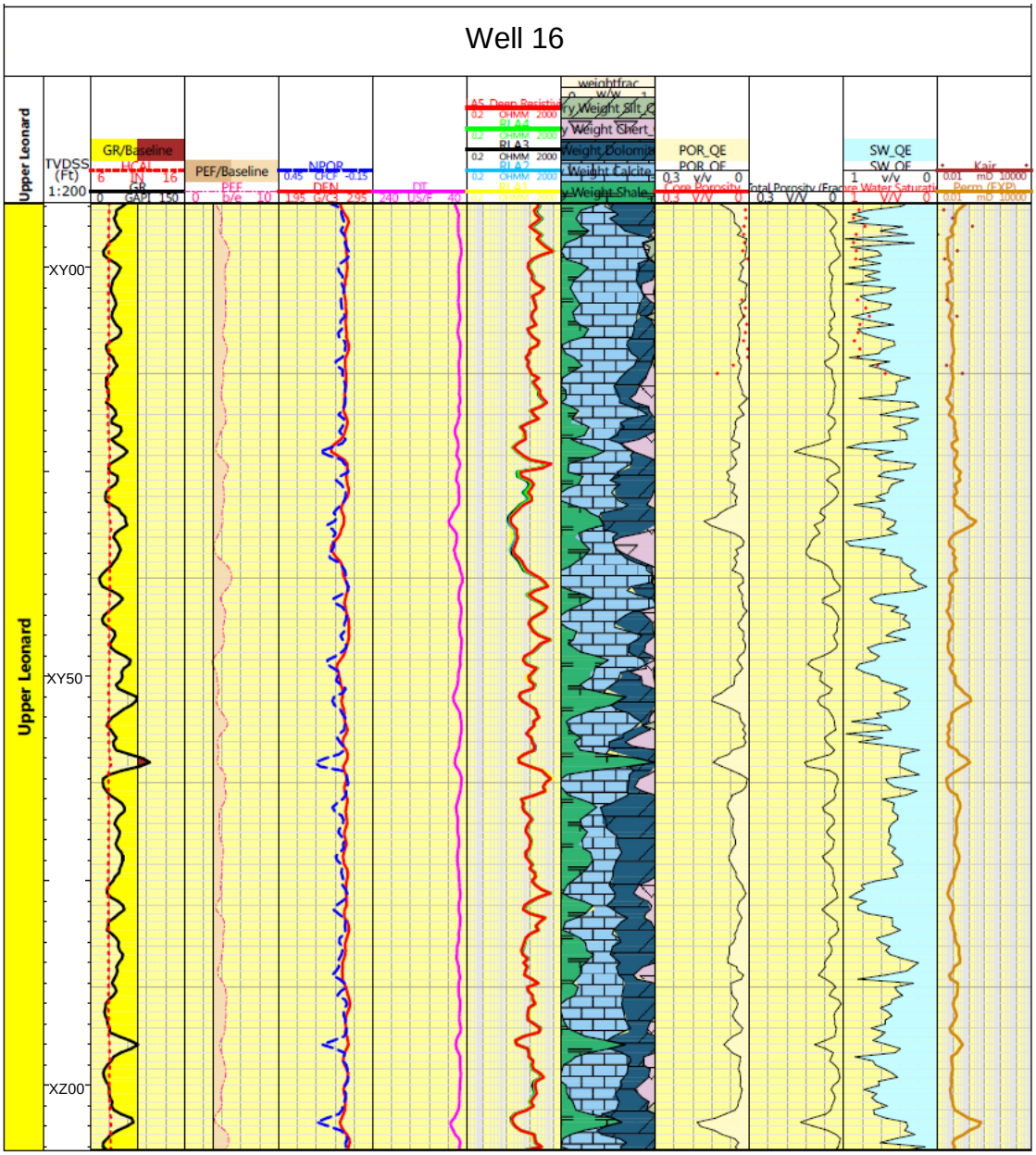
Well 16
Upper Leonard
TVDSS (Ft) 1:200
GR/Baseline
HC_01
IN
GR
GAPI
PEF/Baseline
PEF
b/e
NPOR
DEN
DT
A5_Deep_Resistivity
RI_A4
RI_A3
RI_A2
RI_A1
weightfrac
Weight_Silt_C
Weight_Chert
Weight_Dolomite
Weight_Calcite
Weight_Shale
POR_QE
POR_QF
Core Porosity
Total Porosity (Fracture
SW_QE
SW_QF
Water Saturati
Kair
Perm (EXP)
XY00
XY50
XZ00

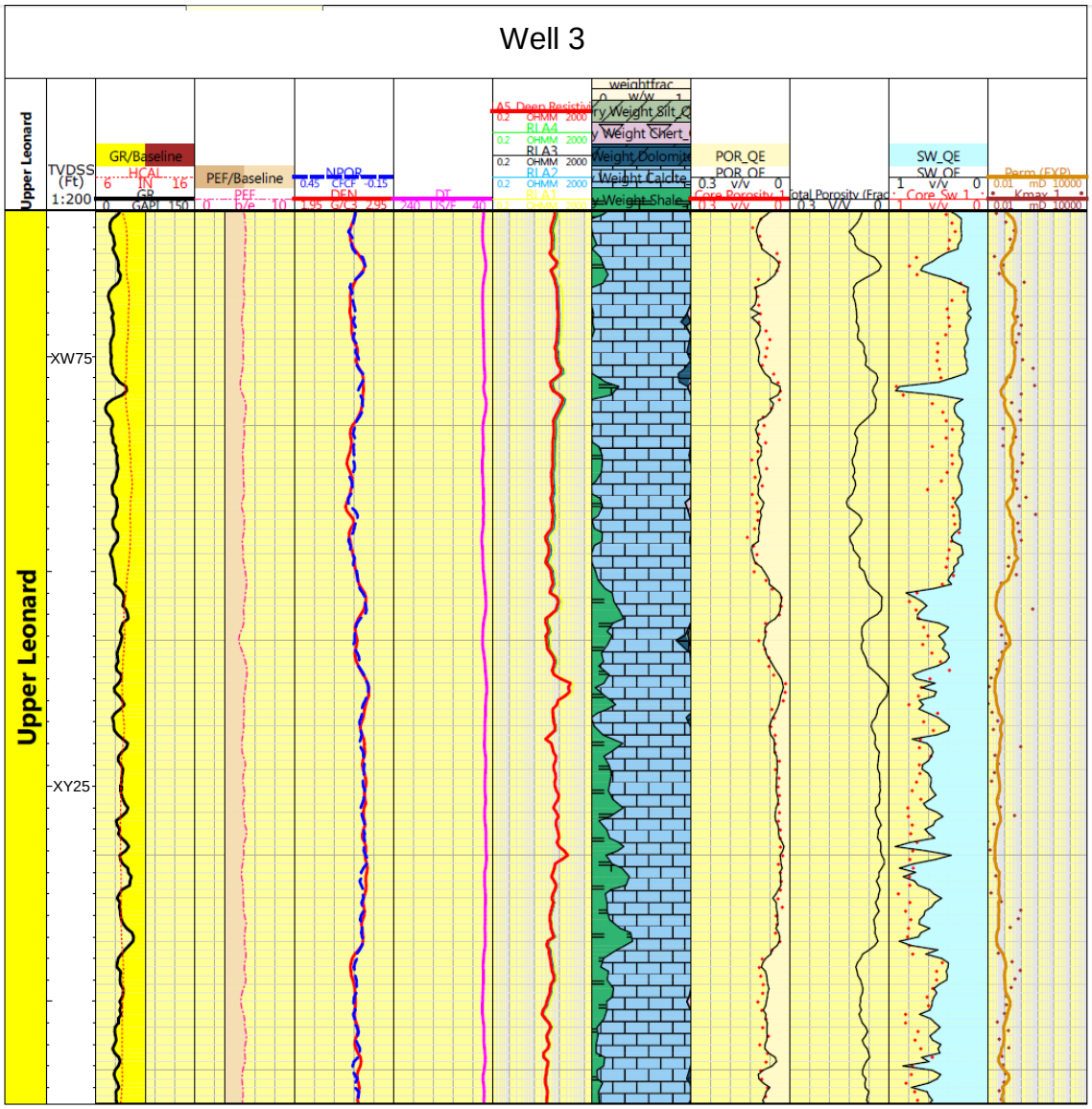
Well 3
Upper Leonard
TVDSS (Ft)
1:200
GR/Baseline
HCAL
IN
GR
GAPI
PEF/Baseline
PEF
b/e
NPOR
DEN
RLA5 Deep Resistivity
RLA4
RLA3
RLA2
RLA1
OHMM
weightfrac
w/w
Weight Dolomite
Weight Calcite
Weight Shale
POR_QE
POR_QF
Core Porosity
Total Porosity (Frac
SW_QE
SW_QF
Core_Sw
Perm (EXP)
Kmax
mD
XW75
XY25
Upper Leonard

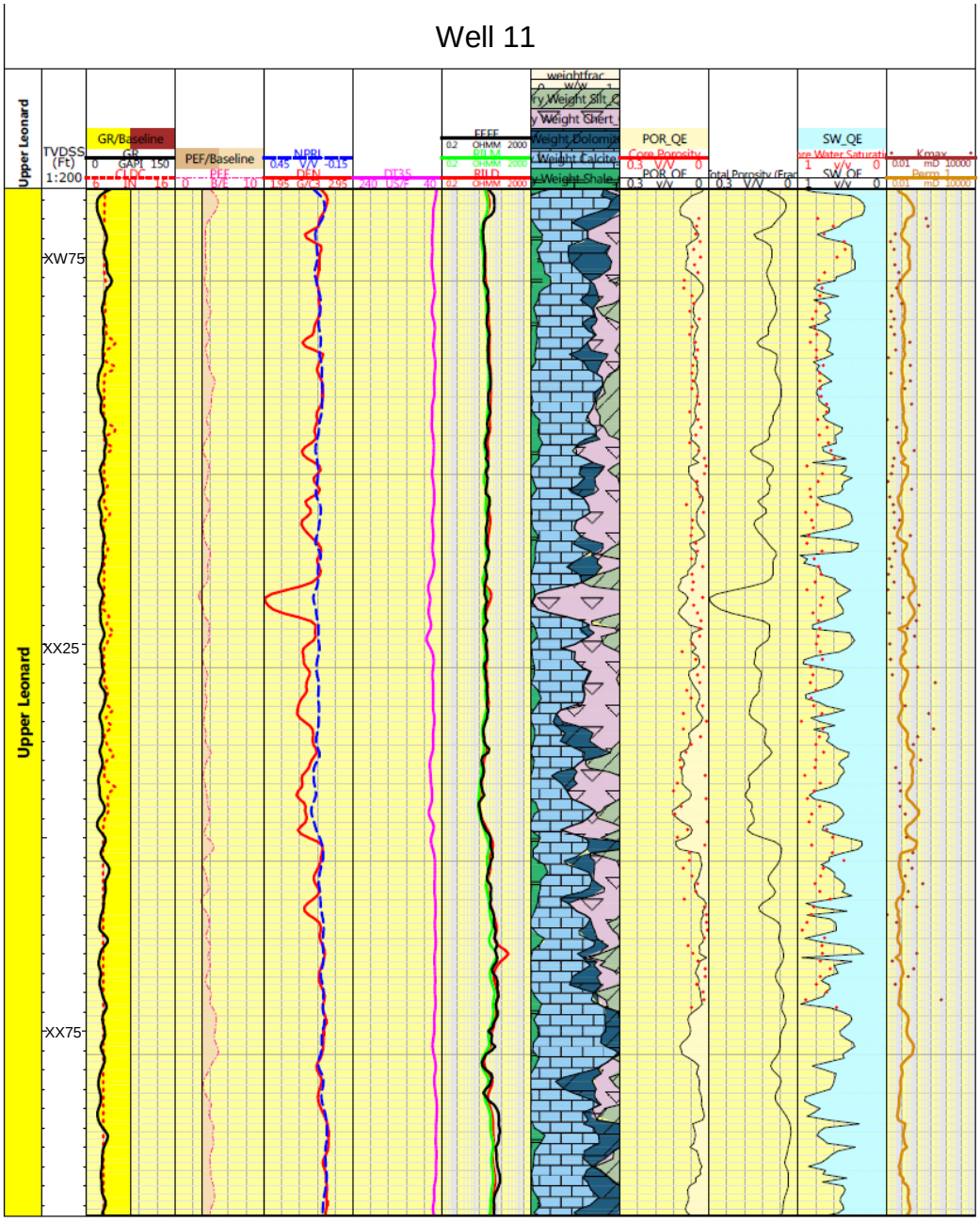
Well 11
Upper Leonard
TVDSS (Ft)
1:200
GR/Baseline
GR
GAPI
CLDC
IN
PEF/Baseline
PEF
PE
NPRL
DEN
DT35
RILM
RILD
OHMM
weightfrac
w/w
Weight Silt
Weight Chert
Weight Dolomite
Weight Calcite
Weight Shale
POR_QE
Core Porosity
POR_QE
Total Porosity (Frac
SW_QE
Water Saturati
SW_QE
Kmax
mD
Dxmp
XW75
XX25
XX75
Upper Leonard

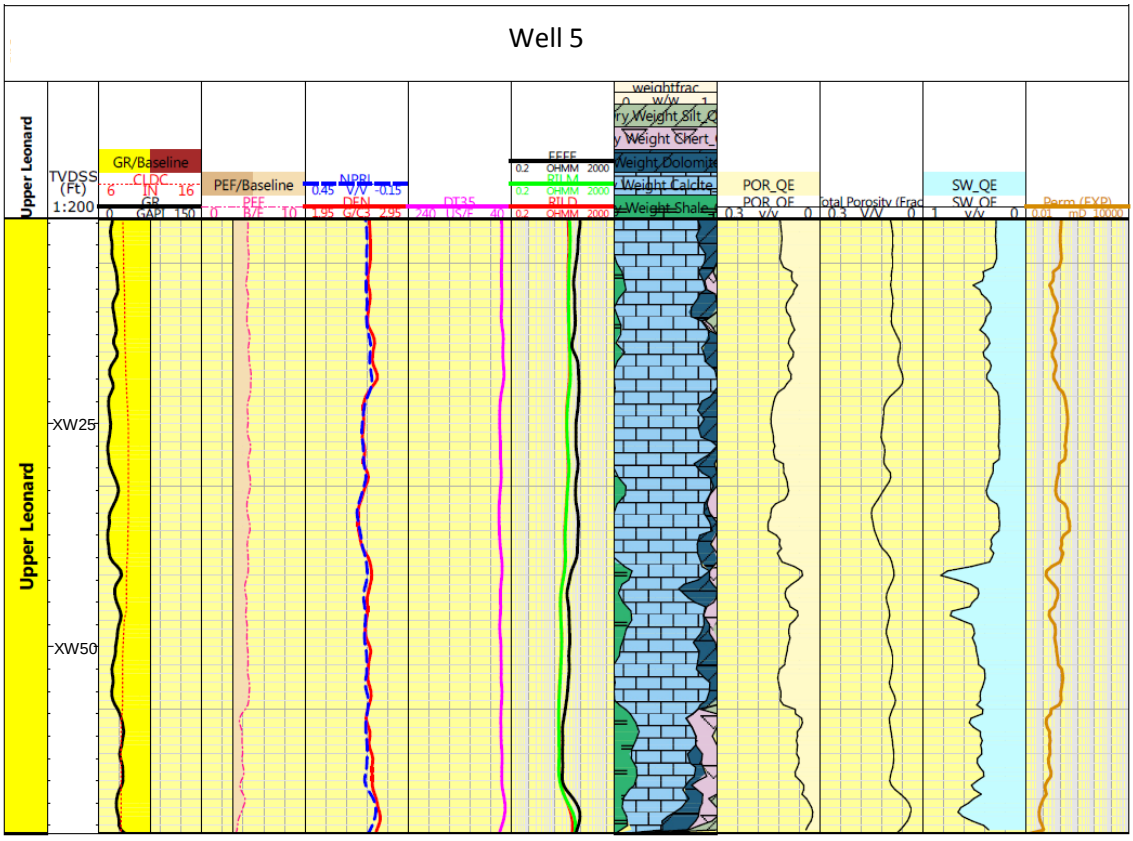
Well 5
Upper Leonard
TVDSS
(Ft)
1:200
GR/Baseline
CLDC
GR
GAPI
PEF/Baseline
PEF
NPRL
DEN
DT35
RILM
RILD
weightfrac
Weight Silt_Q
Weight Chert_
Weight Dolomite
Weight Calcite
Weight Shale
POR_QE
Total Porosity (Frac
SW_QE
Perm (EXP)
XW25
XW50

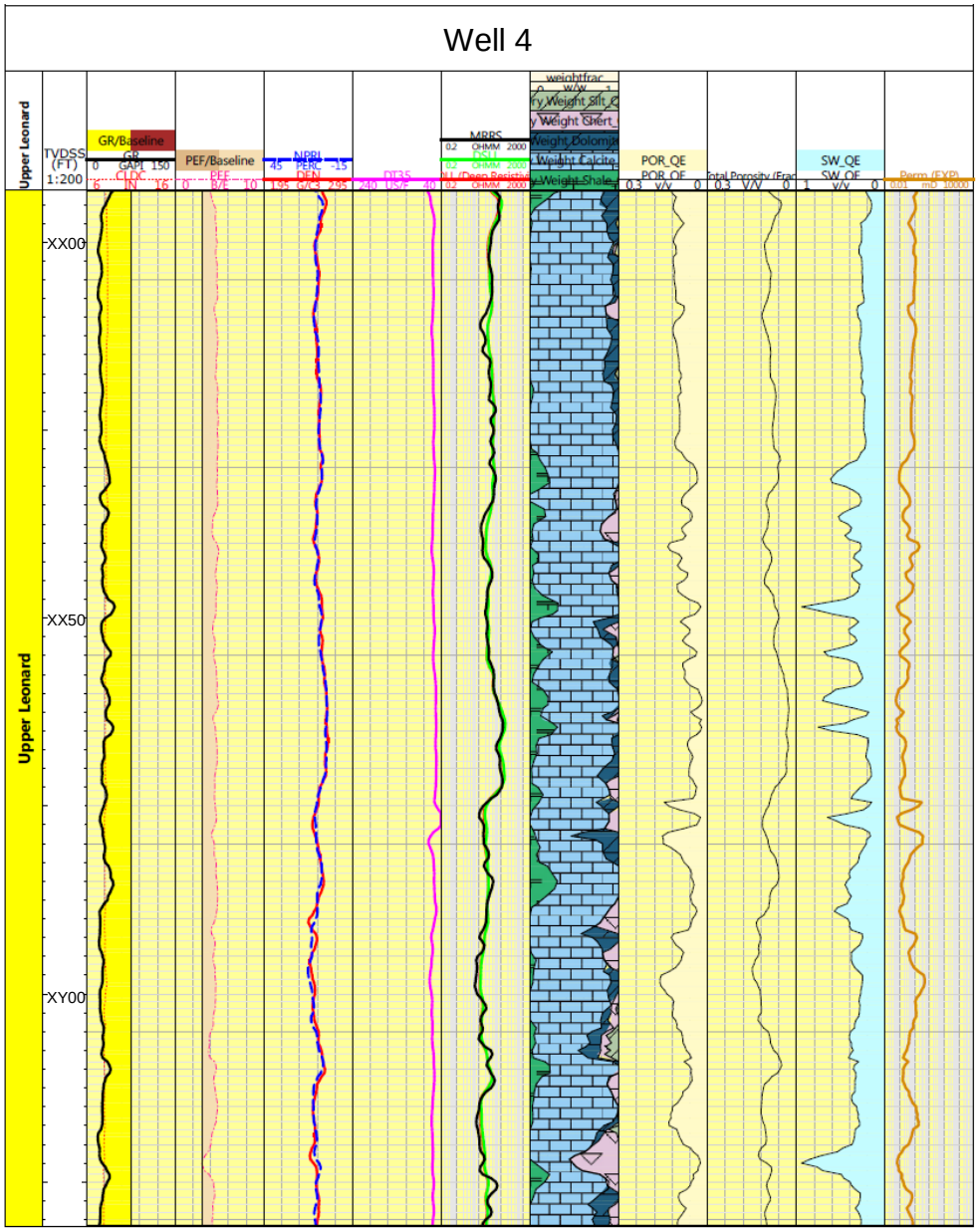
Well 4
Upper Leonard
TVDSS
(FT)
1:200
GR/Baseline
GR
GAPI
CLDC
IN
PEF/Baseline
PEF
B/E
NPRL
PERC
DEN
G/C3
DT3S
USPF
MRPS
OHMM
DSTV
RLL/Deep Resistivity
weightfrac
W/W
Weight_Silt_C
Weight_Chert_
Weight_Dolomite
Weight_Calcite
Weight_Shales
POR_QE
POR_QF
V/V
Total Porosity (Frac
SW_QE
SW_QF
Perm (EXP)
mD
XX00
XX50
XY00
Upper Leonard

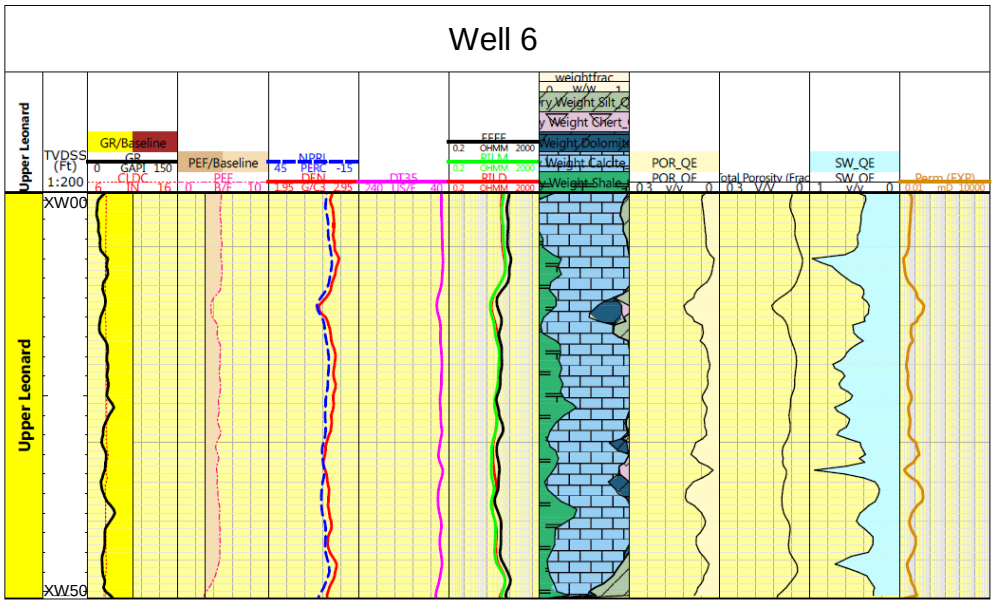
Well 6
Upper Leonard
TVDSS
(Ft)
1:200
GR/Baseline
GR
GAPI
CLDC
PEF/Baseline
PEF
NPRL
PERC
DEN
DT35
RILD
OHMM
weightfrac
w/w
Weight Silt
Weight Chert
Weight Dolomite
Weight Calcite
Weight Shale
POR_QE
POR_QE
Total Porosity (Frac
SW_QE
SW_QE
Perm (EXP)
XW00
XW50
Upper Leonard

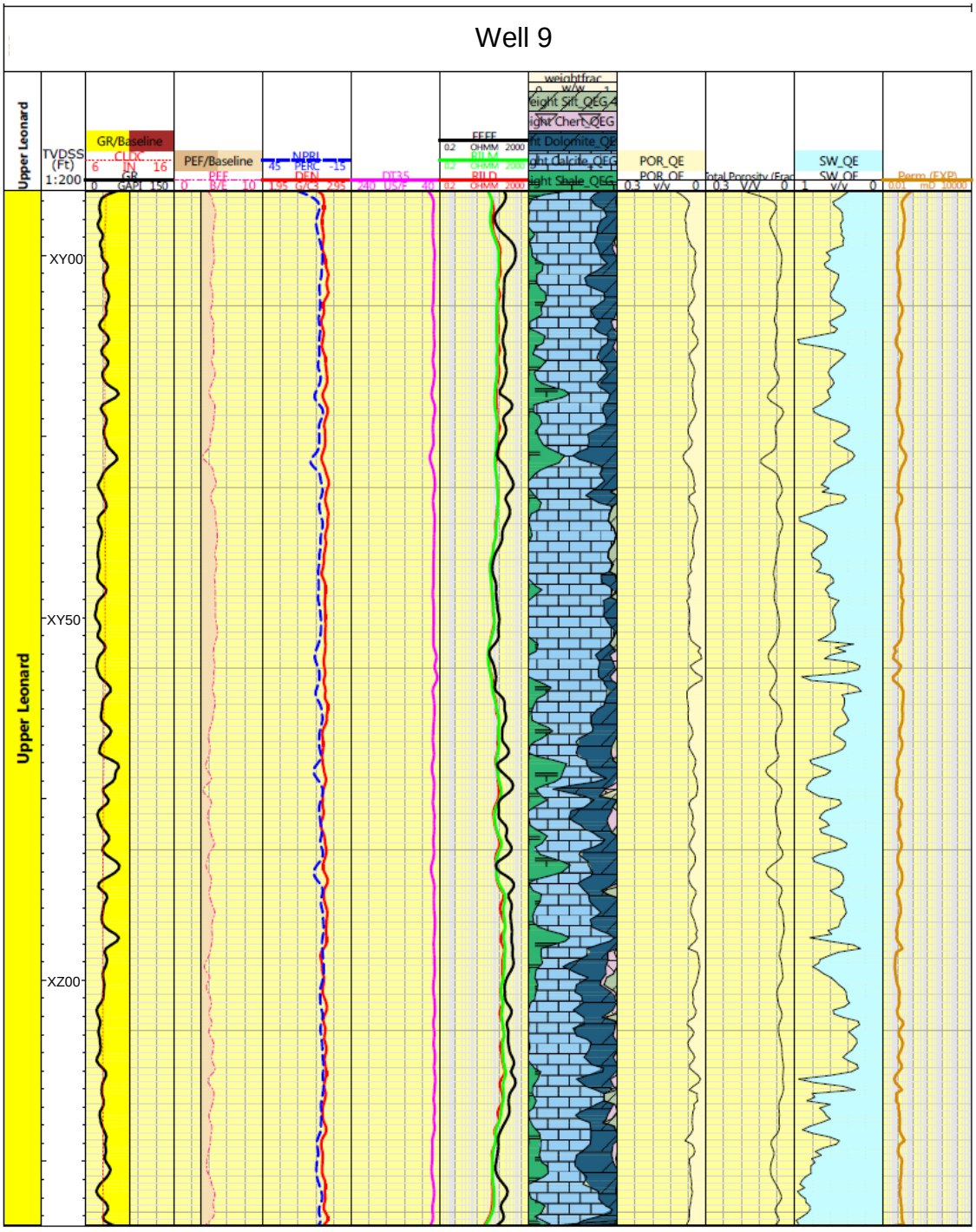
Well 9
Upper Leonard
TVDSS (Ft) 1:200
GR/Baseline
CLDC
GR
GAPI
PEF/Baseline
PEF
RHOB
DEN
NPRL
PERL
DT35
DTSF
FFFF
RILM
RILD
OHMM
weightfrac
w/w
Silt_QEG
Chert_QEG
Dolomite_QE
Calcite_QEG
Shale_QEG
POR_QE
POR_QE
Total Porosity (Frac
V/V
SW_QE
SW_QE
Perm (EXP)
mD
XY00
XY50
XZ00
Upper Leonard

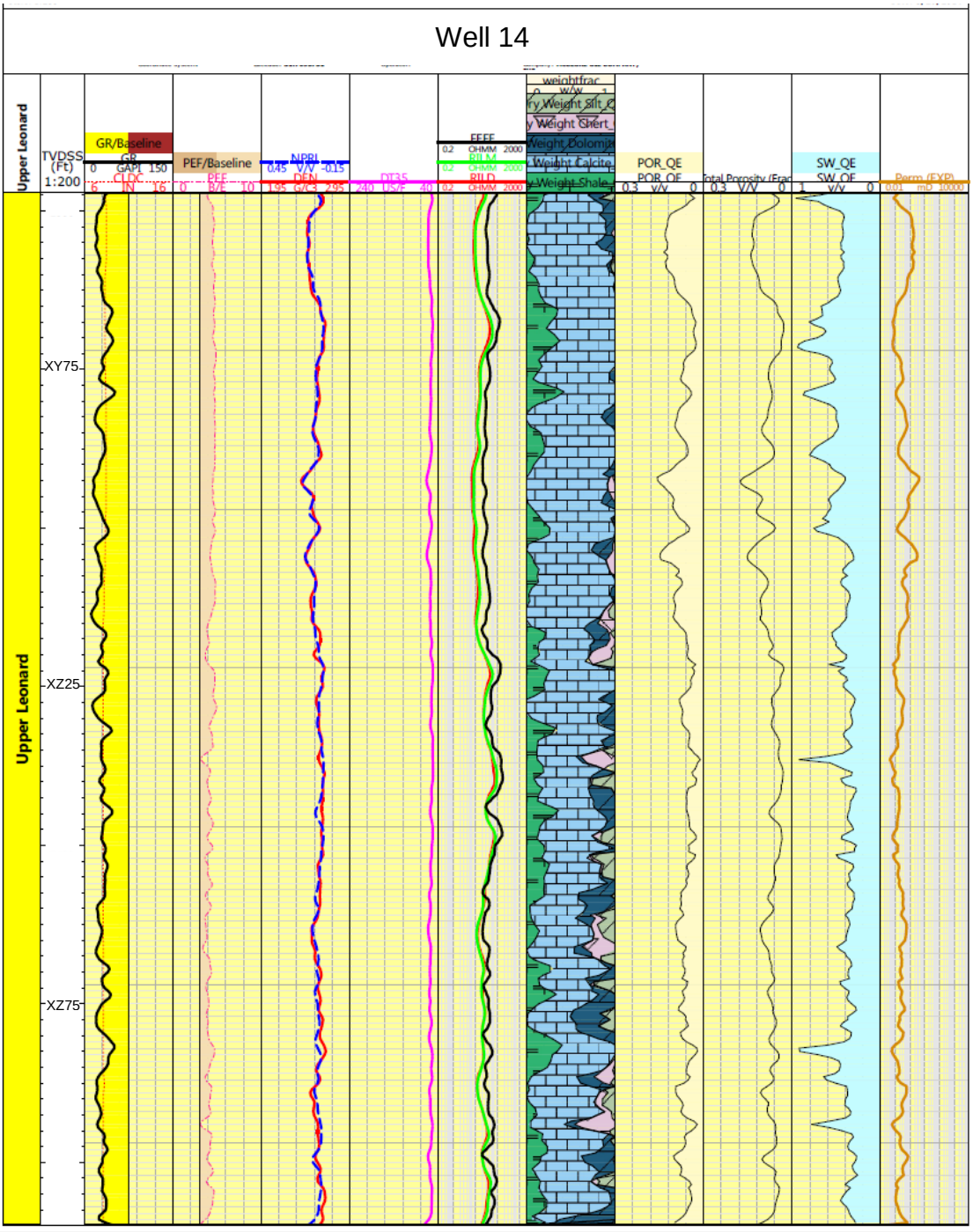
Well 14
Upper Leonard
TVDSS (Ft) 1:200
GR/Baseline
GR
GAPI
CLDC
CN
PEF/Baseline
PEF
BPE
NPRL
DEN
DT35
FEFE
RILM
RILD
OHMM
weightfrac
Weight Silt
Weight Chert
Weight Dolomite
Weight Calcite
Weight Shale
POR_QE
POR_OE
Total Porosity (Frac
SW_QE
SW_OE
Perm (EXP)
XY75
XZ25
XZ75
Upper Leonard

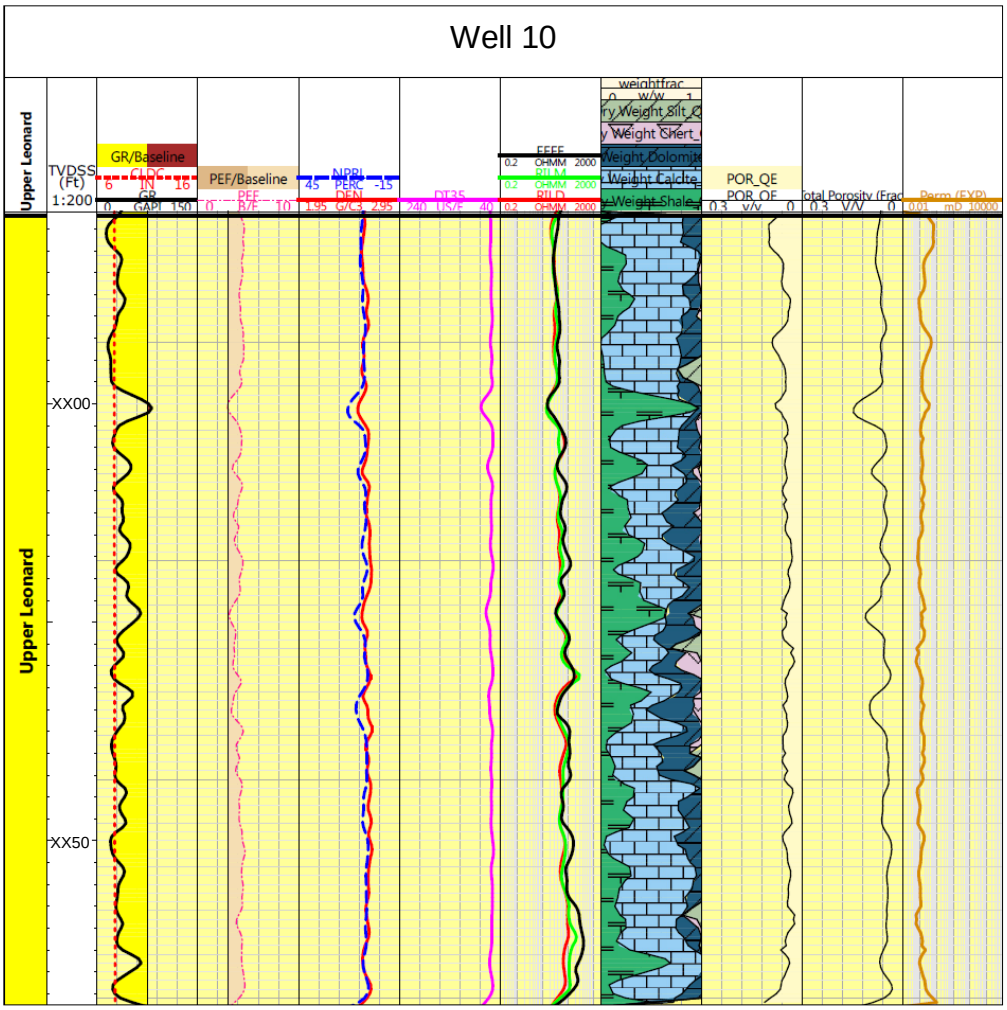
Well 10
Upper Leonard
TVDSS (Ft)
1:200
GR/Baseline
CLDC
CALI
GR
PEF/Baseline
PEF
RHOB
NPRL
PERC
DEN
DT35
RILD
RILM
weightfrac
Weight Dolomite
Weight Calcite
Weight Shale
POR_QE
Total Porosity (Frac
Perm (EXP)
XX00
XX50
Upper Leonard

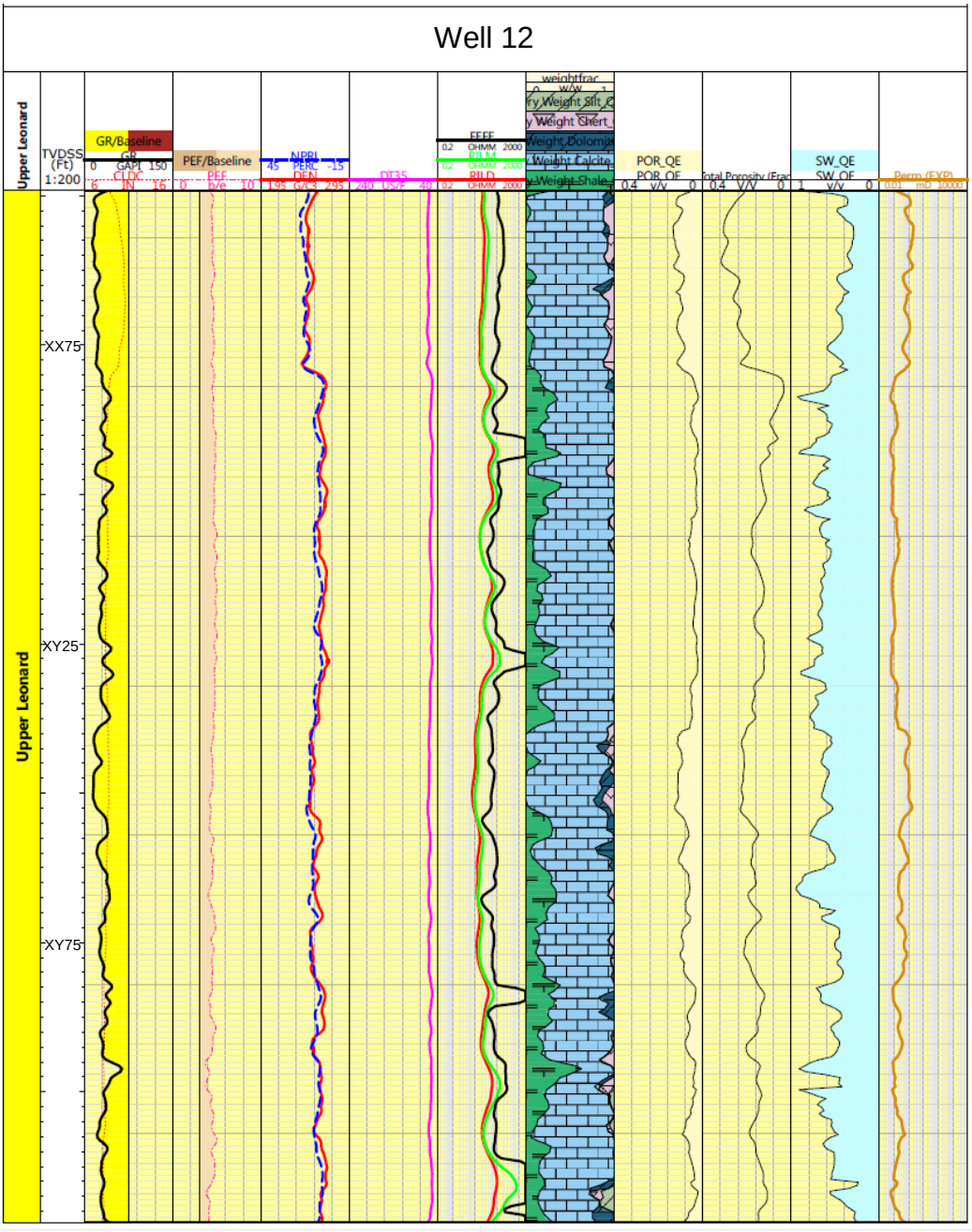
Well 12
Upper Leonard
TVDSS (Ft) 1:200
GR/Baseline
GR
GAPI
CLDC
CN
PEF/Baseline
PEF
DEN
NPRL
PERC
DT35
RILD
RILM
weightfrac
Weight_Dolomite
Weight_Calcite
Weight_Shale
POR_QE
POR_OF
Total Porosity (Frac
SW_QE
SW_OF
Perm (FXP)
XX75
XY25
XY75
Upper Leonard

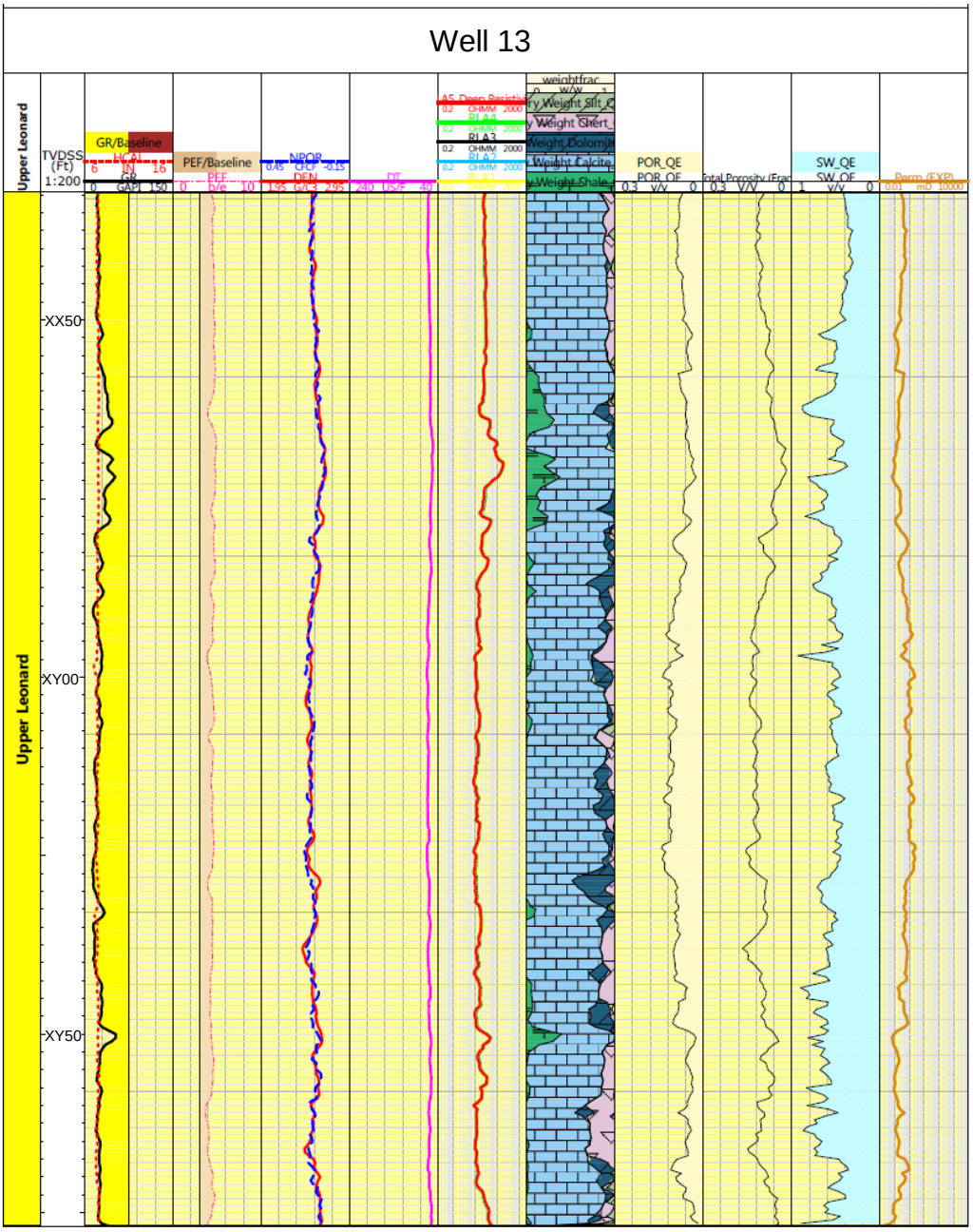
Well 13
Upper Leonard
TVDSS (Ft)
1:200
GR/Baseline
PEF/Baseline
NPOR
DT
POR_QE
SW_QE
XX50
XY00
XY50

APPENDIX 5

THIN SECTION ANALYSIS

TS = Thin Section

DC = Dunham's Classification

F = Fusulinid

B = Brachiopod

C = Crinoid

Sp = Sponge

RC = Rugose Coral

SS = Sponge Spicule

M = matrix

Tr = Trace

TS = Thin Section

MS = Mudstone

FW = Fusulinid Wackestone

RAG = Replacement after Grain

FC = Fringing Calcite

Bcal = Blocky Calcite

Sdol = Saddle Dolomite

Bry = Bryozoan

ITP = Intraparticle Porosity

IP = Interparticle Porosity

PG = Pelletal Grains

Qtz = Quartz

TG = Terrigenous Grains

DR = Dolomite Rhombs

SW = Skeletal Wackestone

FP = Fusulinid-Crinoid Packstone

PW = Partially Silicified Skeletal Wackestone to Mudstone

MC = Matrix-Supported Conglomerate

CC = Clast-supported polymict conglomerate

MF = Mud-Lean Fusulinid-Crinoid Packstone

Well 1

TS No	Facies	Skeletal Grains							M (%)
		F (%)	B (%)	C (%)	Bry (%)	Sp (%)	RC (%)	SS (%)	
1	SW	Tr	8	4	-	-	-	-	70
2	PW	-	8	5	-	-	-	5	60
3	PW	2	8	3	-	-	-	3	60
4	FW	10	5	2	-	-	-	1	65
5	FW	10	4	5	-	-	-	-	60
6	PW	-	5	2	-	-	-	10	50
7	FW	8	5	5	-	-	-	0	70
8	FW	8	5	3	-	-	-	0	60
9	SW	-	8	8	Tr	-	-	0	70
10	SW	Tr	8	5	-	-	-	5	80
11	SW	-	10	5	-	-	-	3	60
12	SW	-	10	5	-	-	-	-	60
13	SW	-	10	6	-	-	-	2	60
14	SW	-	10	5	-	-	-	-	70
15	SW	-	10	6	-	-	-	-	60
16	SW	2	10	4	-	-	-	-	70
17	FP	40	Tr	45	-	-	-	-	5
18	SW	-	8	6	-	-	-	-	70
19	SW	5	8	8	Tr	-	-	-	60
20	FW	8	4	5	-	-	-	-	60
21	FW	5	5	6	-	-	-	-	60

Well 1

TS No	Cement				RAG	Pore Type		TG	PG (%)
	FC (%)	Bcal (%)	Sdol (%)	DR (%)	Silica (%)	IP (%)	ITP (%)	Qtz (Silt;%)	
1	1	5	-	-	-	3	1	-	2
2	-	-	-	3	20	10	<1	2	-
3	-	-	-	-	40	17	2	1	2
4	4	3	1	1	3	7	5	2	1
5	3	2	1	1	-	3	8	2	-
6	-	-	-	5	50	15	1	5	-
7	3	3	2	-	-	8	3	1	1
8	2	10	4	-	-	8	5	1	1
9	-	-	-	3	-	<1	<1	8	2
10	-	-	-	6	8	4	<1	7	1
11	-	-	-	3	5	8	<1	2	1
12	-	-	-	5	-	3	-	5	1
13	-	-	-	2	3	1	<1	5	-
14	-	-	-	4	-	2	<1	6	1
15	-	-	1	-	-	15	-	Tr	-
16	1	1	-	5	5	3	2	5	-
17	2	2	3	-	-	10	2	Tr	-
18		-	-	1	Tr	<1	-	5	-
19	Tr	1	1	-	-	8	2	-	Tr
20	1	1	1	-	-	10	5	-	-
21	Tr	-	2	-	-	6	4	-	1

Well 2

TS No	Facies	Skeletal Grains								Matrix (%)
		F (%)	B (%)	C (%)	Bry (%)	Sp (%)	RC (%)	SS (%)	Other Fossils (%)	
1	MF	40	5	30	10	-	-	-	-	5
2	MF	30	5	40	1	-	-	-	-	10

Well 2

Matrix (%)	Cement				RAG	Pore Type		TG	PG (%)
	FC (%)	Bcal (%)	Sdol (%)	DR (%)	Silica (%)	IP (%)	ITP (%)	Qtz (Silt; %)	
1	Tr	5	2	-	-	8	10	2	-
2	1	3	2	-	-	7	10	3	-

Well 3

TS No	Facies	Skeletal Grains								Matrix (%)
		F (%)	B (%)	C (%)	Bry (%)	Sp (%)	RC (%)	SS (%)	Other Fossils (%)	
1	MC	10	8	10	-	-	-	-	-	50
2	FW	15	6	8	-	-	-	-	-	60
3	SW	-	4	3	-	-	-	-	4	70
4	SW	1	40	30	-	-	-	-	Tr	15
5	MW	-	7	6	Tr	-	-	-	-	90
6	CC	-	5	Tr	10	-	Tr	-	-	50
7	CC	-	5	5	-	-	-	Tr	-	50
8	CC	8	8	5	Tr	-	-	-	-	60
9	CC	5	2	8	-	-	-	-	-	60
10	CC	20	5	15	-	-	-	-	-	15
11	CC	5	2	6	20	-	-	-	-	50
12	CC	-	2	2	-	-	-	-	-	70
13	CC	-	3	2	Tr	Tr	-	-	-	90
14	CC	-	2	3	-	-	-	-	-	60
15	MF	30	10	35	-	-	-	-	-	10
16	MF	30	8	30	-	-	-	-	-	10

Well 3

TS No	Cement				RAG	Pore Type		TG	PG (%)
	FC (%)	Bcal (%)	Sdol (%)	DR (%)	Silica (%)	IP (%)	ITP (%)	Qtz (Silt;%)	
1	5	6	3	-	-	Tr	Tr	2	-
2	2	3	2	-	-	1	5	1	-
3	0	1	-	-	-	Tr	-	2	5
4	Tr	-	Tr	-	Tr	2	1	-	-
5	-	-	-	-	-	-	-	-	2
6	-	10	3	-	-	2	1	1	-
7	-	-	-	2	100	20	2	-	-
8	1	1	1	2	1	1	1	2	-
9	1	1	-	-	Tr	2	2	2	-
10	1	2	1	1	-	10	8	-	-
11	2	3	6	-	-	8	7	-	-
12	-	2	4	-	-	5	2	2	-
13	-	2	1	-	Tr	1	1	2	-
14	-	1	1	-	8	15	2	-	-
15	3	2	1	-	-	2	8	2	-
16	2	2	1	-	-	5	10	-	-

Well 15

TS No	Facies	Skeletal Grains								Matrix (%)
		F (%)	B (%)	C (%)	Bry (%)	Sp (%)	RC (%)	SS (%)	Other Fossils (%)	
1	MS	-	-	-	-	-	-	-	-	100
2	MS	-	-	-	-	-	-	-	-	100
3	MC	Tr	8	4	Tr	-	-	-	-	70
4	SW	-	12	10	-	-	-	-	-	60
5	FW	10	10	5	-	-	-	-	1	70
6	SW	Tr	8	6	-	-	-	-	-	70
7	FP	40	Tr	20	-	-	-	-	5	15
8	SW	-	10	5	-	-	-	-	-	80
9	SW	-	8	5	-	-	-	-	Tr	80
10	Fp	8	5	20	-	-	-	-	Tr	60
11	SW	-	6	5	-	-	-	-	Tr	80
12	CC	10	10	8	-	-	-	-	Tr	60
13	CC	5	10	10	-	-	-	-	-	60
14	FP	40	5	40	-	-	-	-	-	10
15	FP	30	5	50	-	-	-	-	-	10
16	FW	30	5	40	-	-	-	-	-	10
17	SW	5	20	5	10	-	-	-	15	30
18	MS	-	Tr	Tr	-	-	-	-	-	95
19	SW	-	10	1	Tr	-	-	-	-	80
20	MF	45	2	40	-	-	-	-	-	5
21	MS	-	-	-	-	-	-	-	-	100

Well 15

TS No	Cement				RAG	Pore Type		TG	PG (%)
	FC (%)	Bcal (%)	Sdol (%)	DR (%)	Silica (%)	IP (%)	ITP (%)	Qtz (Silt; %)	
1	-	-	-	-	-	-	-	-	-
2	-	-	-	-	-	-	-	-	8
3	<1	<1	-	-	-	<1	-	-	-
4	-	2	1	-	-	5	-	-	-
5	-	2	Tr	-	-	5	1	-	-
6	-	-	4	-	Tr	-	Tr	<1	-
7	3	5	3	-	-	8	6	-	-
8	-	-	-	-	-	8	-	1	5
9	-	-	-	-	-	<1	-	1	8
10	Tr	1	1	-	-	5	3	-	-
11	-	-	-	-	-	-	-	-	5
12	2	5	-	-	-	-	-	-	1
13	Tr	1	-	-	-	5	1	-	-
14	2	4	-	-	-	5	10	-	-
15	Tr	3	2	-		5	10	-	2
16	Tr	1	1	-	-	10	2	-	-
17	-	4	-	-	1	1	Tr	10	-
18	-	1	-	-	-	-	-	5	5
19	-	-	-	-	-	-	-	8	-
20	Tr	5	3	-	-	Tr	-	-	-
21	-	-	-	-	-	-	-	5	-

Well 11

TS No	Facies	Skeletal Grains								Matrix (%)
		F (%)	B (%)	C (%)	Bry (%)	Sp (%)	RC (%)	SS (%)	Other Fossils (%)	
1	MS	-	-	-	-	-	-	-	-	100
2	MS	-	-	-	-	-	-	-	-	100
3	MS	-	-	-	-	-	-	-	-	100
4	MS	-	-	-	-	-	-	-	-	100
5	MS	-	-	-	-	-	-	-	-	100
6	MS	-	-	-	-	-	-	-	-	100
7	MS	-	Tr	-	-	-	-	-	-	100
8	MS	-	-	-	-	-	-	-	-	100
9	MS	-	-	Tr	-	-	-	-	-	100
10	MS	-	-	-	-	-	-	-	-	100
11	MS	-	1	-	-	-	-	-	-	100
12	MS	-	-	-	-	-	-	-	-	100
13	MS	-	Tr	1	-	-	-	-	-	100
14	MS	-	Tr	Tr	-	-	-	-	-	100
15	MS	-	Tr	-	1	-	-	-	-	100
16	WS	5	2	5	-	-	-	-	-	80
17	MS	-	5	10	-	-	-	-	-	80

Well 11

TS No	Cement				RAG	Pore Type		TG	PG (%)
	FC (%)	Bcal (%)	Sdol (%)	DR (%)	Silica (%)	IP (%)	ITP (%)	Qtz (Silt; %)	
1	-	-	-	-	-	-	-	10	-
2	-	2	-	-	40	5	-	2	Tr
3	-	-	-	-	-	-	-	5	2
4	-	1	-	3	10	1	-	-	Tr
5	-	-	-	2	50	1	-	2	-
6	-	-	-	-	5	-	-	2	10
7	-	-	-	-	50	1	-	10	-
8	-	10	-	1	2	-	-	5	5
9	Tr	-	Tr	5	50	1	-	10	-
10	-	Tr	-	5	10	-	-	5	8
11	-	-	-	1	2	-	-	3	5
12	-	-	-	-	20	-	-	10	-
13	-	2	-	-	40	-	-	5	-
14		1	-	-	40	-	-	5	-
15	-	-	-	20	40	-	-	-	-
16	-	1	-	3	30	-	-	2	-
17	-	5	-	2	Tr	1	-	5	-